UNIVERSITÀ
DEGLI STUDI
DI PADOVA

Doctoral School of Space Sciences, Technologies and Measurements
Curriculum in Mechanical Measurements for Engineering and Space
XXVIII Cycle

Fault Tolerant Power Electronics Systems

Director of the School	**:** Ch.mo Prof. Giampiero Naletto
Coordinator of Curriculum	**:** Ch.mo Prof. Stefano Debei
Supervisor	**:** Ch.mo Prof. Giuseppe Buja
Co-Supervisor	**:** Ch.mo Prof. Stefano Debei

Ph. D. Student **:** Syamnaresh Garlapati

University Centre for Space Studies and Activities “Giuseppe Colombo” &
Laboratory of Electric Systems for Automation and Automotive “Industrial Engg.”
University of Padova, Italy

January 31, 2016

UNIVERSITÀ
DEGLI STUDI
DI PADOVA

Sede Amministrativa: Università degli Studi di Padova

CISAS – Centro di Ateneo di Studi e Attività Spaziali "Giuseppe Colombo"

SCUOLA DI DOTTORATO DI RICERCA IN: Scienze Tecnologie e misure Spaziali (STMS)

INDIRIZZO: Misure Meccaniche per l'Ingegneria e lo Spazio

CICLO: XXVIII

Fault Tolerant Power Electronics Systems

Direttore della Scuola: Ch.mo Prof. Giampiero Naletto

Coordinatore d'indirizzo: Ch.mo Prof. Stefano Debei

Supervisore: Ch.mo Prof. Giuseppe Buja

Co-Supervisore: Ch.mo Prof. Stefano Debei

Dottorando: Syamnaresh Garlapati

ABSTRACT

Research work reported in this Ph.D. thesis is in the area of power electronics systems, specifically in the sector of electrical drives. A trustworthy operation of power electronics systems in critical applications like electric vehicles, aircrafts, satellites, and so on, has pushed engineers to develop fault-tolerant solutions. Indeed, in such applications it is necessary for the system to continue its operation, possibly with downgraded performance, even under faulty case. Present thesis reports the studied solutions to make fault-tolerant a class of electric drives under faulty conditions. It has initiated by addressing the need and importance of the usage of power electronic systems in the field of transportation sector, in particular in the automobile and aerospace industry.

Permanent magnet (PM) brushless (BL) drives have become very popular thanks to their higher torque-per-ampere capabilities. Among the two different types of PM BL drives, namely those with sinusoidal back-emf (BLAC) and those with trapezoidal back-emf (BLDC), the latter ones are preferred for light-duty propulsion such as minicars and scooters, and in aeronautics as control-surface actuators. However, some concern have emerged on the use of electrical drives in such applications with regard to the fault tolerance and the power capability per volume unit. A way to effectively cope with these concerns is the adoption of multiphase drives. In this sense, a five-phase drive is a promising solution as it is the most simple multiphase structure of practical interest.

The thesis starts with the study of the phase current and torque behavior in three-phase PM BLDC drive in healthy conditions. To validate the mathematical findings, a study case is used, represented by an electrical drive with in-wheel motor utilized for the propulsion of a city car. Afterwards, various types of faults in voltage source inverter (VSI) of a three-phase PM BLC drive are considered, such as one leg open, one switch open and one switch shorted. Remedial control strategies for the faults of the VSI are envisaged, that enable the three-phase PM BLDC drive to continue to operate even if in a degraded way. The resulting performance is calculated in terms of developed torque and torque ripple. The mathematical findings are substantiated with graphs obtained by simulation.

A five-phase PM BLDC drive is successively considered. First, its operation and its torque capabilities are investigated in healthy conditions under ideal square-wave current supply. The torque capabilities are compared to the three-phase counterpart; torque comparison is carried out by keeping motor size constant and by considering two hypotheses: equal phase back-emf and equal phase rms current. Then, the torque available from a five-phase drive is determined under various supply modes, characterized by the conduction of a reduced number of phases; the torque available is determined by imposing an rms phase current equal to the nominal one. Moreover, the current behavior during the phase commutations for the five-phase PM BLDC drives is analyzed as they exhibit some

differences with respect to the three-phase counterpart. The outcomes of the current analysis are used to derive the effective torque developed by the drive and the torque ripple exhibited as a function of the motor speed. The base speed of the drive is also determined. Also for the torque results, the differences from the well-known characteristics of the three-phase PM BLDC drives are pointed out.

Lastly, an algebraic approach is developed to describe the operation of a five-phase PM BLDC drive in healthy conditions. The approach has led to the formulation of a model of the phase current supply of the motor in healthy conditions. Further, the model has been suitably adjusted to derive the mode (scheduling and magnitude) of current supplying the survival phases in the case of one or more motor open phase faults. The cases of one /two/three open phase faults have been examined and, in the case of two and three faulty phases, the cases of adjacent and non-adjacent faulty phases. For each case, the current magnitude has been found by imposing that the rms value of the current in the most solicited phase is equal to the nominal value, and the torque that the drive is able to develop as well as the maximum value of the torque ripple have been calculated. The obtained results indicate that the reduction in the motor torque as well as the extent of the torque ripple is depending, besides on the number of the faulty phases, on the relative location of the faults.

The thesis work also address the evolution of electrical power generation and conversion methodologies in more electric aircraft, fault-tolerant solutions under faulty Hall sensors, and the concepts of dependability and safety aspects.

The thesis work has been carried out at the Laboratory of “Electric systems for automation and automotive” headed by Prof. Giuseppe Buja. The laboratory belongs to the Department of Industrial Engineering, University of Padova, Italy.

SOMMARIO

Il lavoro di ricerca riportato nella tesi di dottorato è stato svolto nel campo dei sistemi di elettronica di potenza, in particolare degli azionamenti elettrici. Un funzionamento affidabile dei sistemi di elettronica di potenza in applicazioni critiche come i veicoli elettrici, gli aerei, i satelliti, ecc. ha spinto gli ingegneri a sviluppare soluzioni fault-tolerant. Infatti, in tali applicazioni è necessario che il sistema continui a funzionare, eventualmente con prestazioni declassate, anche in caso di guasto. La presente tesi riporta le soluzioni studiate per rendere fault-tolerant il comportamento di una tipologia di azionamenti elettrici in condizioni di guasto. Essa ha inizio con una disamina sulla necessità e sull'importanza dell'impiego di sistemi di elettronica di potenza nel settore dei trasporti, segnatamente nell'industria automobilistica e aerospaziale.

Gli azionamenti a magnete permanente (PM) di tipo brushless (BL) sono diventati molto popolari grazie alla loro capacità di sviluppare elevate coppie per unità di corrente. Tra i due diversi tipi di azionamenti PM BL, quelli con forza controelettromotrice sinusoidale (BLAC) e quelli con forza controelettromotrice trapezoidale (BLDC), questi ultimi sono preferiti per la propulsione leggera come minicar e scooter e nel settore aeronautico come attuatori dei comandi di volo. Qualche timore è emerso sull'uso degli azionamenti elettrici in tali applicazioni in relazione alla tolleranza ai guasti e anche alla potenza sviluppabile per unità di volume. Un modo per affrontare efficacemente questi timori è l'adozione di azionamenti multifase. Sotto questo aspetto un azionamento a cinque fasi è una soluzione promettente in quanto è la struttura multifase di pratico interesse più semplice.

La tesi inizia con lo studio dell'andamento delle correnti e della copia in azionamenti trifase PM BLDC nel funzionamento in condizioni di integrità. Per convalidare i risultati matematici è stato utilizzato un caso di studio rappresentato da un azionamento PM BL con motore ruota utilizzato per la propulsione di city car. Successivamente, la tesi considera vari tipi di guasto dell'invertitore a tensione impressa (VSI) che alimenta il motore PM BL, come ad esempio una gamba aperta, un interruttore aperto o un interruttore cortocircuitato, e propone strategie di controllo correttive che, tenendo conto del tipo di guasto, consentano all'azionamento di continuare a funzionare anche se in modo degradato. Le prestazioni che ne risultano sono calcolate in termini di coppia sviluppata dal motore e di ripple di coppia. I risultati sono supportati da grafici ottenuti per simulazione.

Si è preso quindi in esame un azionamento PM BL a cinque fasi. Dapprima si sono studiati il suo funzionamento e le sue prestazioni di coppia in condizioni di integrità e di andamento ideale delle correnti di fase ed essi sono stati confrontati con quelli di un azionamento PM BL trifase. Il confronto è stato eseguito mantenendo invariate le dimensioni del motore e considerando due ipotesi: parità del valore della tensione controelettromotrice

di fase e parità del valore efficace della corrente di fase. Inoltre è stata determinata la coppia disponibile in varie condizioni di guasto, caratterizzate dalla conduzione di un numero ridotto di fasi, nell'ipotesi che l'ampiezza delle correnti di fase abbia un valore efficace pari a quello nominale. Si è quindi analizzato l'andamento delle correnti durante le commutazioni di fase dell'azionamento PM BL mostrando come esso presenti sensibili differenze rispetto ad un azionamento PM BL trifase. Tale andamento è stato utilizzato per trovare la coppia effettivamente sviluppata dall'azionamento e il ripple di coppia in funzione della velocità del motore. E' stata inoltre determinata la velocità base dell'azionamento. Anche per i risultati di coppia sono state evidenziate le differenze rispetto al caso di azionamento PM BL trifase.

E' stato infine sviluppato un approccio algebrico per descrivere il comportamento di un azionamento PM BL a cinque fasi; esso ha portato a formulare un modello dell'alimentazione in corrente delle fasi del motore in condizioni di integrità. Il modello è stato successivamente opportunamente modificato per derivare le modalità (tempistica e ampiezze delle correnti) di alimentazione delle fasi integre del motore nel caso che un guasto dell'azionamento porti all'apertura di una o più fasi del motore. Sono stati presi in esame i casi di una / due / tre fasi guaste e, nel caso di due e tre fasi guaste, i casi di fasi guaste adiacenti e non adiacenti. Per ogni caso è stata determinata l'ampiezza delle correnti imponendo che il valore efficace della corrente nella fase più sollecitata sia pari al nominale e sono stati ricavati la coppia sviluppabile dal motore e il valore massimo del ripple di coppia. I risultati ottenuti mostrano che la riduzione della coppia del motore e l'ampiezza del ripple di coppia dipendono, oltre che dal numero di fasi guaste, dalla posizione relativa delle fasi guaste.

Il lavoro di tesi discute anche l'evoluzione delle metodologie di produzione di energia elettrica e di conversione nelle applicazioni "more-electric aircraft", soluzioni fault-tolerant in presenza di sensori Hall guasti, e il concetto di affidabilità e di sicurezza funzionale.

Il lavoro di tesi è stato effettuato presso il Laboratorio di "Sistemi elettrici per l'automazione e la veicolistica" diretto dal Prof. Giuseppe Buja. Il Laboratorio fa parte del Dipartimento di Ingegneria Industriale dell'Università degli Studi di Padova, Italia.

Dedicated to my dear parents

ACKNOWLEDGEMENT

My deep appreciation goes to many people whose advice, assistance and encouragement have enabled me to reach this stage in my life. I am really fortunate to have known so many great people so far in my life that my limited memory cannot accommodate. To those who are missing in this brief list, and were supposed to be here, I sincerely apologize.

Foremost, I would like to express my sincere gratitude to my supervisor Prof. Giuseppe Buja for the continuous support of my Ph.D. study and research, for his unlimited patience, motivation, enthusiasm, and immense knowledge. His guidance helped me in all the time of research and writing of this thesis. I am also grateful to Dr. Manuele Bertoluzzo (Associate Professor, Department of Industrial Engineering), whose dedication towards the laboratory remains unparalleled. His support to me and fellow students has always been an ever increasing source of motivation. I would like to thank Prof. Alberto Tessarolo, University of Trieste and his research group for giving me the opportunity to work with them by allotting their valuable time for discussions.

I am greatful to Centro di Ateneo di studi e Attività Spaziali Giuseppe Colombo (CISAS), University of Padova for supporting my study with a grant under Law 170. My sincere appreciations to Prof. Giampiero Naletto, Prof. Stefano Debei and administrative staffs of CISAS, Industrial Engineering department and the University of Padova for their support. I have always found them responsive and supportive not only to me but to all the students, contributing towards an excellent world class research environment.

I am greatful to Dr. Ritesh Keshri for his valuable guidelines and support during the initial stage of my research. I am most grateful to my friend-colleague Mr. Kundan Kumar, for his continuous support and guidelines. I truly appreciate his helpfulness and encouragement in every aspect of life. I would like to extend my salute and thanks to all my friends and colleagues in the Laboratory of Electric Systems for Automation and Automotive, Mr. Christian Fontana, Mr. Rupesh, Mr. Hemanth, Mr. Mattia Forato, Dr. Mude Kishore Naik for their professionalism, company and respect during group work and social activities.

I would like to thank my Indian and Italian friends, Mr. Nisarg Patel, Mr. Jagjit Singh, Mr. Kishore Yadav, Dr. Maiti, Dr. Varun Kumar Sharma, Mr. Mauro, Mr. Shashank, Ms. Federica, Mr. Federico, Ms. Anna, Ms. Maria, for lots of support and making my stay more memorable in Padova. In addition, I would like to thank all my school mates and college mates from India, specifically Mrs. T. Devi, Mr. K. Naresh Kumar, Mr. V. Bheemudu for their continuous support and motivation.

Finally, I thank again Mr. Rupesh Kumar Jha and Ms. Anna Tuzzato for staying beside me during tough situations. I am especially indebted to my family members for their patience and constant support throughout my way.

TABLE OF CONTENTS

Page

Chapter 3

Chapter 4

Chapter 5

Chapter 8

LIST OF FIGURES

FIGURE Page

FIGURE Page

LIST OF TABLES

Chapter 1

Introduction

1.1 Background

Transportation sector needs to be improved day-by-day, to meet the increase in public demand. Higher dependability is a new challenge in power electronics especially in applications such as electric and hybrid electric vehicles, more electric aircrafts, chemical industries, transportation systems, renewable energy systems, and space-crafts [1]. Looking into the history of air transportation, there is drastic change in the commercial aircraft technologies used since last decade.

Power converters are principally used to convert power from one level to other, power conditioning, and also to feed the electrical motor. According to a recent survey, power electronic switches are responsible for the main part of power converter failures [2]. Existing literature gives a review on faulty modes and detection methods of power switches and its diagnosis methods, etc.

Reliability, easy control and ease of maintenance are the main reasons for adopting electrical drives in transportation and aviation applications. Most of the household and industrial applications uses induction motor drives, whereas light and mid-duty propulsion apparatuses are served by permanent magnet (PM) brushless drives due to their higher power density and torque-per-ampere capability than other motor of same size. Out of two different types of PM BL drives, namely PM BL DC type and AC type, PM BLDC drives are most preferred for light and traction applications. Due to the recent advancements in power electronics, the PM BLDC drives have been also utilized within the framework of more-electric aircraft paradigm as flight control actuators, for instance (f.i.) for positioning ailerons, flaps, and

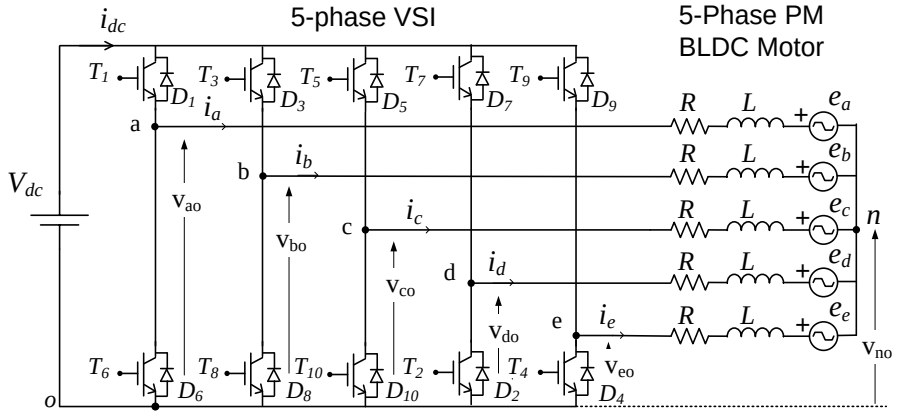

Fig. 1.1. Circuit representation of a five-phase PM BLDC drive.

rudders. Design of these drives aimed at achieving fault tolerant capabilities, leads to devote special attention towards multiphase drives. So that they are able to operate in faulty conditions although with degraded performance. The most promising multiphase structure of a PM BLDC drive has five number of phases, because of its limited complexity with respect to other multiphase topologies with higher phase count.

The circuit scheme of a five-phase PM BLDC drives is shown in *Figure 1.1*. Similar to the three-phase PM BLDC drives, the five-phase PM BLDC drives require the injection of square-wave phase currents synchronized with the flat portion of the back-emfs for the drives to develop constant torque with maximum torque-per-ampere factor. In the existing literature, five-phase PM BL drives with sinusoidal phase currents have been mostly investigated in spite of the fact that their set-up needs a high-resolution transduction of the rotor position for the current synchronization. Less attention, has been paid to the five-phase PM BL drives with square-wave current supply even if they have a more robust set-up due to the use of less troubling Hall sensors.

1.2 Objective and Approach

A five-phase voltage source inverter (VSI) is used to feed the five-phase PM BLDC drive. There are different possibilities to make a PM BLDC drive fault tolerant like (a) by implementing suitable strategies of control that give continuity to the operation of the PM BLDC drive even under a fault, eventually with downgraded performance; this solution is more economical and can be readily adopted in the existing PM BLDC drives used in both the industrial and transportation sectors, (b) either by adding an auxiliary healthy leg to the VSI or increasing the number of motor phases so as to reduce the dependency of the drive operation during faults. Addition of an auxiliary leg is not a cost effective solution, as the use of extra VSI leg is during faulty case only and it remains ideal during normal (healthy) operation. But the increased number of motor phases appears most convenient for a PM BLDC drive to be tolerate a fault without a large penalization of its performance. With reference to the subjects (a) and (b), the following activities have been done:

- Study on various possibilities of fault occurrence and their effects on the performance of a three-phase BLDC drive has been summarized. Possible control solutions, some of them supported with additional hardware, have been analyzed for common fault cases.
- A state-of-art study has been carried out on multi-phase fault tolerant BLDC motor drive. A study is initiated by examining the possible conduction modes of a multi-phase PM BLDC drive that has five-phases considering both healthy operation and faulty operation.

Five-phase PM BLDC drives are exemplified with its real fault-tolerant behavior in the presence of a fault in either the motor or the motor-supplying converter, although with degraded performance. As an initial step, the torque capability of the five-phase PM BLDC drives has been evaluated and compared to those of the three-phase counterpart under the same motor size and loading.

Afterwards the torque performance, namely the torque vs. speed characteristic and the torque ripple vs. speed curve, has been calculated for a five-phase PB BLDC drive taking into account the current commutations. Furthermore, the time behavior of the phase currents of a five-phase PM BLDC drives has been investigated by a computer-assisted analysis in the PSIM environment. To this purpose a suitable model of the drive has been formulated and hysteresis controllers have been implemented for the phase current regulation. Data of the model has been obtained from a 2 kW study case available in laboratory. Different strategies have been considered for the switching of the transistor legs (like switching of only upper or lower transistors of the legs of the voltage source inverter supplying the motor or a combination of them), finding out that an efficient chopping strategy consists in switching the transistor of the leg that conducts the incoming current and in continuing to chop as long as the respective phase conducts. Various possible faults are considered and the effective algorithm is chosen, that maximizes the drive performance is maximum among the possible best choices provided by satisfying the constraints.

1.3 Research contributions

The research contributions of this thesis work are summarized as follows:

- Software/Control scheme for three-phase Voltage Source Inverter (VSI) switch faults of a three-phase PM BLDC drive.
- Performance evaluation of a five-phase PM BLDC motor under various supply modes.
- Phase current and torque behavior during commutation in both three-phase and five-phase PM BLDC drives.
- Algebraic algorithms for generation of reference supply currents for faulty operation of five phase PM BLDC drive. In particular, two algorithms have been developed are intended to keep torque ripple at a minimum and the other one intended to keep the motor torque at a maximum.
- Software simulation (PSIM) of the five phase PM BLDC drive with hysteresis phase current control by applying the algebraic algorithm for reference current generation.

1.4 Thesis outline

The thesis is organized in eight Chapters whose outline is given below.

Current chapter summarizes with background, objective and approach of thesis

Chapter 2 discuss the need of power electronics systems and elaborates the way that the commercial aircraft improvised with the updated technologies by time. Increased demand of electrical energy for the aircraft lead engineers to put a greater emphasis on the use of technologies towards innovative architecture (design, operation and maintenance) in order to save system mass and the fuel that consume. It details the traditional power generations and conversion methodologies like constant frequency/speed power generation using gear

mechanism followed by the integrated generator system are modernized with the high power converters which can handle the variable frequency AC power and further transformed into difference levels of AC and DC as per load requirements. A typical levels of power requirement in aircraft for various loads like avionics, motor loads, lightning and galley loads are served with the help of semi-conductors filled power converters, which are more compact, efficient, cost effective and with fault tolerant capability.

Chapter 3 discuss the working operation of a regular (three-phase) PM BLDC drive. Starting with basic equations followed by the behavior of phase current is analyzed during the commutation period. Further, torque behavior is analyzed during commutation with respect to speed variation. Appropriate speed limits are also calculated for successful completion of commutation in specified interval for continuous operation of the drive. The theoretical results on the motor torque have been verified by considering a case study.

Most of the existing literature discussed on the problems of torque ripple and dropping speed-torque characteristics arising in PM BLDC drive during phase current commutation. It also need to be focused on the fault-tolerant solutions for regular PM BLDC drives i.e. the capabilities of overriding a fault to ensure the uninterrupted mobility of the system/vehicle. Chapter 4 deals with various general VSI switch faults that usually downgrades the PM BLDC drive performance. Various types of fault are considered such as one leg open, one switch open and one switch shorted. Remedial control strategies for the healthy devices of the VSI are envisaged, that make the drive operating even if in a degraded way. The analysis is carried out to obtain the maximum performance by effective modifications done to current reference/control strategy. The resulting torque performances are calculated in terms of developed torque and torque ripple. The mathematical findings are substantiated with graphs obtained by simulation on an in-wheel PM BLDC drive used for the propulsion of light electric vehicles.

Most of the literature is focued on fault detection and fault tolerant control, which is confined to the faults in power electronic switches of VSI and stator winding of motor. Hall senesor faults in a PM BLDC drive are also need to be focused inorder to make the system more realiable and fault-tolerant. In chapter 5 it is discussed about the Hall Sensor faults that occur due to the flaws in core, temperature variation, and also due to unbalneced positioning. Hall sensor plays a major role in extraction of information about the rotor position. Each Hall effect signal of BLDC motor has specific value at each instant of time with respect to permanent magnet rotor position. A hall effect sensor fault flag (HFF) method is used to detect the fault but identification of faulty Hall Sensor is obtained by Discrete Fourier Transform (DFT) analysis for the pattern recognition of the line voltage (as the line voltage is deteriorated due to position sensor fault) followed by computing the Spectral Energy Density (SED) for the successive time intervals reveals the faulty position sensor. Once the fault is detected, it is over written by a simple algorithms with a closed loop control scheme of reliable operation of BLDC motor.

Chapter 6 deals with the torque capabilities of a PM BLDC drive with a five-phase structure, which is a promising solution for its simplicity with respect to the ones with a greater number of phases to attain high torque, better efficiency and fault-tolerant features. Differently from what is usually done in the literature, the five-phase PM BLDC drive has been investigated by assuming the motor supplied with square-wave currents. The first point discussed is the torque capabilities of a five-phase PM BLDC drive compared to a three-phase counterpart having a motor with equal dimensions and magnetic structure. From the comparison it has been found that the five-phase PM BLDC drive is able to develop a torque 9.5% higher than the three-phase one. The second point discussed is the torque capabilities of the five-phase PM BLDC drive when the simultaneous conduction does not involve four motor phases like in the standard supply. Two supply modes have been evaluated, where three or two phases are conducting simultaneously with conduction intervals of $3\pi/5$ and $2\pi/5$, respectively. It has been found that in these supply modes the torque capability of a five-phase PM BLDC drive decreases of about 20% and 30% respectively, compared to the standard supply. Therefore, it does not appear convenient to use these supply modes in healthy five-phase motor. However, their study has represented a preliminary analysis of the drive behavior in faulty conditions, i.e. when one or more motor phases are out-of-service.

Chapter 7 deals with the commutation behavior of a five-phase PM BLDC drives with square-wave current supply of the motor phases. Current behavior during phase commutations has been analyzed for low- and high-speed operation by keeping regulated the current of two non-commutating phase, one situated on the same side of the phase of the incoming current and the other one in the opposite side. This basically entails that the current behavior reproduces that one in a three-phase PM BLDC drive. Resulting expressions, however, are quite divergent from the three-phase case for both the current excursion of the non-commutating phase and the length of the commutation interval because of the different space shift of the motor phases. From the current behavior during the phase commutation, the effective torque developed and the torque ripple exhibited by the five-phase PM BLDC drives have been found.

Chapter 8 proposes an algebraic approach to determine the current supply in an automatic way for a 5-phase PM BLDC drive in faulty conditions. At first, an algebraic approach has been developed to formulate a matricial model of the drive in healthy conditions. Afterwards, constrains on the model have been posed to extend its application to the case of one or more phases open because of a fault in a phase either of the motor or of the VSI supplying the motor. With the help of the constrained model, scheduling and magnitude of the current supply for a faulty drive are obtained. The analysis reveals that during the single open phase fault the drive can deliver two third of its rated power. The same criteria have been applied to determine the supply current sequences when two or three phases are faulty. It has been demonstrated that, with the proposed current sequence, the power that can be extracted from the drive as well as the torque waveform change depending not only on the number of faulty (open) phases, but also on their relative location. In particular, it has been shown that, with

two open phases the drive can deliver 40% and 50% of its rated power depending on whether the two open phases are adjacent or non-adjacent, respectively. Furthermore, in the former case the output torque exhibits a ripple, while in the latter case is ripple-free. As regards the faulty scenario with three open phases, it has been demonstrated that the drive can deliver 20% or 34.7% of its rated power depending on whether the open phases are adjacent or not, respectively. For both adjacent and non-adjacent open phases, a ripple arises in the output torque.

A review on dependability features are reported in Appendix.

Chapter 2

Power Electronic Systems for Electric Vehicles/Aircrafts

2.1 Introduction

Global transportation requirements are growing with the increase in standard of living and population. Today it is postulated that the air traffic market growth is estimated at a rate of 5% per year till 2020 [3–4]. In this regard, the aerospace industry is going to face both economic and environmental issues [5]. An increased demand of electrical energy for the aircraft led engineers to put a greater emphasis on the use of technologies toward innovative architecture (design, operation and maintenance) in order to save system mass. This can also influence both the overall cost and the fuel burn. In addition to the aerodynamic structural layout and the engine optimization, the advancements in the electrical equipment systems will also play a major role in reducing operating costs, especially by making minimum maintenance and maximum availability of the aircraft. For many years, electrical power for aerospace applications has been generated using a variable ratio gearbox-mounted wound-field synchronous machine to obtain a three-phase 115 V AC system at a constant frequency of 400 Hz. However, operating experiences under the new requirements of lower cost, increased reliability, easier maintenance and higher operating speed have shown that a replacement for the gearbox using power electronics has obvious advantages. It consequently becomes necessary to employ power converters not only to convert electrical power from one form to another, but also to convert the generated electricity to higher or lower voltage levels [6–7]. Besides, the prime initiatory aspect for the development of the electrical systems and power electronic components and systems is to enhance the reliability, power density, fault-tolerance, and performance to build the concept of *More Electric Aircraft (MEA)* a reality.

In order to control the electrical power levels (needed to supply different aircraft loads), power electronic converters are required [8]. With the advent of second and third generation semiconductor devices made the things easier in molding the electrical energy in desired form (AC or DC). Continued improvements in the power electronic circuitry, magnetic materials, capacitors, motor structures and integrated control components are expected to reform size, weight and reliability issues of ‘more electric’ technology (MET) applications in aerospace systems [9]. A key premise of MET is to replace the traditional auxiliary devices and bleed air extraction equipment with integral engine starter/generator(S/Gs), electrical energized actuators and engine-gear box driven fuel pumps. The replacement eliminates the hydraulic, pneumatic and mechanical power devices which minimizes and/or eliminates their associated costs as well as maintenance.

Merits:

- Improved System Efficiency
- Reduced Size and weight
- Flexibility
- Load sharing

Challenges:

- Losses
- Reliability
- Fault-tolerant
- System integration

2.2 Aircraft philosophy towards more electric

The emerging technological improvement in structural design, aerodynamics, and power electronics changed the usage of energy platform in an aircraft. Aircraft uses a combination of different energy systems rely on secondary power types such as mechanical, pneumatic, hydraulic, and electrical sources. In a conventional civil aircraft, the fuel driven engine serves as a primary source for the propulsion of aircraft and a part of its energy is transformed into different forms for feeding non-propulsive loads inside the aircraft. A brief description of extraction and utilization of secondary power types in aircraft are as follows.

- ***Mechanical power*** is produced by the main engine shaft and is extracted via gearbox to drive the loads such as electrical generator, compressors, fuel and oil pumps local to engine, hydraulic pumps.
- ***Electrical power*** is obtained from the main generator to feed the avionics (inside the cockpit), lightening loads, galleys and various commercial loads such as entertainment systems.
- ***Hydraulic power*** is provided by the central hydraulic pump to the entire aircraft subsystems such as flight control actuation systems, landing gear, doors, steering, engine actuation, and other ancillary systems.
- ***Pneumatic power*** is obtained by the high pressure compressors that are coupled to the main engine. It serves in driving the environmental control systems (ECS), wing anti-ice, cabin pressurization, flaps, doors, windows, engine startup systems.

The combination of all the above systems is becoming more complicated and reduces the whole system efficiency, accuracy, interface, and safety. Hydraulic and Pneumatic systems have high power density but it occupies more on-board space and weight. These systems are not fault-resistant or fault-tolerant, malfunctioning/leakage in the system turns

to outage of every linked sub-system resulting in grounding the aircraft and flight delays. Generally such leakages are difficult to locate and cannot be accessed easily even after locating.

Electrical systems serve as a feasible solution for the non-propulsive power needs of the aircraft. The interpretation of 'all electric' aircraft is not a new concept, it was considered in mid 1950s for the design of electrical aircrafts like Bristol Brabazon and Vickers Valiant V-Bomber. The trend was not continued due to the lack of advancements in the electrical power generation capabilities, power conditioning equipment, advanced control systems, power electronic components.

Since the early 1990s, the research advancements in transportation system changed the aircraft architecture. The research revealed that the replacing or eliminating centralized hydraulic and pneumatic systems with electrical power gives more benefits listed below.

- Saving aircraft on-board space and weight
- Efficient and reliable system operation
- Less maintenance
- Reduced cost
- Economical fuel consumption with less emission of CO_2 into atmosphere

All the above aspects comes true due to the development that took place in the field of power electronic systems, fault-tolerant electrical machines, electro-mechanical and electro-hydraulic actuators, fault-tolerant electrical power systems, etc. The research renovation of the electrical power as a secondary source in aircraft fulfilled the needs of commercial and civil transportation by *more electric aircrafts (MEA).*

2.3 On-board aircraft power generation

The evolution of electrical power in the aircraft was grown up in a step by step manner since early 1950s. The MEA concept introduces new techniques in extraction and utilization of the electrical energy. Earlier days the electric power system was twin 28 V DC system, which suits for the twin generator system. Later in 1960s power generation at constant frequency seems less reliable. As a matter of fact, generation of 115 V AC at 400 Hz forced the requirement of a constant speed drive (CSD) for the wide speed variation of the aircraft engine. Even though the CSD system is abided by the constraints like huge on-board space, poor efficiency (due to the hydro-mechanical gear system) and less reliability, it is carried for a long time in most of the commercial and civil aircrafts as shown in *Figure 2.1*.

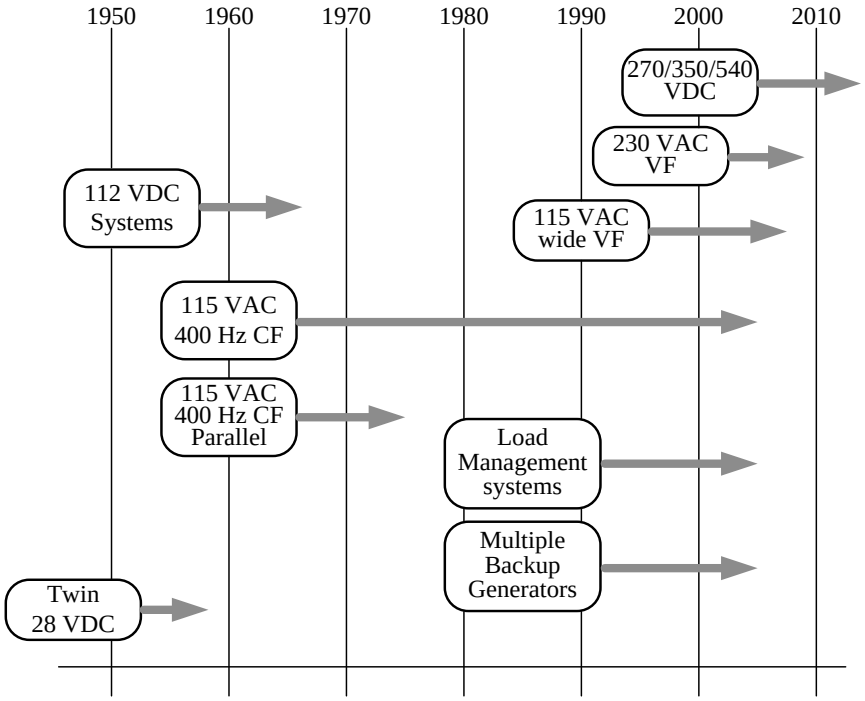

Fig. 2.1. Aircraft electrical power evolution.

Most of the traditional methodologies like fixed frequency power generation using gear mechanism followed by integrated generator system are modernized with the advent of high power converters in handling the variable frequency AC power. From [10] the layout reveals the major blocks of conventional and MEA power distribution as shown in *Figures 2.2 and 2.3*.

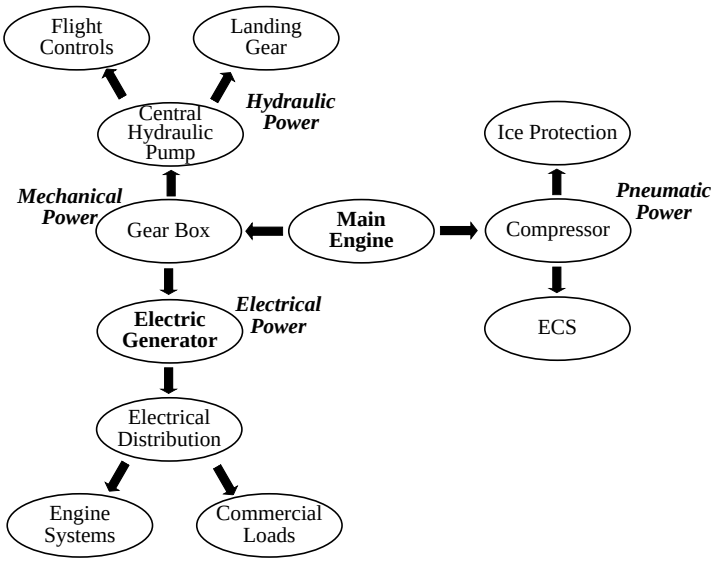

Fig. 2.2. Layout of conventional power distribution.

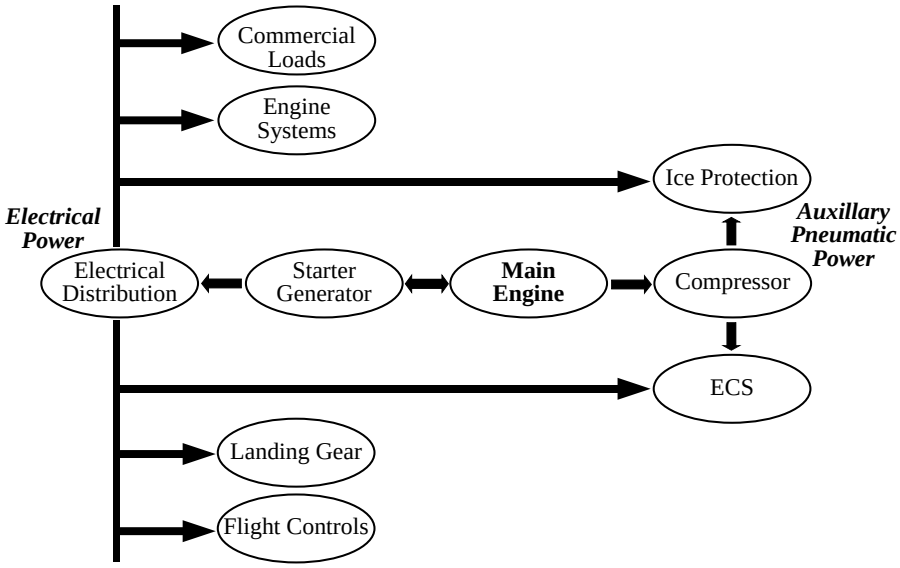

Fig. 2.3. Layout of MEA power distribution.

The advanced power electronic system came up with a Variable Speed Constant Frequency (VSCF) system, which is being carried out in the recent decades for on-board power generation. VSCF system uses a power electronic converter in converting the Variable Frequency (VF) generated electrical power into a fixed desired frequency. It not only eliminates the cumbersome gear system but also improves the system efficiency, reliability, fault-tolerant capability, efficiency, wastage of fuel. Further development in the machine design turned to generate VF AC supply.

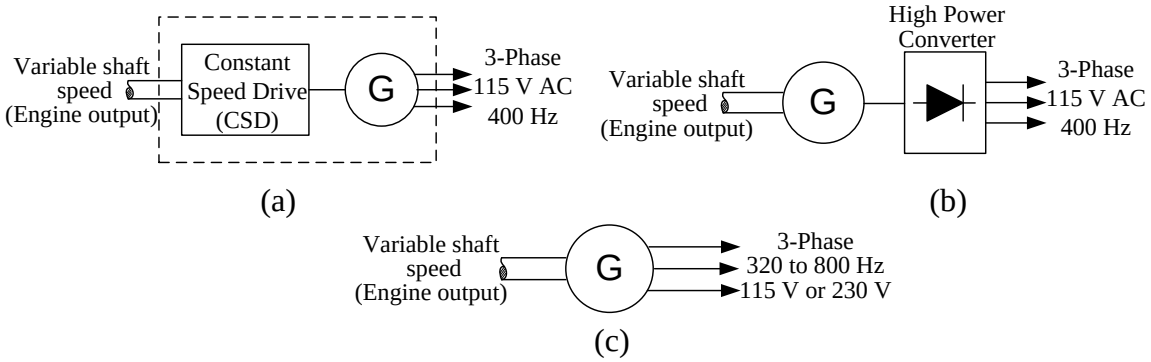

Fig. 2.4. Aircraft electric power generation with [11] (a) Constant frequency, (b) Variable speed constant frequency, (c) Variable frequency.

The More electric aircraft trend taken place from fixed to variable frequency electrical power generation as shown in *Figure 2.4*, is briefly described in short as follows:

1. *Constant frequency (CF)* is a sustained methodology of power generation since past decades. It requires hydro-mechanical gear system that drives the generator (at constant speed) under variable speed main engine as shown in *Figure 2.4a*. Its

cumbersome structure, control, and size forced to pay more in terms of overall cost, reduced efficiency, and increased risk factor.

2. *Variable speed constant frequency (VSCF)* systems came into picture with advanced power electronic converters. The use of Constant speed drive (CSD) is replaced with the high power electronic converters which are more reliable, compact, efficient and fault-tolerant. The requirement of both AC power and DC power in aircraft gave an opportunity for the designers to go for the efficient and reliable method.

    a. *DC link*: In this system the generated AC power with slight variation in the frequency (f ±Δf) is converted into DC power with the help of high power rectifiers/bi-directional converters. Which is mostly used for military applications.

    b. *AC link*: A Cycloconverter or an advanced matrix converter plays a major role in converting the variable frequency generator output AC power into AC power with fixed frequency and amplitude.

3. *Variable frequency (VF)* system is a new trend which needs lot more care in handling the high power converters for VF applications. The cost effectiveness of this system is analyzed based on the motor controllers required in handling the variable frequency. The prominent features of VF system are small size, volume, compact, and efficient in feeding galley loads.

MEA uses an electric generator to generate variable frequency AC supply. This electric generator is coupled with main engine shaft which is rotating at a variable speed. This arrangement reduces the on-board weight and space with increased efficiency and reliability of the aircraft. Further, generated power is converted into fixed frequency AC using static power electronic converters offering better flexibility and improved controllability of the AC

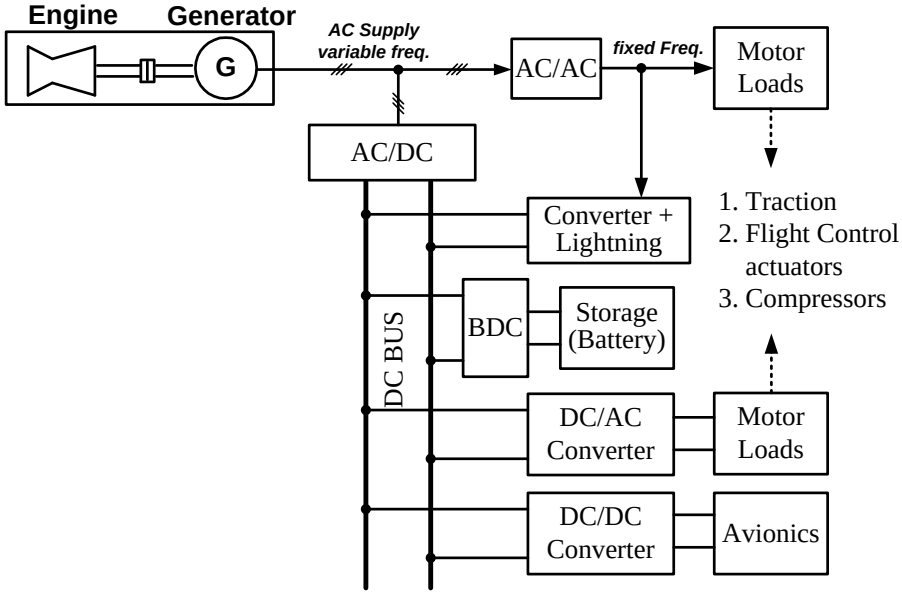

Fig. 2.5. Schematic diagram of basic aircraft loads.

bus. MEA uses both AC and DC bus power distribution network as per the different requirements of the load. Schematic of the possible applications connected with the bus are shown in *Figure 2.5*.

2.4 Electric energy conversion

Applications associated under this category are

- Variable frequency AC to fixed frequency AC conversion.
- AC/DC conversion to form DC bus
- DC/DC conversion for avionics and storage of energy in on board batteries.
- DC/AC for motor loads

2.4.1 Variable frequency AC to fixed frequency AC

The power distribution in MEA uses both AC and DC supply. From *Figure 2.5* it is clear that the aircraft consists of different loads and it is not possible to generate different voltages of AC or DC power directly from the generator. In this situation a static power electronic converter play a major role in obtaining the fixed frequency (400Hz) AC supply by eliminating the tedious gearbox mechanism. In precise, a Matrix converters (or) a Cycloconverters (or) AC/DC/AC converters are used in achieving the fixed frequency (400 Hz) 230 V/115 VAC supply. Appliances like motor drives, lightning loads, galley loads are connected to the AC bus.

2.4.2 AC/DC conversion to form DC bus

The generated AC power is converted to DC and is transmitted over the flight body, as it reduces wiring losses, skin effect, etc. It is necessary to have an AC to DC converter to form a 270V DC bus, where all the emergency/important DC loads are connected.

2.4.3 DC/DC conversion for storage and avionics

The aircraft consists of many electronic circuits, computers, commercial, and entertainment applications which need various voltage levels of DC supply. The 270V DC bus is further converter to various voltage levels to feed the appliances like avionics, DC motors, and ultra-capacitors/batteries, etc.

2.4.4 DC/AC conversion for motor load

The DC to AC converters plays a vital role in feeding the ac loads from the DC bus. Such types of loads play a vital role in flying of the aircraft. For example, in case of engine failure the flight control actuators remain idle due to AC bus failure. As the DC bus consists of a storage system in terms of battery/ultra-capacitors, few important loads like avionics, flight control actuators, fuel pumps, etc. are feed with the help of DC to AC converter for proper function even under engine failure conditions.

2.5 Electro-mechanical energy conversion

This category of energy conversion includes different types of electric drive [12] applications dedicated for

- Flight control actuators
- Compressors for fuel-pump, cabin air pressurization and air conditioning

2.5.1 Flight Control Actuators

An aircraft wings consists of different control surfaces (flaps, slats, spoilers, rudder, elevators) in order to elevate, tilt, and landing purpose. Earlier aircraft uses two hydraulic motors, which are mechanically summed via a shaft running over the wing span. The relative displacement of the flaps on both wings is monitored to maintain symmetry, which is more important in balancing the flight. A failure in a single flap cause the whole flap system failure which leads to the loss of flight control and also cause a structure failure.

An individual electrical drive for every single flap is a good choice in replacing centralized the hydraulic-motor control. As the flaps are several meters long [55], a dedicated motor drive is a best choice in order to move both the ends of the flap simultaneously. An example prototype for flap control is shown in *Figure 2.6*. The flap is driven by a modular fault-tolerant drive, with overall system control undertaken by a flap control computer. The drive is operated with position control using speed, torque, and position loops. The angle of the

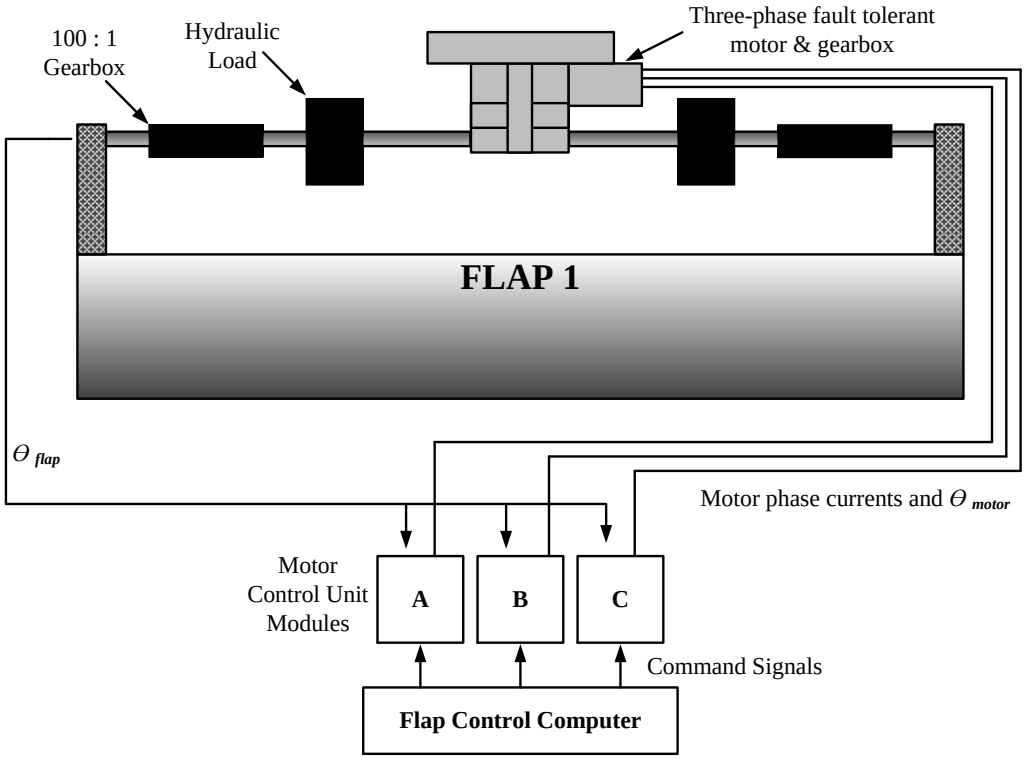

Fig. 2.6. Layout of flap drive [55].

flap is continuously monitored with the help of sensors to locate the position and a feedback signals are feed to the drive modules (A, B, C in *Figure 2.6*).

2.5.2 Compressors for fuel-pump, cabin air pressurization and air conditioning

The new trend compressors are driven using electrical drives for serving the aircraft needs like heating, ventilation, and air conditioning. The power levels of these electrical driven compressors starts from 100 W to a few kilowatts. There several compressors with their respective merits and applications in heating, ventilation and air conditioning (HVAC) or air pressurization for aircraft cabins. The turbo compressor shown in *Figure 2.7* has both size and efficiency advantages over other compressor types, such as scroll, lobe or screw compressors. These systems ideally have rotational speeds between 100000 and 1 000 000 r/min at power levels of 100 W up to several kilowatts. A miniature two-stage electrically driven turbo-compressor system with a rated rotational speed of 500 000 r/min is explained in [13]. It serves as a cabin air pressurization system for solar impulse plains but the specifications also suits to the other aircraft applications.

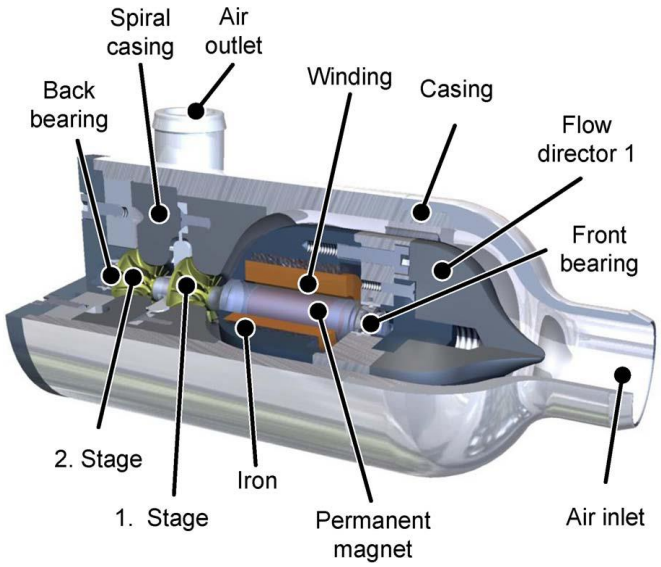

Fig. 2.7. Cross-sectional view of the integrated two-stage electrically driven turbo-compressor system.

2.6 Selection of electric drives

From the schematic structure of the aircraft shown in *Figure 2.5*, a starter/generator is associated to each engine to start the turbine engine and provide primary electrical power, an integrated power unit with an integral starter/generator to provide emergency, auxiliary and main engine start power. Mostly the generated power is distributed in DC bus with the help of power electronics systems that plays a major role in power conversion from one level to other level with AC to DC and vice-versa. The primary loads include a conventional avionics system, all electric flight control system, electrically driven environmental control system, electric fuel management and delivery system, electrically driven pneumatic system

for pulsed actuators, electrically driven landing system (i.e., landing gear actuation, nose wheel steering, etc.) and other miscellaneous subsystem (i.e., lighting, heaters, fire protection, etc.). *Table 2.6.1* identifies the type and numbers of motor drives systems necessary to support a generic MEA [14–15].

From *Table 2.6.1* it is proved that, MEA requires around 86 number of drives to perform various operations at different locations and weather conditions. For example, ECS requires a total power of 40 kW for 10 motor drives while the largest one is 10 kW among them (i.e the remaining motors constitute 30 kW). So, on an average the remaining motors are of less than 3.5 - 5 kW range. In a similar manner, other than largest drive the flight controls, fuel system, landing systems, and other miscellaneous motors comes under this category.

Tab. 2.6.1 Requirement of electrical drives in MEA.

System description	Continuous max. total power (kW)	No. of motor drives	Largest motor drive (kW)
Flight controls	80	28	50
Environmental control systems (ECS)	40	10	10
Fuel pump system	35	10	9
Pneumatic system	30	2	15
Lading System	30	20	5
Misc. other	20	10	1
Engine starter/ generator system	125 per channel	6	125
Total no. of power contributing units	-	86	-

But the duty of operation varies as per their work location. For example, the motor drives the flight control actuators for a small time when it is necessary to take off, change the direction, and landing. The motor drive must have high torque at low speeds to drive the actuator and also must be fault tolerant. So, the selection of motor drive [15], [56] plays a vital role at its particular location as per their operational characteristics in attaining the required/desired performance, which are listed in *Table 2.6.2.*

Tab. 2.6.2 Performance comparison of motor technologies.

Performance	Induction motor	Switched reluctance motor	Permanent magnet motor
Fault tolerant	Low	High	High
Power density	Moderate	Moderate	High
Robustness	√	√	×
Efficiency	Moderate	High	High
Cost	Low	Low	High
Wide speed range	×	√	√
Open-loop control	√	×	×
Close-loop simplicity	√	√	√
Torque ripple	×	High	Low
Acoustic noise	×	Moderate	Low
Areas of application	Actuators	High-temp. engine	Flight control actuators

Permanent Magnet (PM) motors can be of brushless AC type (synchronous motor) and brushless DC type, fed with sinusoidal and rectangular (or trapezoidal) currents, respectively. PM motors are characterized with high power density, efficiency, reliability and also capability with modular approach to achieve electrical, magnetic, thermal, and physical isolation among the phases with simple controls techniques. Thereafter, hereafter more focus is given to the PMBL drives characterized by trapezoidal phase back-emfs and commonly termed as PM BLDC drives and its fault tolerant capabilities which are discussed in details with respective strategies.

2.7 Conclusion

This chapter reveals the structure of power generation and demand in an aircraft since beginning. With the advancements in the power electronics systems, electrical systems (drives) replaces the hydraulic and the pneumatic systems, which in turn made a huge impact to avionic industry and as well as to the environment (reduced weight leads to consumption of less fuel). The power generation and distribution schematic shows the requirement of power electronics systems for various loads of different power ratting. It also elaborated in this chapter that the necessity of electrical drives for different purposes, based on the performance characteristics of that particular drive.

Chapter 3

Three Phase Permanent Magnet (PM) Brushless (BL) DC Drive

3.1 Introduction

Flexibility in control, reliability and ease of maintenance are the main reasons in favor of the adoption of electric drives in the motion equipment from household to transportation and aviation applications, for powers ranging from fraction of kW to hundreds of kW. Majority of the drives used in household and industrial applications are induction motor drives whereas for light and mid-duty propulsion apparatuses are served by permanent magnet (PM) brushless (BL) drives due to the comparatively much higher power density and torque per ampere [16–18].

A three-phase PM BLDC drive consists of a motor with permanent magnets on the rotor and three phase star connected concentrated windings with neutral point *n* on the stator and a three-phase voltage source inverter (VSI) supplying the motor. *Figure 3.1* shows the schematic diagram of a three-phase PM BLDC drive, where V_{dc} and i_{dc} are the dc source voltage and current. T_1-D_1, …., T_6-D_6 are the transistors and its associated anti-parallel diodes, and v_{jo} with j=*a, b, c* are the inverter voltages referred to the negative pole *o* of the dc source.

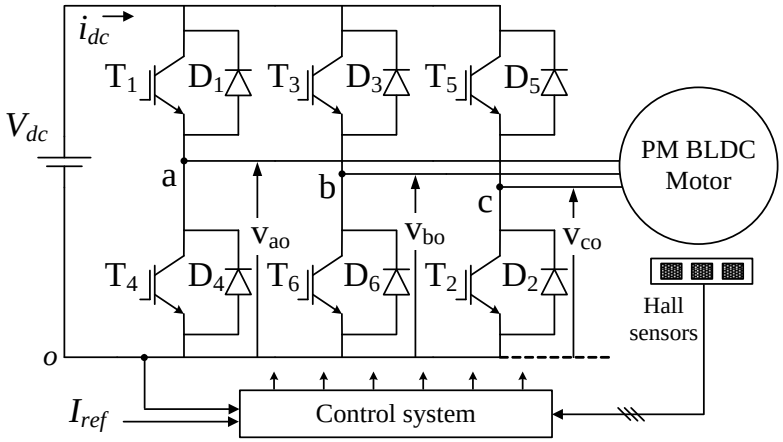

Fig. 3.1. Schematic diagram of three-phase PM BLDC motor drive.

3.2 Operation and equations

As shown in *Figure 3.1*, a three-phase PM BLDC drive is composed of a PMBL motor with trapezoidal phase back-emfs, a voltage source inverter (VSI) supplying the motor feeding energy from DC voltage source connected to dc-link, and a control system governing

the motor-VSI operation. Specifically, the control system commands the VSI switches to inject square-wave phase currents that are synchronized with the flat-top potion of the back-emfs as per the information of rotor position through three Hall sensors mounted on the stator. Magnitude of the phase currents is regulated as per the required torque. With the help of hall information and dc-link current sensor dc-link current control can be realized. It is also possible to implement phase current control through current sensors for phase currents and estimated continuous rotor position from the hall sensor information. Phase back-emfs and currents are traced in *Figure 3.2*, where θ_e is the rotor position in electrical radians, E and I are the magnitudes of the phase back-emfs and phase currents. Commutation phenomena are disregarded at this moment in tracing the currents so that square waveforms are taken for them.

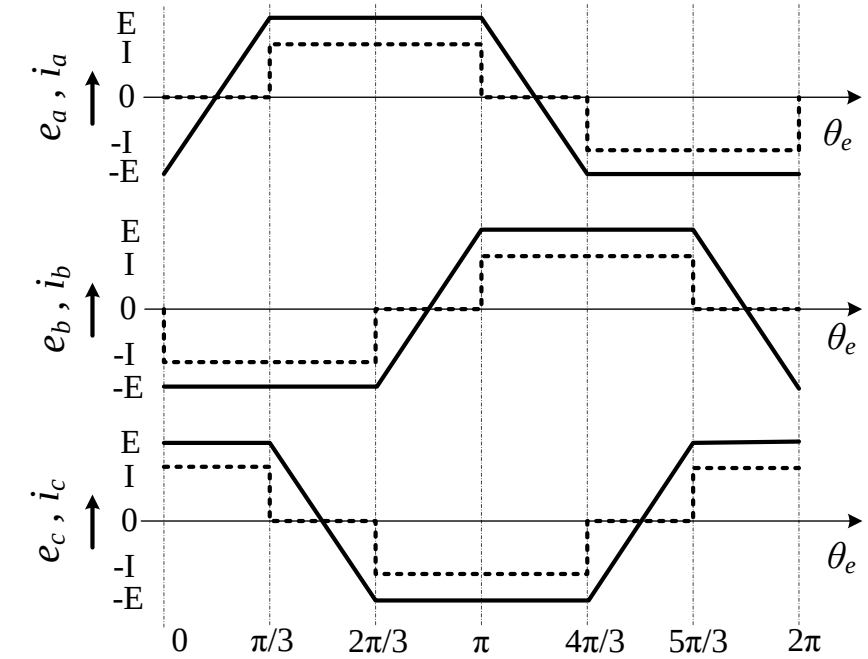

Intervals conducting transistors	S1	S2	S3	S4	S5	S6
	T_5-T_6	T_6-T_1	T_1-T_2	T_2-T_3	T_3-T_4	T_4-T_5

Fig. 3.2. Back-emfs (bold line), phase currents (dashed line), and supply intervals of three -phase PM BLDC motor drive.

The current reference I_{ref} is compared with the feedback current i_{dc} coming from the dc-link before being manipulated by the PI regulator. The latter one outputs the dutycycle δ for chopping one of the two conducting transistors. In the study, I_{ref} is set at the nominal current magnitude I_N and the current regulator is assumed to deliver the maximum effort in presence of a small current error. During out of commutation

$$V_{dc} = 2E + 2RI \tag{3.2.1}$$

where V_{dc} becomes δV_{dc}. The electrical power p converted into mechanical form is given by

$$p = \sum_{j=a,b,c} e_j i_j \tag{3.2.2}$$

where electrical power p is constant over the supply period and equal to $2EI$. By assuming here and henceforth that the motor rotates at a constant speed Ω, the torque τ developed by the drive is also constant and expressed as

$$\tau = p / \Omega \tag{3.2.3}$$

For the normal operation of the drive with the ideal square-wave current supply shown in *Figure 3.2*, the average torque developed by the motor becomes

$$T = 2kI_N \tag{3.2.4}$$

where I_N and k are nominal phase current square-wave magnitude and motor constant respectively.

3.3 Commutation

PM BLDC motors should be fed by square-wave phase currents for the production of flat and ripple free torque. However in practice due to phase inductance and limited supply voltage, phase currents deviate from their ideal square-wave shape. This results in reducing the average torque and increases the torque ripple with increase in motor speed. The same concept has been described by R. Carlson et. al [19] about the phase current commutation due to the inductance effect and enhanced DC link current sensing technique to analyze the overall behavior. The machine model adopted in this study has a Y-connection with a neutral point n and is represented by its equivalent circuit as shown in *Figure 3.3*.

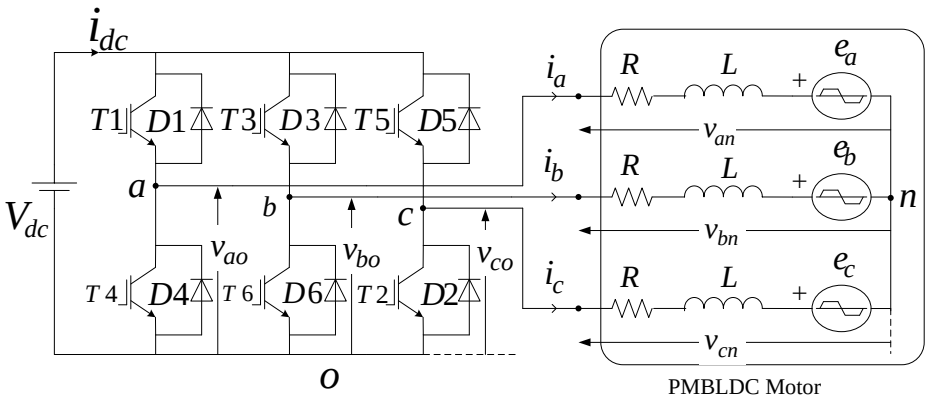

Fig. 3.3. Equivalent circuit representation of a three phase PM BLDC drive.

A new transistor conducts for every π/3 electrical radians and continues to operate for 2π/3 electrical radians. *Figure 3.2* shows the trapezoidal back-emfs and ideal current of square wave as a function of the angular phase θ_e in electrical radians. The trapezoidal waveform of the back emfs has a flat-top magnitude E given by

$$E = k\Omega \tag{3.3.1}$$

Where k and Ω are the motor constant and mechanical speed. With respect to the equivalent circuit arrangements shown in *Figure 3.3,* circuit variables are expressed as

$$\left.\begin{aligned} v_{jn} &= Ri_j + L\frac{di_j}{dt} + e_j \\ v_{jn} &= v_{jo} - v_{no}; \quad \sum_{j=a,b,c} i_j = 0 \\ v_{no} &= \frac{1}{3}\sum_{j=a,b,c}\left(v_{jo} - e_j\right) \end{aligned}\right\} \tag{3.3.2}$$

where $j = a, b$ and c. V_{jn} is phase to neutral point voltage; i_j is phase current; e_j is phase back-emf and v_{no} is the neutral point voltage. Term 'o' corresponds to the negative terminal of the battery and the reference point for the measurement of voltages. R is the phase resistance and L is the phase inductance including the effect of mutual inductance. As the phase resistances are very small, therefore it is neglected in further analysis.

3.3.1 Phase Current behavior

Operation of BLDC motor drive (*Figure 3.2*) is divided into six supply intervals where current commutation takes place in changing from one supply interval to the other. As discussed in *Section 3.2*, the nature of commutation is similar for all the supply intervals of six switch VSI fed three-phase BLDC drive. As a template, the commutation at $\theta_e = \pi/3$ is examined. At this position, transistor T1 is turned ON to allow the incoming current i_a to reach the required value I, T5 is turned OFF to force the outgoing current i_c to vanish by circulating through freewheeling diode D2 and T6 is kept ON. Both the incoming and outgoing transients take time to be completed.

Therefore, from (3.3.2) variation in phase currents i_a, i_b, and i_c with respect to θ_e is expressed as

$$\left.\begin{aligned} \frac{di_a}{d\theta_e} &= \frac{2\left(V_{dc} - E\right)}{3n_p\Omega L} \\ \frac{di_b}{d\theta_e} &= -\frac{\left(V_{dc} - 4E\right)}{3n_p\Omega L} \\ \frac{di_c}{d\theta_e} &= -\frac{\left(V_{dc} + 2E\right)}{3n_p\Omega L} \end{aligned}\right\} \tag{3.3.1.1}$$

Where n_p is the number of pole pairs and Ω is the motor mechanical speed. For small values of θ_e, e_c can be approximated to its flat-top value E.

Let I_N, V_{dc} and Ω_N be the nominal current, terminal voltage and nominal motor speed respectively. From (3.3.1.1) can be solved by considering the initial conditions of the phase currents and expressed as follows

$$\left.\begin{aligned} i_a &= \frac{2(V_{dc}-E)}{3n_p\Omega L}\theta_e \\ i_b &= -I - \frac{(V_{dc}-4E)}{3n_p\Omega L}\theta_e \\ i_c &= -I - \frac{(V_{dc}+2E)}{3n_p\Omega L}\theta_e \end{aligned}\right\} \qquad (3.3.1.2)$$

Once the switch *T5* is turned OFF and *T1* is turned ON, keeping *T6* ON, incoming current i_a starts rising through *T1* and *T6*. At the same time outgoing current i_c freewheels through *T6* and body diode *D2* until it extinguishes. Three states of the inverter before, during and after the end of commutation are shown in *Figures 4.2.3a, 4.2.3b and 4.2.3c* respectively.

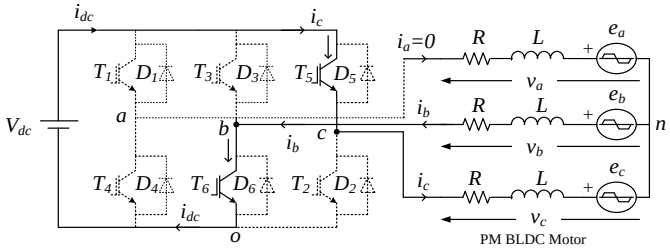

(a)

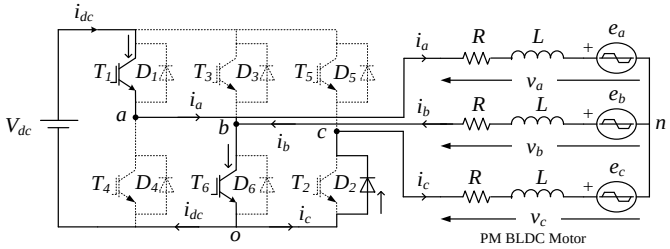

(b)

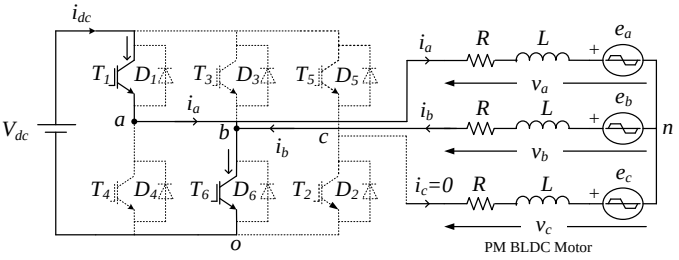

(c)

Fig. 3.3.1. Phase currents a) before; b) during and c) after the commutation $\theta_e=\pi/3$.

Depending upon the rate of rise or fall of the commutating currents, which in turn is a function of speed, either of commutating current can reach to their final value earlier or simultaneously. The three possible cases are: a) incoming current i_a reaches to final value *I* before the outgoing current i_c vanishes (*Figure 3.3.1a*); b) i_a reaches to final value after

outgoing current i_c vanishes (*Figure 3.3.1b*) and c) both the incoming current i_a and outgoing current i_c reaches to their final value at the same instant (*Figure 3.3.1c*).

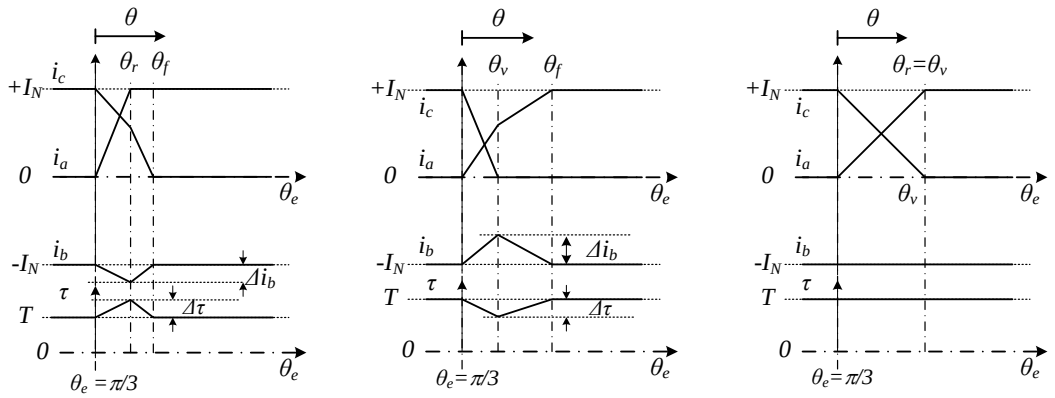

(a) (b) (c)

Fig. 3.3.2. Phase commutations with: a) $\theta_r < \theta_v$; b) $\theta_r > \theta_v$; and c) $\theta_r = \theta_v$.

Therefore from (3.3.1.2) rise interval θ_r of i_a and vanishing interval θ_v of i_c are given by

$$\left.\begin{aligned}\theta_r &= \frac{3n_p\Omega L}{2(V_{dc}-E)}I\\ \theta_v &= \frac{3n_p\Omega L}{(V_{dc}+2E)}I\end{aligned}\right\} \qquad (3.3.1.3)$$

Expressions for θ_r and θ_v are not valid at the same time. θ_r is less than θ_v in the speed zone $\Omega < \Omega_N/2$ (low-speed zone) whilst θ_r is greater than θ_v in the speed zone $\Omega > \Omega_N/2$ (high-speed zone). It is clear that the commutation interval consists of two parts: in the first part both the commutating currents are subjected to transients toward their final values whilst in the second part only one of them is subjected to the transients. The angular interval taken by the slowest commutating current to reach its final value is denoted by θ_f and represents the (total) commutation interval.

In the case of $\theta_r < \theta_v$, behavior of i_c can be explained the help of KVL equation for its freewheeling path written as

$$-2L\frac{di_c}{dt} = e_c - e_b - L\frac{di_a}{dt} = 2E - L\frac{di_a}{dt} \qquad (3.3.1.4)$$

Once i_a reaches to its final value, it is modulated to maintain the desired value. Thus second term in (3.3.1.4) vanishes after θ_r and increase in slope of i_c takes place.

Along the commutation interval, current i_b undergoes a fluctuation due to unbalanced behavior of the commutating currents. The fluctuation is superimposed to the constant amplitude of $-I_N$ and attains its maximum magnitude at the angle where the quicker of the commutating currents reaches its final value.

In terms of voltage quantities, the low-speed zone is encountered when $V > 4E$ and the high-speed zone when $V < 4E$. The speed $\Omega_N/2$ separates the two zones. For this speed value, θ_r is equal to θ_v, no unbalance occurs in the commutating currents and i_b does not undergo any fluctuation. The transients of both the commutating currents and the non-commutating current in the two speed zones are exemplified in *Figure 3.3.2*. The traces clearly show the different behavior of the currents in the two speed zones. Therefore it is convenient to study separately in each speed zone the torque characteristics ensuing from the behavior of the commutating currents.

3.3.2 Torque behavior during commutation

The general torque expression of torque was given in (3.2.3), and the torque between commutations is given by

$$\tau = \frac{2EI}{\Omega} \tag{3.3.2.1}$$

The instantaneous torque developed by the drive, obtained by applying (3.2.2), (3.2.3) and the first Kirchhoff's principle to the neutral point, is given by

$$\tau(\theta_e) = -2k\, i_b(\theta_e); \qquad \forall\, \theta_e \in \left(\frac{\pi}{3}, \frac{2\pi}{3}\right) \tag{3.3.2.2}$$

Equation (3.3.2.2) shows that the torque is equal to the opposite of non-commutating negative current. Similar torque equations can be derived for the other supply intervals and in the two speed zones as shown in *Figure 3.3.2*. The torque in two speed zones is exemplified as follows:

By the end of first part of the commutation interval (i.e. θ_r or θ_v from *Figure 3.5*), the non-commutating phase current i_b deviates to its maximum value from its nominal value, which is also termed as ripple. If Δi_b is the ripple in the non-commutating current, the phase current i_b can be expressed as

$$i_b(\theta_e) = -I + \Delta i_b(\theta_e) \tag{3.3.2.3}$$

During the commutation interval, the non-commutating negative phase current i_b undergoes a deviation Δi_b from the steady-state value of $-I_N$. It can be realized as follows

$$\Delta i_b = I - i_a - i_c \tag{3.3.2.4}$$

Equation (3.3.2.4) attains its maximum magnitude at the end of the first subinterval of commutation. Then the effective torque, given by the average value of the instantaneous torque over the supply period (that coincides with the average value over the supply interval), is given by

$$T = 2kI - \frac{3}{\pi}\int_0^{\theta_f} \Delta i_b(\theta_e)\, d\theta_e \tag{3.3.2.5}$$

Because of the triangular behavior of i_b during the commutation interval, (3.3.2.5) can be rewritten as follows

$$T = 2kI - \frac{3k\theta_f}{\pi}\Delta i_b(\theta_m) \tag{3.3.2.6}$$

From (3.3.2.2) torque ripple is defined as the peak-to-peak excursion and is equal to the magnitude of current excursion.

$$\Delta T = 2k\left|\Delta i_b(\theta_m)\right| \tag{3.3.2.7}$$

where θ_m is equal to θ_r for low speed zone (i.e. $\Omega<\Omega_N/2$) and to θ_v for high speed zone (i.e. $\Omega>\Omega_N/2$).

3.3.2.1 Torque characteristics for $\Omega<\Omega_N/2$

In the low-speed zone, i_a reaches the reference value I_N before i_c vanishes. The rising interval θ_r of i_a is given by the first of (3.3.1.3); its maximum value is θ_m and is taken for $\Omega=\Omega_N/2$. This proves that the approximation $e_c \cong E$ is well grounded for $\theta_e<\theta_r$. The amplitude of i_c at θ_r is

$$i_c(\theta_r) = I\,\frac{V_{dc} - 4E}{2(V_{dc} - E)} \tag{3.3.2.8}$$

Along θ_r, the current regulator keeps T_1 ON until the current reaches I_N and when i_{dc} is equal to i_a for $\theta_e>\theta_r$, T_1 is chopped to maintain constant I_N. Taking into account that i) the feedback current is i_{dc} and ii) i_{dc} coincides with i_a when T_1 is ON, the control scheme must operate in a discrete way and sample i_{dc} during the ON time of T_1 to regulate (i_a) at I. Due to the chopping of T_1, VSI is no more applied with the source voltage V_{dc} across the motor phases but δV_{dc}. Then the term V_{dc} in (3.3.1.1) must be substituted for by δV_{dc}. For the second part of commutation rate of variation of i_c is given by

$$-2L\frac{di_c}{dt} = 2E; \quad \forall\theta_e \in (\theta_r, \theta_f) \tag{3.3.2.9}$$

By (3.3.2.8) and (3.3.2.9), the expression of i_c in the second part of the commutation interval is

$$i_c(\theta_e) = -\frac{V_{dc} + 2E}{3Ln_p\Omega}(\theta_e - \theta_r) + i_c(\theta_r); \quad \forall\theta_e \in (\theta_r, \theta_f) \tag{3.3.2.10}$$

Phase current i_c vanishes for

$$\theta_f - \theta_r = \frac{3n_p\Omega L(V_{dc} - 4E)}{2(V_{dc} - E)(V_{dc} + 2E)}I \tag{3.3.2.11}$$

By substituting the first equation of (3.3.1.3) in (3.3.2.10), it turns out that the commutation interval is equal to

$$\theta_f = \frac{3n_p \Omega L I}{(V_{dc} + 2E)} \tag{3.3.2.12}$$

From (3.3.2.3), (3.3.2.4) and (3.3.2.8), the amplitude of Δi_b at θ_r is calculated in

$$\Delta i_b(\theta_r) = -I \frac{V_{dc} - 4E}{2(V_{dc} - E)} \tag{3.3.2.13}$$

by substituting (3.3.2.12) and (3.3.2.13) in (3.3.2.6) and (3.3.2.7), the motor torque and the torque ripple are formulated as a function of the speed for a PM BLDC drive operating in the low-speed zone. They are expressed as

$$T = 2kI + \frac{9kn_p \Omega L I^2}{2\pi} \frac{(V_{dc} - 4E)}{(V_{dc} + 2E)(V_{dc} - E)} \tag{3.3.2.14}$$

$$\Delta T = 2kI \frac{V_{dc} - 4E}{2(V_{dc} - E)} \tag{3.3.2.15}$$

(3.3.2.14) shows that the motor torque exceeds the requested value of a quantity that is maximum as the speed approaches zero and reduces as the speed increases, becoming nominal at $\Omega = \Omega_N/2$. Equation (3.3.2.15) shows that the torque ripple has the same profile vs. the speed as the excess of the motor torque. (3.3.2.14) and (3.3.2.15) do not apply at zero speed, i.e. at standstill, where the motor develops a torque exactly equal to its rated value and the torque ripple due to the commutations disappears.

3.3.2.2 Torque characteristics for $\Omega > \Omega_N/2$

In the high-speed zone, i_c vanishes before i_a reaches to I_R. The vanishing interval θ_v of i_c is given by (3.3.1.3). Value of i_a at θ_v is

$$i_a(\theta_v) = I \frac{2(V_{dc} - E)}{(V_{dc} + 2E)} \tag{3.3.2.16}$$

Along θ_v, i_{dc} is equal to i_a. For $\theta_e > \theta_v$, T1 is kept ON since i_a is still less than I, and i_{dc} remains equal to i_a. As phase c is now no more conducting, so rate of variation of i_a can be obtained from the voltage equation for the mesh formed by phase a and phase b.

$$2L \frac{di_a}{dt} = V_{dc} - 2E; \quad \forall \theta_e \in (\theta_v, \theta_f) \tag{3.3.2.17}$$

By (3.3.2.16) and (3.3.2.17), the expression of i_a in the second part of the commutation interval is

$$i_a(\theta_e) = \frac{(V_{dc} - 2E)}{2n_p \Omega L}(\theta_e - \theta_v) + i_a(\theta_v); \quad \forall \theta_e \in (\theta_v, \theta_f) \tag{3.3.2.18}$$

Phase current i_a reaches to I for $\theta_e > \theta_v$

$$\theta_f - \theta_v = -\frac{2n_p \Omega L (V_{dc} - 4E)}{(V_{dc} - 2E)(V_{dc} + 2E)} I \tag{3.3.2.19}$$

Substituting (3.3.1.3) in (3.3.2.19), then the commutation interval becomes

$$\theta_f = \frac{n_p \Omega L I_N}{(V_{dc} - 2E)} \tag{3.3.2.20}$$

To calculate the motor torque and the torque ripple in the high-speed zone it is necessary to determine Δi_b at θ_v. From (3.3.2.3), (3.3.2.4) and (3.3.2.16), we get

$$\Delta i_b(\theta_v) = -I \frac{(V_{dc} - 4E)}{(V_{dc} + 2E)} \tag{3.3.2.21}$$

on substituting (3.3.2.20) and (3.3.2.21) in (3.3.2.6) and (3.3.2.7), we get

$$T = 2kI - \frac{3kn_p \Omega L I^2}{\pi} \frac{(-V_{dc} + 4E)}{(V_{dc} - 2E)(V_{dc} + 2E)} \tag{3.3.2.22}$$

$$\Delta T = 2kI \frac{(-V_{dc} + 4E)}{(V_{dc} + 2E)} \tag{3.3.2.23}$$

Equations (3.3.2.21) and (3.3.2.22) formulate the torque characteristics of a PM BLDC drive in the high-speed zone. (3.3.2.22) reveals that the motor torque drops below the requested value by a quantity ΔT, which is zero for $\Omega = \Omega_N/2$ and increases to a maximum as the speed approaches the no-load speed. (3.3.2.23) explains that the torque ripple has a similar profile vs. the speed as the drop of the motor torque.

3.4 Base speed

Base speed Ω_B is defined as the maximum speed at which the source voltage is able to bring the incoming phase current to the rated value of current I_R, at maximum by the end of every supply interval i.e. at every electrical angular duration of $\pi/3$ the successive current commutation starts. Under this situation, θ_f coincides with $\pi/3$. By equating (3.3.2.20) to $\pi/3$, we get the base speed as follows

$$\frac{n_p \Omega L I_N}{(V_{dc} - 2E)} = \frac{\pi}{3} \tag{3.4.1}$$

3.5 Case study

Tab. 3.5.1 PM BLDC motor data.		
Data	Symbol	Value
Rated motor voltage	V_{dc}	48 V
Rated motor current	I_N	50 A
Rated torque	T_N	32 Nm
Pole pairs	n_p	8
Phase resistance	R	50 mΩ
Inclusive phase inductance	L	75μH
Motor constant	k	0.32 V·s/rad

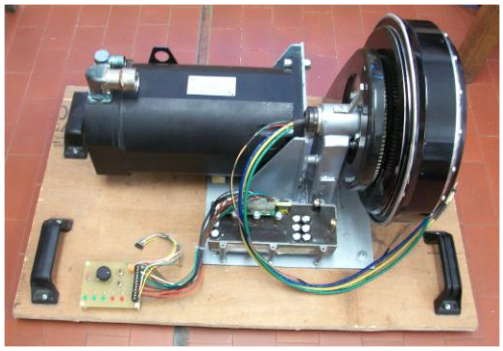

Fig. 3.5.1 In-wheel PM BLDC drive [20].

The study case is meant for the propulsion of light road vehicles as in-wheel surface mounted PM BLDC drive is considered from [20] to exemplify the above findings. The nominal/rated quantities and parameters of the drive those are considered from [20] are listed in *Table 3.5.1*. Calculated values of motor like nominal speed *(Ω_N)*, base speed *(Ω_B)* are 75 rad/s and 71.7 rad/s respectively. Equation (3.3.2.23) proves that the base speed is lower than the nominal speed of the motor.

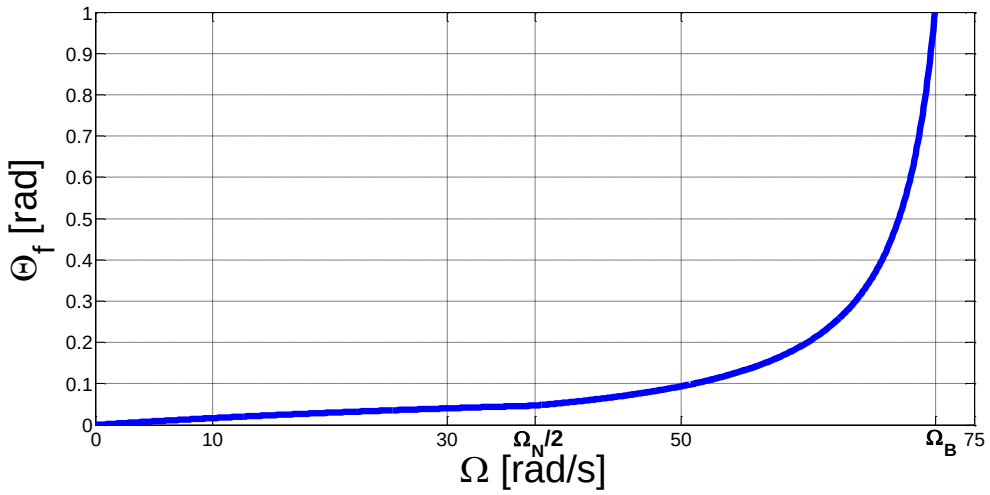

Fig. 3.5.2. Commutation interval vs. motor speed.

Figure 3.5.2 plots the rising interval θ_r of i_a and the commutation interval θ_f in the low-speed zone, and the vanishing interval θ_v of i_c and again the commutation interval θ_f in the high-speed zone. The graph point out that i) the commutation interval increases notably in the high-speed zone, reaching the value of π/3 at the base speed, ii) in the low-speed zone the

rising interval increases from zero to commutation interval at $\Omega = \Omega_N/2$, and iii) in the high-speed zone the vanishing interval starts from the value of 46.8 m rad at $\Omega = \Omega_N/2$.

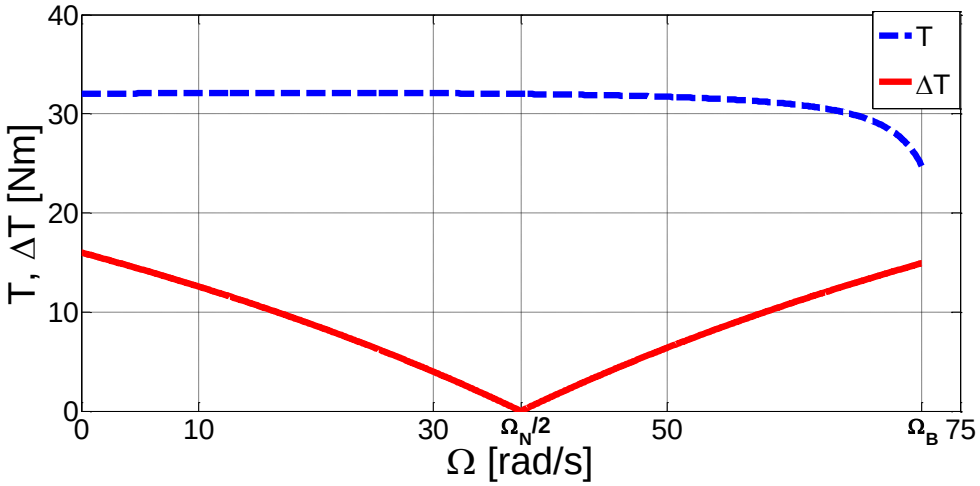

Fig. 3.5.3. Torque (blue dashed line) and torque ripple (red solid line) vs. motor speed.

The motor torque and the torque ripple are plotted in *Figure 3.5.3* with the blue solid line and the red dotted line, respectively. The graph show that i) the motor torque continuously drops with the increase in speed and falls by 23% of the rated value at the base speed, ii) the torque ripple has a symmetrical profile with respect to $\Omega = \Omega_N/2$, as it can easily deduced by inspecting (3.3.2.15) and (3.3.2.23), and is as high as 50% both at low speeds and at high speeds.

3.6 Conclusion

An analytical study of the torque characteristics of a PM BLDC drive with DC-side current control is carried, stressing the effects of the commutations on motor torque and torque ripple. The study has divided the speed range into two zones each of them having a proper behaviour of the phase currents during the commutations. The calculated motor torque exhibits a continuous drop with the speed whilst the calculated torque ripple is high both at low and high speeds, becoming zero just at half the speed range. The theoretical results are in good agreement with the motor torque have been verified by drive data which was executed on a commercial in-wheel PM BLDC drive.

Chapter 4

Remedial Control Strategies for a Three-Phase PM BLDC Drive

4.1 Introduction

Three-phase PM BLDC motors made its major existence in industrial and transportation applications due to its performance [17]. The literature on these drives has given a large emphasis on analyzing and proposing the appropriate solutions to overcome the problems of torque ripple and dropping speed-torque characteristics arising in the PM BLDC drive from phase-current commutations [19–20]. However, especially for the applicative sectors of the electric vehicles, a great interest is emerged towards the analysis and the proposal of solutions giving the PM BLDC drives fault-tolerant capabilities, i.e. the capabilities of overriding a fault to ensure the uninterrupted mobility of the electric vehicles. Considerable faulty states refer to the components of the drive such as the PM BLDC motor, the voltage source inverter (VSI) supplying the motor, and the electronic control unit (ECU) [21–26]. Differently from the more electric aircraft applications where human safety is supreme, requirements against the fault of the propulsion drive for the road vehicles are less stringent and can accept that the drive continues to operate even if in a degraded way, i.e. with worst performance compared to the nominal one. Typically for a drive, this means the development of a torque less than the nominal one and/or the upset of in-excess torque ripple.

Different types of faults possible within the motor are open circuit winding, short circuit of coils of the same phase or phase to ground, and short circuit of the terminals. Similarly the VSI can suffer from open/short circuit of single or both switches of a leg of VSI. The above-mentioned situations and the arrangements for fault-tolerant drive operation have been discussed in [21–23]. For the case of PM BLAC drives, in [24] a few VSI faults have been discussed and a solution consisting in an extra VSI leg, i.e. a four-leg VSI has been taken on, to tolerate the faults. Opposing to [24], paper [25] inserts a capacitor leg across the VSI DC-link and connects the mid-point of the capacitor leg to the motor phase that was supplied by the faulty VSI leg. Solution in [25] appears to be cost-effective in the sense that i) it does require neither an extra VSI leg nor the access to the neutral point of the motor, and ii) it replaces the DC-link capacitor with a mid-point capacitor arrangement. With this arrangement, commutation phenomena affects the torque ripple in a different manner with respect to the healthy VSI operation due to fixed voltage of the phase terminal, equal to half the DC-link voltage. In [26] the problem of compensating the torque ripple ensuing from the mid-point capacitor arrangement is dealt with.

4.2 Voltage source inverter (VSI) faults

During VSI faults, the drive can stop or undergo a corrupted behavior. By properly controlling the healthy section of the VSI, the drive can be continued to operate with performance that, even if degraded, is taken at an optimum value. In order to get the better performance of BLDC motor, the effected faulty phase is compensated with possible modifications in software/control or hardware solutions. In the present thesis more focus is given to the possible software/control strategies rather than the costly hardware schemes.

The possible cases of faults that occur in voltage source inverter (VSI) [27] that feed a three-phase PM BLDC motor are as follows

i) Open circuit fault in both switches of same leg (f.i. T1 and T4)
ii) Open circuit switch fault (f.i. T4)
iii) Short circuit switch fault (f.i. switch T1)

4.2.1 Open circuit fault in both switches of same leg (f.i. T1 and T4)

A three-phase BLDC motor is fed by a three-phase VSI consists of six switches (i.e. two switches in each leg). An open circuit fault in switches T_1 and T_4 (or) open circuit fault in phase *a* of VSI which is feeding PM BLDC motor as shown in *Figure 4.2.1* is considered. Both the cases create same impact in degrading the motor performance, but the location of the fault may varies. In both cases the leg *a* is isolated from the BLDC motor (i.e. only phase-a). So, the possible solutions that are going to be derived are also same for both the cases. In order to get the better performance, the absence of faulty switches T_1 and T_4 (i.e. VSI leg *a*) can be compensated with possible modifications in software/control by altering the current strategy for the remaining healthy phases (i.e. phases *b* and *c*).

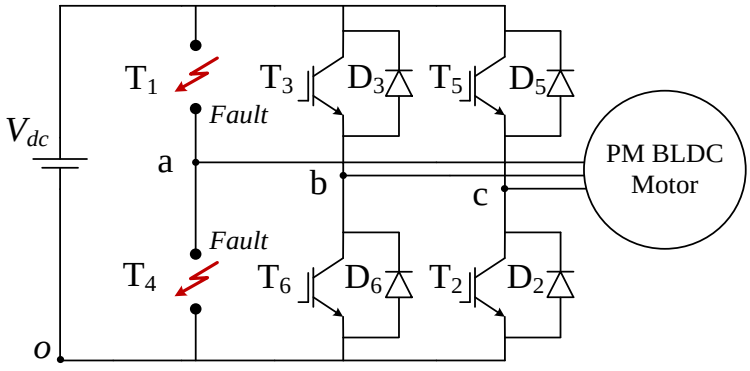

Fig. 4.2.1. Open circuit fault in two switches of same leg

Before going to the solution, it is necessary to examine the effect of fault under normal working control strategy of BLDC motor and its performance by observing the performance indices like average torque, and torque ripple. *Figure 4.2.2* shows the back EMF and current waveforms, while the highlighted area indicates the absence of phase current (i_a) such that the output power available during that supply interval become zero.

During the supply intervals S_2 and S_3 in *Figure 4.2.2*, the current cannot make a closed path to flow through the switches T_1 and T_4 which are open due to fault. Similarly in the supply interval S_5 and S_6 there is no outgoing path for i_b and i_c to flow because switch T_4 is open. And hence in supply intervals S_2, S_3, S_5, S_6 torque will be zero. The Average torque under fault condition and the corresponding torque ripple is given by

$$\tau_{avg} = \left(\frac{1}{3}\right)\frac{2EI}{\Omega} \tag{4.2.1}$$

$$\tau_{ripple} = \frac{\tau_{\max} - \tau_{\min}}{\tau_{avg}} = 3 \tag{4.2.2}$$

where Ω = mechanical speed

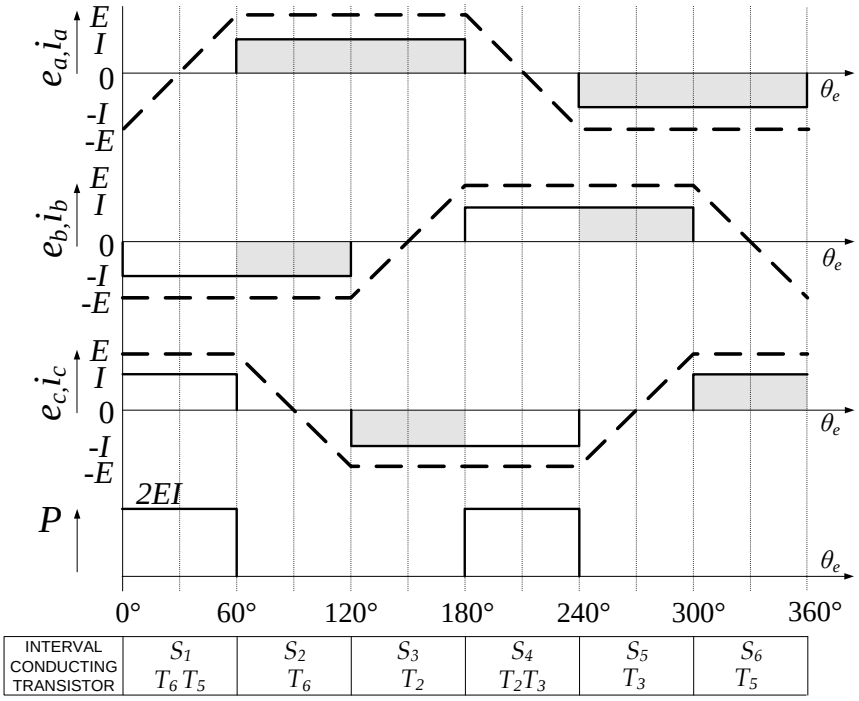

Fig. 4.2.2. Back EMFs and phase currents under open circuit fault in two switches of same leg (i.e. Leg *a*) with normal control strategy.

4.2.1.1 Operation of remaining phases (f.i b and c) in 180° conduction mode

Due to absence of phase *a*, the output power obtained from three-phase PM BLDC motor in one complete cycle is reduced to one third as shown in (4.2.1). This can be overcome by proper utilization of the remaining healthy phases with change in control strategy of 180° conduction mode. Now the VSI consists of two legs (i.e. four switches only) which is also termed as H-Bridge inverter. It can be operated either in bipolar or in unipolar pulse width modulation. Here in this case, phase *b* and phase *c* can be operated in 180° conduction mode. Selection of commutation location plays a prominent role in obtaining maximum average power and average torque as shown in *Figure 4.2.3*. Depending on the back emf and the phase current synchronization, the amount of average power and average

torque varies. The possible chances of getting maximum power can be evaluated by considering total average power in terms of commutation angle α. Where α is angle from zero to which the phase current (i_b and i_c) changes its sign.

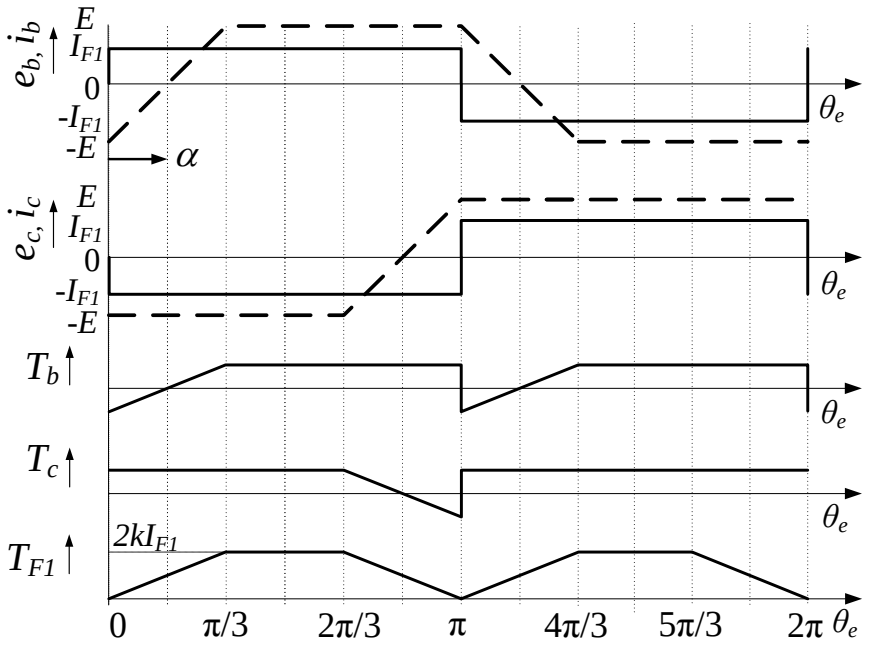

Fig. 4.2.3. Choice of phase current commutation with 180° conduction mode (considering back emf of phase *b* as a reference for this moment).

Here in this case, phase *b* and phase *c* can be operated in 180° conduction mode and the selection of commutation location plays a prominent role in obtaining maximum average power and average torque as shown in *Figure 4.2.3*. Depending on the location of phase current commutation and the back emf synchronization, the amount of average power and average torque varies. Where I_{F1} is the magnitude of the phase current that flow in remaining phases.

The possible chances of getting maximum power can be evaluated by considering total average power in terms of commutation angle α. Where α is angle from zero to which the phase current (i_b and i_c) changes its sign. With the variation of commutation angle α, average power varies. The commutation angle α can be varied from 0 to π, since the torque (T_{F1}) waveform (*Figure 4.2.2*) having a symmetry for a period of π radians. By plotting the variation of total average torque ($T_{F1,\,avg}$) in terms of α, location of commutation angle for maximum torque can be evaluated. The total average value of torque for different ranges of α is given below. The total torque is a combination of average torque obtained from phase *b* and phase *c*

$$T_{avg} = T_{b,avg} + T_{c,avg} \tag{4.2.1.1}$$

The average torque is obtained from the basic equation

$$p = \sum_{j=a,b,c} e_j i_j \; ; \quad \tau = \frac{p}{\Omega} \tag{4.2.1.2}$$

where p is constant over the supply period and equal to $2EI$. By assuming here and henceforth that the motor rotates at a constant speed Ω, the torque τ developed by the drive is also constant and expressed as (4.2.2). For the normal operation of the drive with the ideal square-wave current supply, average torque T_{avg} is equal to $2kI$. Where I and k are phase current square-wave magnitude and motor constant respectively.

In *Figure 4.2.3* it is shown that the back emf of phase *b* is considered as a reference and the commutation angle (α) is varied. For change in commutation angle (α) from the origin the total average power and torque can be obtained as follows:

I. For commutation angle varying from $0 < \alpha < \pi/3$

Average power for phase *b* is obtained as,

$$P_{b,avg} = \frac{1}{\pi}\left[\int_0^{\alpha}(-I)e_b \; d\alpha + \int_{\alpha}^{\pi/3}(I)e_b \; d\alpha + IE\int_{\pi/3}^{\pi} d\theta_e\right] \tag{4.2.1.3}$$

Where, $e_b = -E + \frac{6E}{\pi}\alpha$

substituting value of e_b in (4.2.1.3) and integrating we get

$$P_{b,avg} = \frac{IE}{\pi}\left[2\alpha + \frac{2\pi}{3} - \frac{6}{\pi}\alpha^2\right] \tag{4.2.1.4}$$

similarly for phase *c*,

$$P_{c,avg} = \frac{1}{\pi}\left[\int_0^{\alpha}(I)(-E) \; d\alpha + \int_{\alpha}^{2\pi/3} IE \; d\alpha + \int_{2\pi/3}^{\pi} e_c(-I)d\theta_e\right] \tag{4.2.1.5}$$

solving (4.2.1.5) we get

$$P_{c,avg} = \frac{IE}{\pi}\left[\frac{2\pi}{3} - 2\alpha\right] \tag{4.2.1.6}$$

we can write,

$$P_{F1,avg} = P_{b,avg} + P_{c,avg} \tag{4.2.1.7}$$

substituting (4.2.1.4) and (4.2.1.6) in (4.2.1.7) we get

$$P_{F1,avg} = \frac{IE}{\pi}\left[\frac{4\pi}{3} - \frac{6}{\pi}\alpha^2\right] \tag{4.2.1.8}$$

II. For commutation angle varying from $\pi/3 < \alpha < 2\pi/3$

Average power for phase *b*, is given by

$$P_{b,avg} = \frac{1}{\pi}\left[\int_0^{\pi/3}(-I)e_b \; d\alpha + \int_{\pi/3}^{\alpha}(-I)E \; d\alpha + IE\int_{\alpha}^{\pi} d\theta_e\right] \quad (4.2.1.9)$$

Integrating (4.2.1.9) we get

$$P_{b,avg} = \frac{IE}{\pi}\left[-2\alpha + \frac{4\pi}{3}\right] \quad (4.2.1.10)$$

similarly, for phase *c*,

$$P_{c,avg} = \frac{1}{\pi}\left[\int_0^{\pi/3} I(-E)\; d\alpha + \int_{\pi/3}^{\alpha} I(-E)\; d\alpha + IE\int_{\alpha}^{2\pi/3} d\theta_e + \int_{2\pi/3}^{\pi}(-I)e_c \; d\theta_e\right] \quad (4.2.1.11)$$

Integrating it we get

$$P_{c,avg} = \frac{IE}{\pi}\left[-2\alpha + \frac{2\pi}{3}\right] \quad (4.2.1.12)$$

using (4.2.1.7) we can write

$$P_{F1,avg} = \frac{IE}{\pi}\left[-4\alpha + 2\pi\right] \quad (4.2.1.13)$$

III. For commutation angle varying from $2\pi/3 < \alpha < \pi$

Average power for phase *b*, is given by

$$P_{b,avg} = \frac{1}{\pi}\left[\int_0^{\pi/3}(-I)e_b \; d\theta_e + \int_{\pi/3}^{2\pi/3}(-I)E \; d\theta_e - IE\int_{2\pi/3}^{\alpha} d\alpha + IE\int_{\alpha}^{\pi} d\theta_e\right] \quad (4.2.1.14)$$

solving it we can write

$$P_{b,avg} = \frac{IE}{\pi}\left[-2\alpha + \frac{4\pi}{3}\right] \quad (4.2.1.15)$$

similarly for phase *c* we get,

$$P_{b,avg} = \frac{1}{\pi}\left[\int_0^{2\pi/3} I(-E)\; d\theta_e + \int_{2\pi/3}^{\alpha}(I)e_c \; d\alpha + \int_{\alpha}^{\pi}(-I)e_c d\alpha\right] \quad (4.2.1.16)$$

Where, $e_c = -5E + \frac{6E}{\pi}\alpha$

substituting value of e_c in (4.2.1.16) and integrating we get

$$P_{c,avg} = \frac{IE}{\pi}\left[-10\alpha + \frac{10\pi}{3} + \frac{6}{\pi}\alpha^2\right] \quad (4.2.1.17)$$

similarly using (4.2.1.7) we can obtain P_{avg} which can be given as

$$P_{F1,avg} = \frac{IE}{\pi}\left[-12\alpha + \frac{14\pi}{3} + \frac{6}{\pi}\alpha^2\right] \quad (4.2.1.18)$$

For change in commutation angle from $0 < \alpha < \pi$, the total average torque can be obtained using (4.2.1.8), (4.2.1.13), and (4.2.1.18)

$$T_{F1,avg} = \frac{kI}{\pi}\left[\frac{4\pi}{3} - \frac{6}{\pi}\alpha^2\right] \text{ for } \left(0 < \alpha < \frac{\pi}{3}\right) \quad (4.2.1.19)$$

$$T_{F1,avg} = \frac{kI}{\pi}\left[-4\alpha + 2\pi\right] \text{ for } \left(\frac{\pi}{3} < \alpha < \frac{2\pi}{3}\right) \quad (4.2.1.20)$$

$$T_{F1,avg} = \frac{kI}{\pi}\left[-12\alpha + \frac{14\pi}{3} + \frac{6}{\pi}\alpha^2\right] \text{ for } \left(\frac{2\pi}{3} < \alpha < \pi\right) \quad (4.2.1.21)$$

From (4.2.1.19) to (4.2.1.21) the variation of total average torque T_{avg} w.r.t to commutation angle (α) is plotted in *Figure 4.2.4*. It reveals that maximum average torque can be obtained, when α is equal to zero with phase *b* and phase *c* are operated at 180° conduction mode.

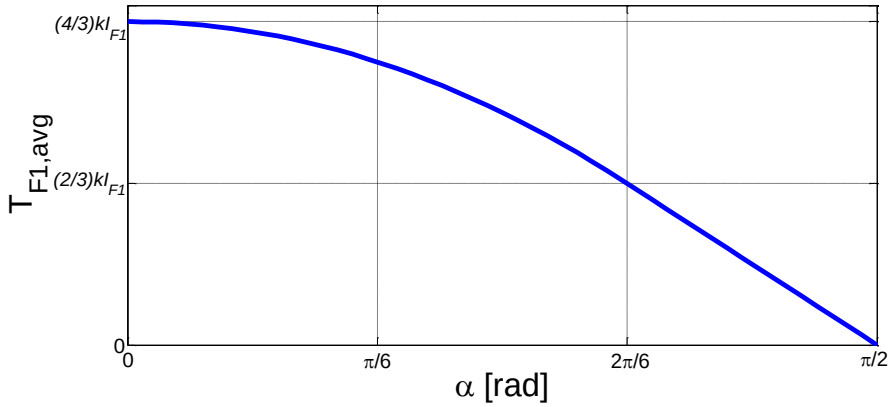

Fig. 4.2.4. Variation of average torque ($T_{F1,\,avg}$) with respect to commutation angle (α).

4.2.1.2 Considering equal rms values

For the comparison of torque, it is assume that to ensure the same cu-loss per phase. The rms values of the phase currents during healthy and faulty case motors must be same, and the corresponding magnitudes of the flat portion of phase currents are I_N and I_{F1} respectively as shown in *Figure 4.2.5*.

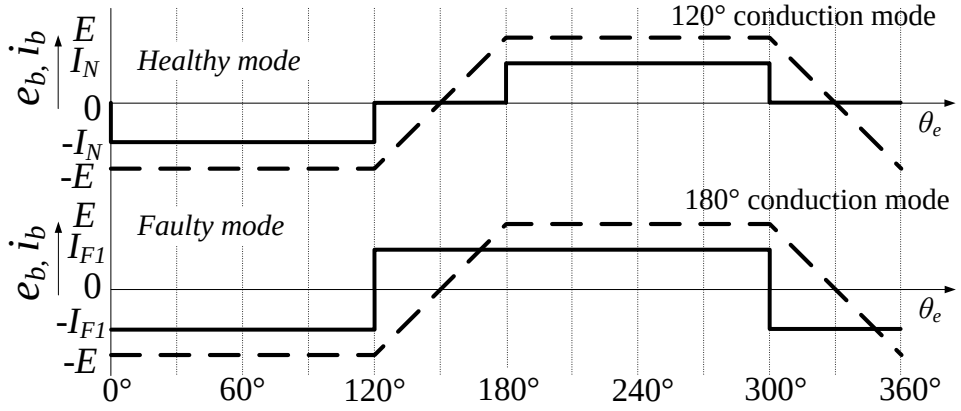

Fig. 4.2.5. Back EMFs and phase current in healthy mode and in faulty mode.

$$I_{rms,N} = \sqrt{\frac{2}{3}} I_N \tag{4.2.1.22}$$

$$I_{rms,F} = I_F \tag{4.2.1.23}$$

by ensuring same copper loss per phase, equating (4.2.1.22) to (4.2.1.23) I_N and I_{F1} are correlated as

$$I_{F1} = \sqrt{\frac{2}{3}} I_N \tag{4.2.1.24}$$

and the corresponding motor torque are correlated as

$$\tau_{F1} = \frac{2}{3}\left(\frac{2EI_F}{\Omega}\right) = \frac{2}{3}\left(\frac{2E}{\Omega}\right)\left(\sqrt{\frac{2}{3}} I_N\right) = 0.54\,\tau_N \tag{4.2.1.25}$$

Thus for the same cu-loss per phase, the motor offers only 54% rated torque of a three-phase PM BLDC motor.

4.2.1.3 Considering commutation effect

Behavior of motor in 180° conduction mode is already discussed without considering commutation effect. In practice, due to motor phase inductance effect the sudden rise and fall in current is being opposed. From *Figure 4.2.3* it is clear that commutation takes place twice in a complete cycle and is briefly explained in the following section with appropriate schematic diagrams.

Considering supply interval S_3, where i_b is going from $-I$ to I and i_c is going from I to $-I$ which will take some finite time to complete this commutation process as shown in *Figure 4.2.6*.

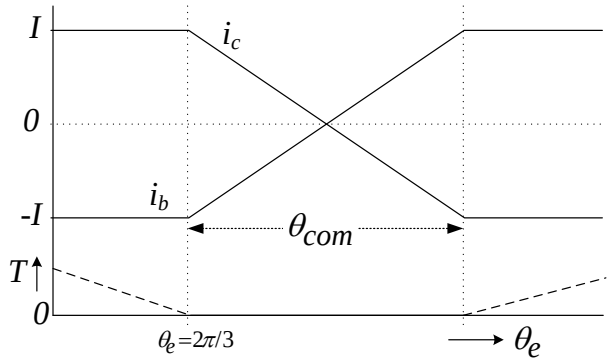

Fig. 4.2.6. Current and torque behavior in supply interval S3.

Electric equivalent circuit before commutation and during the commutation is shown in *Figures 4.2.7, 4.2.8* and *4.2.9*. Before supply interval S_3, switches T_5 and T_6 are conducting (*Figure 4.2*) and during commutation i.e. from $\left[\frac{2\pi}{3}\right]$ to $\left[\frac{2\pi}{3} + \theta_{com}\right]$ the switches T_3, T_2

and diodes D_3 and D_2 are taking part in current flow. So the path of current flow in motor phases during the commutation remains unchanged as that of *Figure 4.2.7* and *Figure 4.2.8*.

(a) Just before commutation (i.e. during supply interval S_3)

By appyling KVL over the loop, in *Figure 4.2.7*,

$$V_{cb} = L\frac{di_c}{dt} + e_c - e_b - L\frac{di_b}{dt} \tag{4.2.1.26}$$

where $i_b = -i_c$, $e_c = -E$, $e_b = -E$

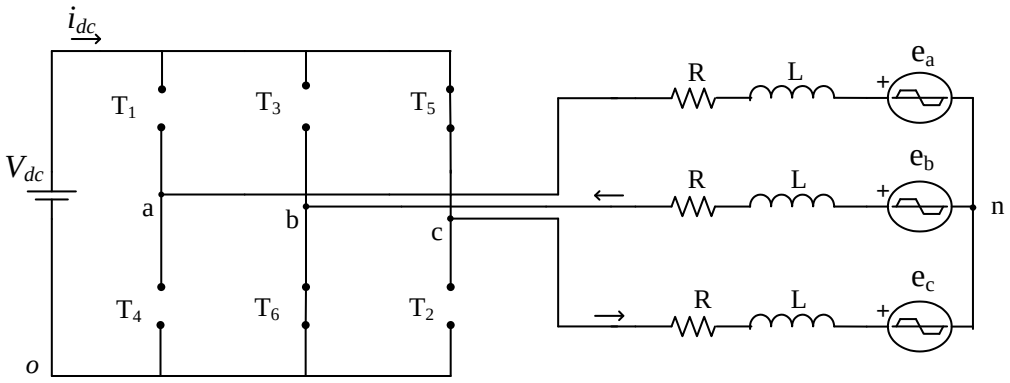

Fig. 4.2.7. Before commutation (i.e. supply interval S3).

$$V_{cb} = 2L\frac{di_c}{dt} \tag{4.2.1.27}$$

Differentiation for a constant value is equal to zero (i.e. for i_c= constant), therefore

$$V_{cb} \cong 0$$

(b) During commutation interval $\left[\frac{2\pi}{3} < \theta_e < \left(\frac{2\pi}{3} + \theta_{com}\right)\right]$

By applying KVL over the loop in *Figure 4.2.8*, we get

$$V_{bc} = L\frac{di_b}{dt} - e_b + e_c - L\frac{di_c}{dt} \tag{4.2.1.28}$$

where $e_b = -E\left[1 - \frac{6}{\pi}\theta_{com}\right]$, $i_b = -i_c$, $e_c = -E$, $V_{bc} = V_{dc}$

Back emf of phase *b* is assumed to be equal to $-E$ for a small commutation interval (θ_{com})

Therefore, $e_b \cong -E$

$$V_{dc} = L\frac{di_b}{dt} + E - E + L\frac{di_b}{dt} \tag{4.2.1.29}$$

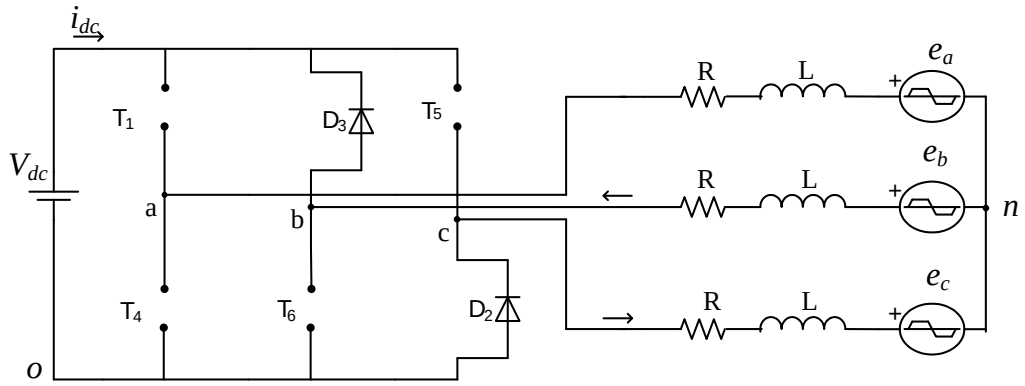

Fig. 4.2.8. During commutation $\left[\frac{2\pi}{3} < \theta_e < \left(\frac{2\pi}{3} + \frac{\theta_{com}}{2}\right)\right]$.

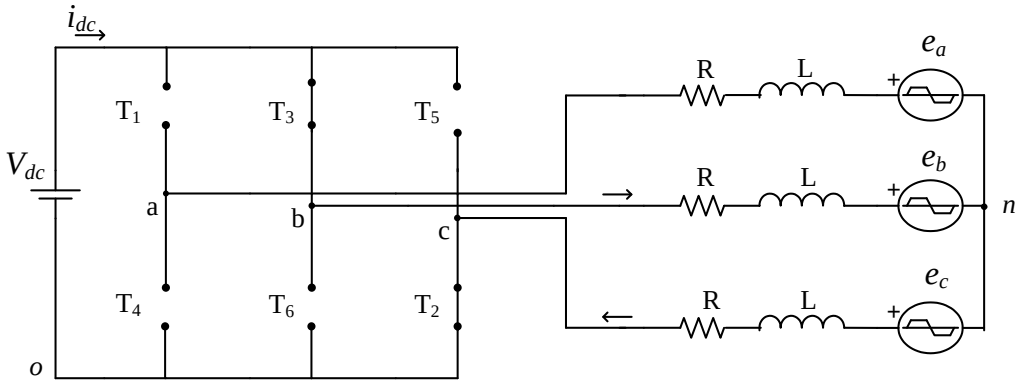

Fig. 4.2.9. During commutation $\left[\left(\frac{2\pi}{3} + \frac{\theta_{com}}{2}\right) < \theta_e < \left(\frac{2\pi}{3} + \theta_{com}\right)\right]$.

$$\frac{di_b}{dt} = \frac{V_{dc}}{2L} \tag{4.2.1.30}$$

We know that $\theta_e = \Omega_e * t$

$$\frac{di_b}{d\theta_e} = \frac{V_{dc}}{2L\Omega_e} \tag{4.2.1.31}$$

Integrating on both sides of (4.2.1.31), we get

$$\int_{-I}^{I} di_b = \frac{V_{dc}}{2L\Omega_e} \int_{2\pi/3}^{(2\pi/3+\theta_{com})} d\theta_e \tag{4.2.1.32}$$

$$\theta_{com} = \frac{4IL\Omega_e}{V_{dc}} \tag{4.2.1.33}$$

During this commutation interval back EMFs are same and $i_b = -i_c$, So the torque produced is equal to zero.

$$\tau = \frac{e_b i_b + e_c i_c}{\Omega} = 0 \tag{4.2.1.34}$$

Similar commutation operation takes place during the negative crossing edge of phase current (i_b) at θ_e = 300°. Therefore the average torque for one complete cycle considering commutation is

$$\tau_{avg} = \left(\frac{2}{3} - \frac{\theta_{com}}{2\pi}\right)\frac{2EI}{\Omega} \tag{4.2.1.35}$$

4.2.1.4 Simulation Result

The switches T_1 and T_4 in VSI are replaced with a high resistance of 10k ohm. Parameters of BLDC motor considered for simulation are given in *Table 4.2.1*.

Tab. 4.2.1 PM BLDC motor data.

Parameters	Values
Phase resistance (R_s)	50m Ω
Phase inductance (L_s)	75μ H
Electric torque/back emf constant	0.32
Number of pole pair(n_p)	8
DC Voltage source (V_{dc})	48 V

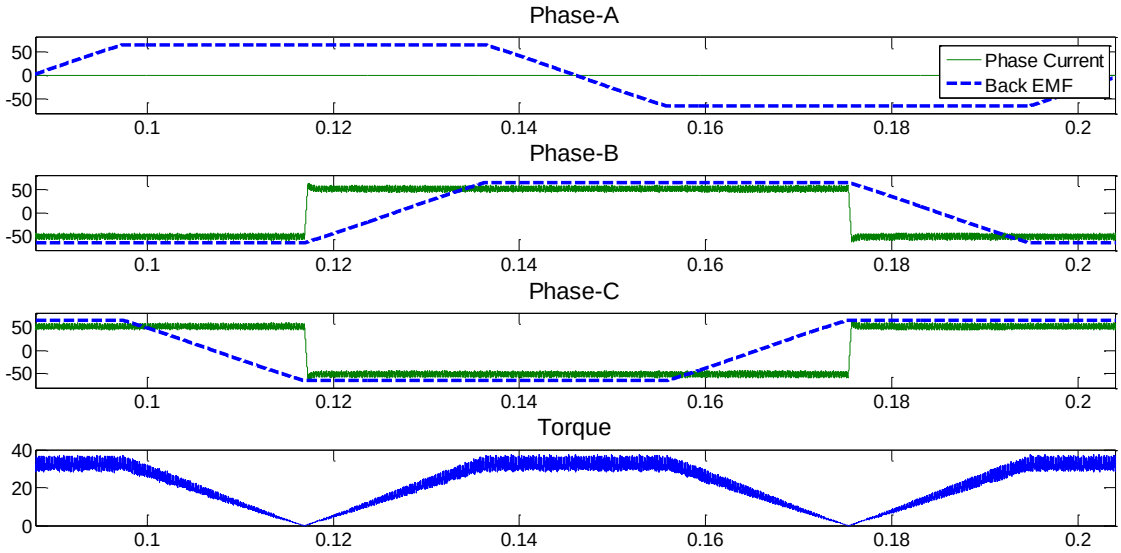

Fig. 4.2.10. Simulation result of BLDC motor when phase *a* is open circuit (faulty) and phase *b* and *c* are operated in 180° conduction mode.

4.2.2 Open circuit switch fault (f.i. T4)

A three-phase BLDC motor should be fed by a three-phase VSI consists of six switches. Let us consider an open circuit switch fault occurred in phase *a* i.e. either T_1 or T_4 is faulty. For

instance (f.i.), it is considered that the switch T_4 is open and isolated from the circuit as shown in the *Figure 4.2.2.1*. As the lower switch of the leg-*a* is open, there is no path for the phase current i_a to flow in reverse direction and also the possibility of modulating the upper switch T_1 is unmanageable due to the absence of freewheeling diode path as well (i.e. diode D_4). In order to get the better performance of BLDC motor, the effect of absence of switch T_4 can be compensated with possible modifications in software/control or hardware solutions as follows:

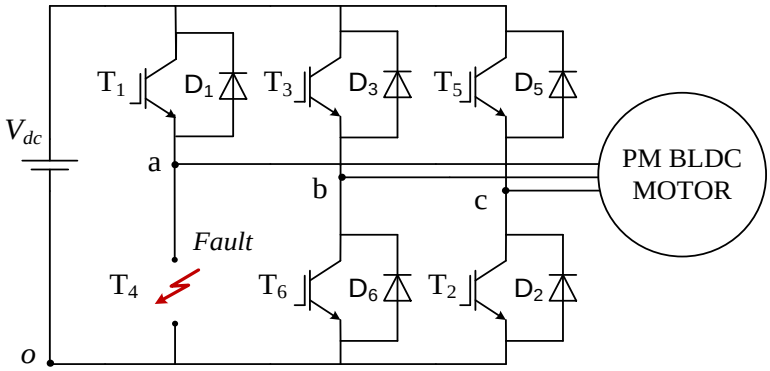

Fig. 4.2.2.1. Open circuit fault in single switch (f.i. T_4).

The motor can also work under faulty condition without any hardware modifications. An immediate fault identification and appropriate changes in the control strategy can make the motor to operate with better performance (i.e. lesser as compared to that of the normal operation performance). Since switch T_4 is the three-phase VSI is already open due to an open circuit fault as shown in *Figure 4.2.2.1*, now switch T_1 cannot be modulated further due to the absence of freewheeling diode path (D_4) and it is considered as ON for the supply intervals S_2 and S_3. During those supply intervals (i.e. during S_2 and S_3) the torque produced due to phase current i_a is positive. In order to get more positive torque, the phase current i_a must become zero before its back EMF starts decaying from supply interval S_4. Unless the current passing through T_1 becomes zero, switch T_1 cannot be turned off. As there is no path for T_1 to freewheel, the possible way for making the phase current i_a to zero after supply interval S_3, is to turn ON the switch T_5. During this approach the phase current i_b becomes negative for the commutation duration to make the faulty phase current zero. The equivalent circuit during this situation is as shown in *Figure 4.2.2.2*.

By applying basic Kirchhoff's law as considered in *Chapter 3*, for the sequence of *Figure 4.2.2.2* the current derivatives are obtained as follows

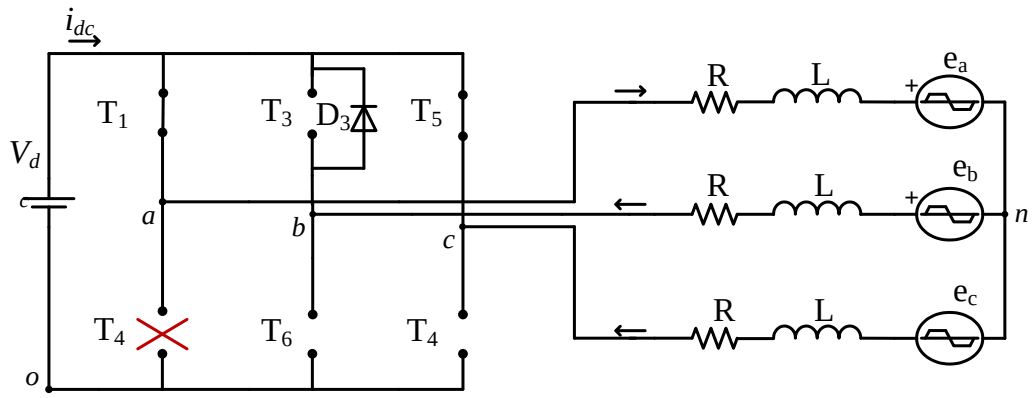

Fig. 4.2.2.2 Equivalent circuit of switch T_4 open circuit fault with T_5 turn ON.

$$\left.\begin{aligned} \frac{di_a}{dt} &= -\frac{2e_a}{3L} \\ \frac{di_b}{dt} &= -\frac{3E-e_a}{3L} \\ \frac{di_c}{dt} &= \frac{3E+e_a}{3L} \end{aligned}\right\} \qquad (4.2.2.1)$$

Integrating (4.2.2.1) by considering the end of supply interval S_3 as initial condition for i_a, i_b and i_c as $+I$, 0 and $-I$ respectively, we get

$$i_a = I_{F2} - \frac{2e_a}{3n_p L\Omega}\Delta\theta_e \qquad (4.2.2.2)$$

$$i_b = -\frac{3E-e_a}{3n_p L\Omega}\Delta\theta_e \qquad (4.2.2.3)$$

$$i_c = -I_{F2} + \frac{3E+e_a}{3n_p L\Omega}\Delta\theta_e \qquad (4.2.2.4)$$

As the switch T_5 is ON, the phase current i_c can be positive and there is no restriction of phase current i_c being only negative. During this situation, phase Current i_a reaches zero for a duration of $\Delta\theta_e$ and its duration can be evaluated by equating (4.2.2.2) to zero. Where e_a is assumed to be constant and equal to E.

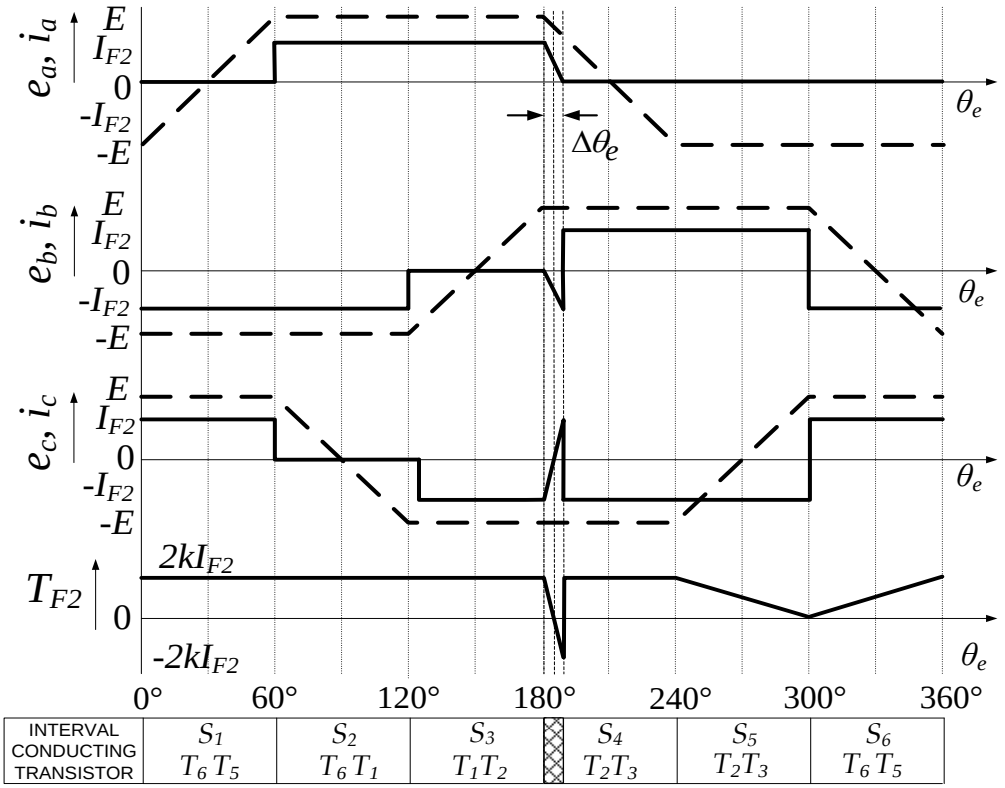

Fig. 4.2.2.3. Back-emf and phase current waveforms for making phase current i_a zero by turning ON switch T5.

$$\Delta\theta_e = \frac{3n_p L I_{F2}}{2k} \tag{4.2.2.5}$$

Equation (4.2.2.5) clearly states that $\Delta\theta_e$ is independent of back emf and does not depend upon motor speed. So that, after a duration of $\Delta\theta_e$, gate pulse for switch T_1 can be removed and rest of the operation is carried with the new reference currents provided by phase *b* and phase *c* alone as shown in *Figure 4.2.2.3*.

For the comparison of torque, it is assume that to ensure the same cu-loss per phase. The rms values of the phase currents during healthy and faulty case motors must be same, and the corresponding maximum value of the phase current I_{F2} is as shown in *Figure 4.2.2.3*. Since the value of $\Delta\theta_e$ is very small, it is neglected in calculation of rms values of the phase currents and average torque.

$$I_{b,rms} = I_{c,rms} = \sqrt{\frac{5}{6}}\ I_{F2} \tag{4.2.2.6}$$

For the equal cu-loss per phase for the healthy and faulty mode, rms value of the phase-currents should be equal. Thus the peak magnitudes I_N and I_{F2} phase currents are correlated as

$$I_{F2} = \sqrt{\frac{4}{5}} I_N \tag{4.2.2.7}$$

and the corresponding motor torque is co-related as

$$T_{F2} = \frac{5}{6}.2kI_{F2} = \frac{5}{6}.\sqrt{\frac{4}{5}}.2kI_N = 0.745\,T_N \tag{4.2.2.8}$$

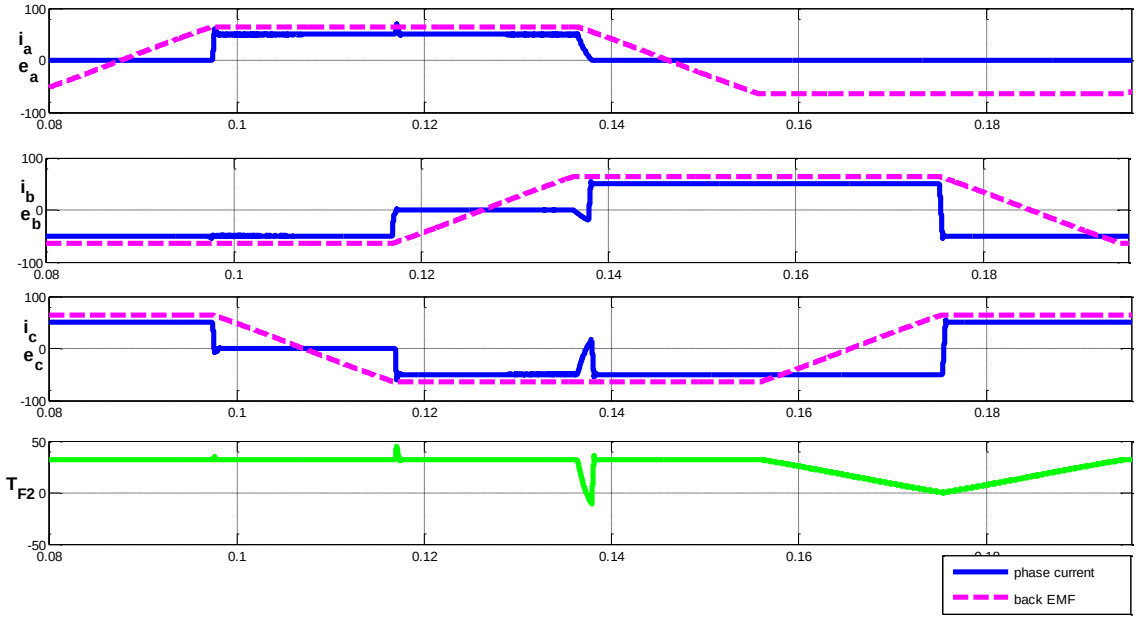

Fig. 4.2.2.4. Simulation response of BLDC motor with switch T_4 open circuited (faulty) and phase *b* and *c* are operated in current extension mode.

Thus for the same cu-loss per phase, the motor offers only 74.5% rated torque of a three-phase PM BLDC motor. Simulated response for this case of fault is shown in below *Figure 4.2.2.4*.

4.2.3 Short circuit switch fault

There could be two possibilities of short circuit fault in a particular leg of the VSI: a) say switch T_1 is being modulated and it gets shorted, and b) T_1 is being modulated and T_4 gets short circuited. In case b) occurrence of a fault can be handle by turning off the switch being modulated, with this two cases turns into a similar one.

4.2.3.1 Short circuit of a switch being modulated (f.i. switch T1)

Considering the case that prior to occurrence of short circuit fault at T_1, VSI was being operated with the modulation of upper switches and keeping corresponding lower switches ON in a supply interval. For example under normal condition in supply interval S_2, Switch T_1 is being modulated and T_6 is kept ON. *Figure 4.2.3.1* shows a short circuit switch fault at T_1.

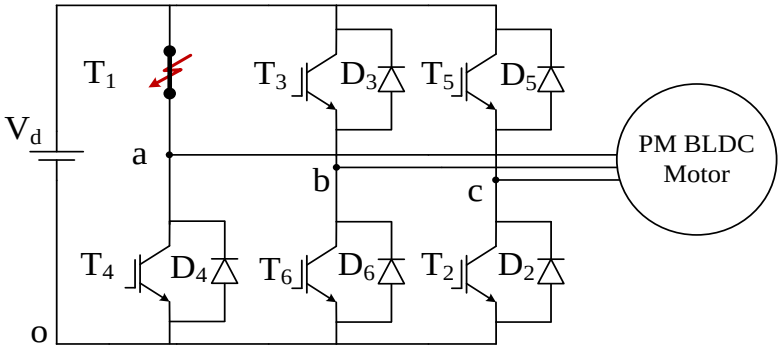

Fig. 4.2.3.1. Short circuit switch fault (f.i. switch T_1).

In case of fault in T_1, as a strategy to ensure functionality of VSI, modulation of switches for further supply intervals is shifted to lower switches and the upper switches are kept ON in a supply interval. During the interval S_2 and S_3, as a first sight there should not be any problem with the operation of the drive under an ideal case of operation. On the arrival of interval S_4, upper switch of phase *b* (T_3) can be turned ON and the lower switch of phase *c* can be modulated to maintain phase *c* current to the level of *-I*. So this can facilitate equal sharing of currents by the switches T_1 and T_3. As the T_1 is short circuited, its complementary switch can never be operated to avoid shorting of phase *a* leg. So the operation corresponding to the normal operation of intervals S_5 and S_6 are prohibited. During interval S1, upper switch of phase *c* can be turned on and T_6 can be modulated to regulate phase-c current to the level of *–I*. During S_5, as none of the healthy switches are modulated, phase-a current will start to free-wheel through T_1-D_3-T_1 and T_1-D_5-T_1. It is important to note that during S_5 and S_6, negative back-emf of phase-a supports i_a to rise. Rate of variation of i_a during interval S_5 and S_6 are given by (4.2.3.1) and (4.2.3.2) respectively.

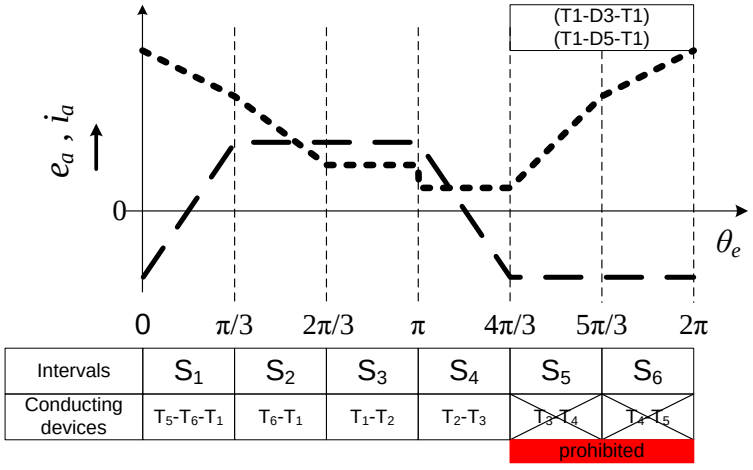

Fig. 4.2.3.2. Phase current and back-emf under switch T_1 short-circuit fault.

$$\frac{di_a}{dt} = \frac{V_d}{3L}\left[\delta_b + \delta_c + \frac{2E}{V_d}\left(1 + \frac{3}{\pi}\theta\right)\right] \qquad (4.2.3.1)$$

$$\frac{di_a}{dt} = \frac{V_d}{3L}\left[\delta_b + \delta_c + \frac{2E}{V_d}\left(\frac{3}{\pi}\theta\right)\right] \tag{4.2.3.2}$$

where θ is measured from the instant of the start of a particular interval.

From (4.2.3.1) and (4.2.3.2) it can be concluded that as rate of variation of i_a remains positive (for the present consideration $\delta_a = \delta_b = 0$). So it will continue to rise, even with any regulatory effort by modulating T_2 and T_6, rate of variation in i_a remains positive. So in any case current will continue to rise during S_5 and S_6. It can be shown that during the interval S_1 and S_2, rate

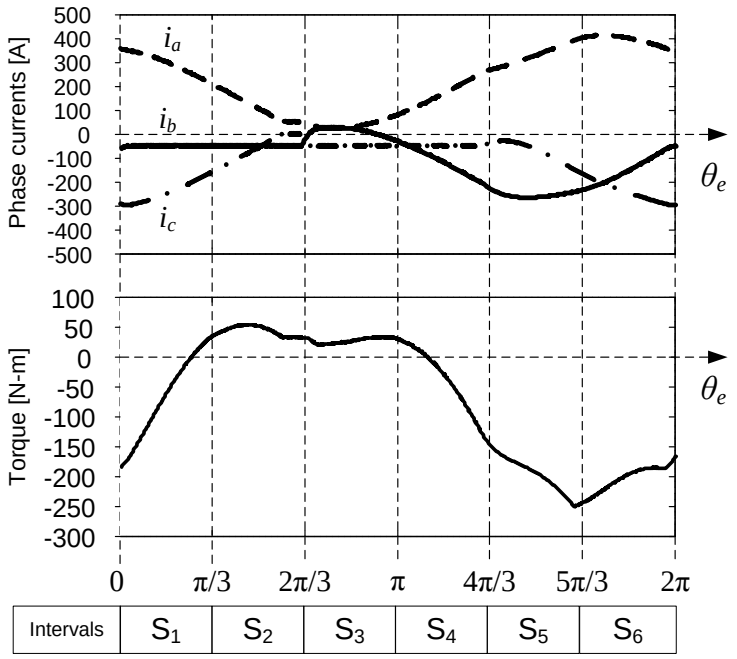

Fig. 4.2.3.3. Simulated phase currents and motor torque under switch T_1 short-circuit fault.

of variation of i_a becomes negative so, current starts reducing from the maximum value. Such a case with ideal commutation is demonstrated in *Figure 4.2.3.2*. Response of the drive under simulated fault is shown in *Figure 4.2.3.3*.

It can be observed that i_a and corresponding other phase current rises to an un acceptable value, with the development in very high value of average negative torque which will result in hard braking of the drive and the destruction of the healthy switches and overall drive system. Magnitude of the faulty current can be reduced by an advanced turn OFF of lower switches T_2 and T_4 in the interval S_3, where e_a is positive so free wheel current can be forced to rise to lower value.

Disadvantage under such a case will be a braking torque of even much higher value and is not permissible. Thus to handle such a situation, arrangements other than the improvement switching strategy would be beneficial like switching to an auxiliary healthy leg or use of mid-point capacitor arrangement [25].

4.3 Conclusion

This chapter dealt with the possible general VSI switch faults that usually downgrades the PM BLDC drive performance. The analysis is carried out to obtain the maximum performance by effective modifications done to current reference/control strategy. Same copper loss per phase is considered in all the cases to make an evaluation on a common platform. The motor performs its continuity even under faulty condition, with a downgraded torque performance of about 54% of nominal torque for a two switch fault and 74.5% of nominal torque for a single switch fault.

Chapter 5

Remedial Control Strategies for a Hall Sensor Faults in Three-Phase PM BLDC Drive

5.1 Introduction

A PM BLDC motor require rotor position information to switch the transistors of the motor phases in the right sequence. In this aspect, a simple cost effective solution that comes front is Hall effect sensors. Hall Effect sensors are mounted inside the BLDC motor (with 120 degree electrical phase difference) to detect rotor position. Output of each sensor is high (logic '1') for 180 electrical degree and is low (logic '0') for the next successive 180 degree with respect to rotor position. Decoding Hall effect signals result to choose the proper supply of applied voltage by switching the three-phase voltage source inverter (VSI) of BLDC motor as shown in *Figure 5.1*.

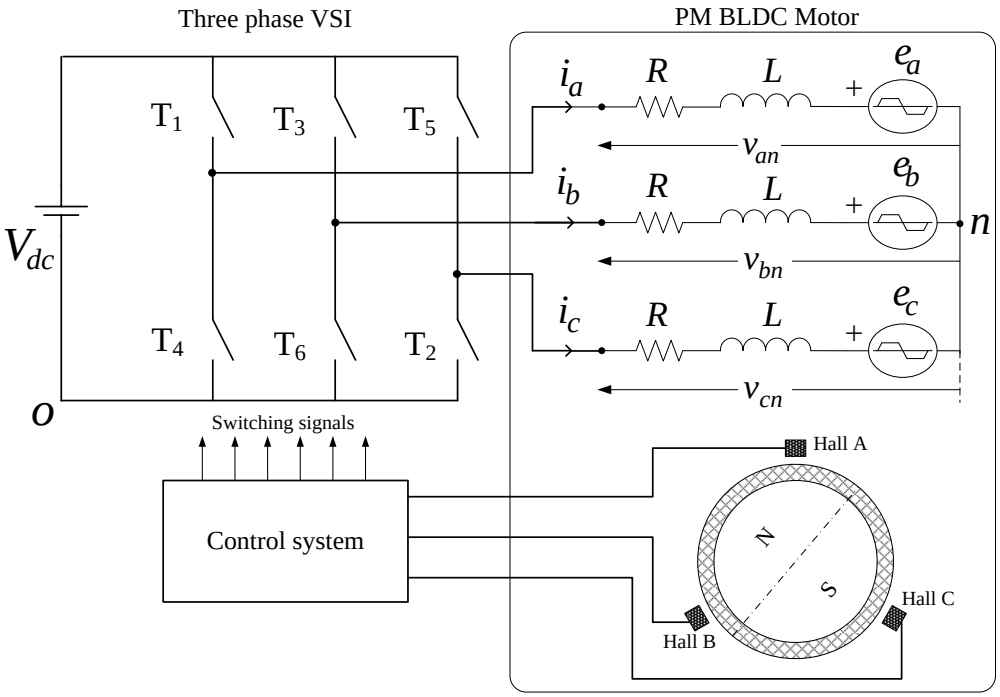

Fig. 5.1. Three-phase PM BLDC drive system.

In order to obtain the maximum power/torque, the phase currents or the VSI switches are commutated in each supply interval (possible combination of all the Hall Effect signals A, B and C with respect to the maximum value of the respective back emf of each phase. The switching sequence/signals are generated by the control system in an appropriate manner as per the *Table 5.1*, to obtain maximum output power (or torque) from the drive.

Tab. 5.1 Switching sequence decided by Hall signal.				
Supply interval	Hall A	Hall B	Hall C	Conducting switches
S1	1	0	1	T1, T6
S2	1	0	0	T1, T2
S3	1	1	0	T3, T2
S4	0	1	0	T3, T4
S5	0	1	1	T5, T4
S6	0	0	1	T5, T6

Failure of Hall Effect sensors directly effects the applied voltages to the BLDC motor and degrade the performance of overall motor drive. [28–31] proposes a few methodologies to compensate the sensor faults. A sensorless approach was given in [32] using digital pwm technique for vehicular applications. The fault tolerant control system mainly should fulfil the following tasks,

1) Fault detection

2) Fault identification

3) Remedial strategies

5.2 Hall Effect Sensor

A voltage potential, called Hall voltage, appears across a sample when a magnetic field is applied with a given angle to the current flow. In common applications, it is orthogonal to both the magnetic field and the current and its magnitude is proportional to both the magnetic flux density and the current as shown in *Figure 5.2*.

The magnetic field causes a gradient of carrier concentration across the sample. A larger number of carriers on one side of the sample, compared to the other side, causes a voltage potential [33].

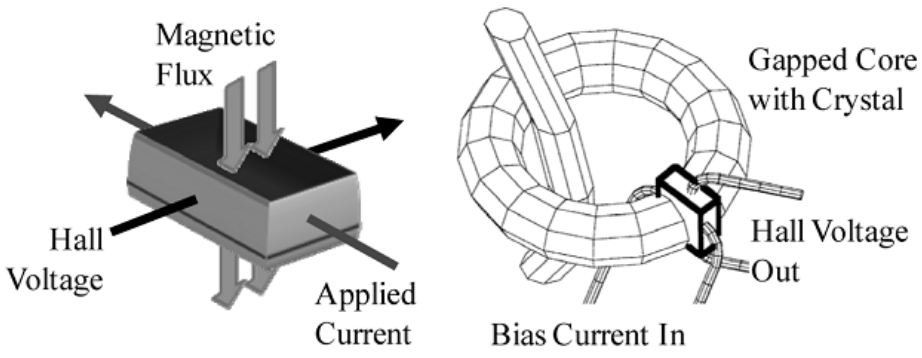

Fig. 5.2 (a) Hall effect in a conductor, (b) Hall effect current sensor [33].

Faults in Hall effect sensors:

Different possible Hall effect sensor faults [29] are as follows:

1) Flaws in the core, such as degradation (corrosion, cracks), residual magnetic fields, or core breakage can result in a bias[1].
2) Changes in the bias current through the sensor can result in bias[1] or scaling[2].
3) Temperature variations can change the magnetic properties of the ferrite core, resulting in decrease (or increase) of the induced magnetization, causing a bias in the readings.
4) Changes in the orientation of the induced magnetic field in the sensor (due to mechanical shocks or other reasons) can change the value of Hall voltage and lead to a scaling error.

Any of these faults may result to breakdown of the Hall effect sensor in BLDC motor. Unbalanced positioning of Hall effect sensors is also another common fault in BLDC motor discussed in [30] that increases the low-frequency harmonics in torque ripple and degrades the overall drive performance, however it does not result in sensor breakdown. There are a few research work on Hall Effect sensor failure of BLDC motor specifically for electric vehicle applications. Jeong, et al. have presented a control strategy that provides fault tolerance to the major sensor faults which may occur in an interior-permanent-magnet-motor (IPMM)-based electric vehicle propulsion drive system [31].

5.3 Position sensor failure

Position sensors fault is detected through difference between the estimated rotor angle and the actual measured one through a sensorless algorithm based on extended EMF in rotating reference frame. In this approach, reconfiguration to sensorless control scheme need to be introduced to rectify the fault and maintain the proper operation ofthe motor after fault occurrence is detected. Complexities of sensorless control scheme and transition algorithm to sensorless control are the main drawbacks of the proposed method.

Breakdown of the position sensor cause the output signal of sensor to be whether constant high (logic ‘1’) or constant low (logic ‘0’) and it does not change according to the rotor position. Therefore behaviour of BLDC motor is studied for the both conditions (H_A = 0 and H_A = 1) separately during failure of Hall effect position sensor of phase A.

Malfunction of Hall effect sensor with constant value zero (H_A=0):

Hall Effect sensor failure causes change of the switching signals of VSI and affects directly on the applied line voltage of the BLDC motor. Due to the malfunction of hall sensor

[1]*Bias*: A constant offset from the nominal sensor signal statistics. Another way to describe bias is as the sensor output at zero input. Bias can occur due to incorrect calibration or physical changes in the sensor system.
[2]*Scaling:* Magnitudes are scaled by a factor, where the form of the waveform itself does not change.

(H_A) the switching sequence becomes altered for the half of the supply cycle, which indirectly isolate the switches to work. The switching signals for the switches T1 and T2 are constant zero (switches T1 and T2 remain open circuit) for H_A = 0 fault condition. Change of applied voltages cause variation of the stator phase currents of the BLDC motor that effects directly on electrical torque of motor and increases torque ripple. Similarly, the effect of various Hall effect sensor fault for constant value zero are shown in *Table 5.3.1*.

Tab. 5.3.1 Switching signals during hall sensor fault (constant zero).	
Faulty hall sensor	Non-conducting switches
H_A=0	T1, T2
H_B=0	T3, T4
H_C=0	T5, T6

Malfunction of Hall effect sensor with constant value one (H_A=1):

In this case of hall sensor fault i.e. for $H_A=1$, the performance of the drive remains unaltered to the ones for $H_A=0$ fault condition. However during this faulty condition by checking the switching signals for the VSI switches, it can be realized that the switches T5 and T4 remain OFF after fault, which is different to that of the previous fault condition (H_A=0). Similarly, the effect of various Hall effect sensor faults for constant value one are shown in *Table 5.3.2*.

Tab. 5.3.2 Switching signals during hall sensor fault (constant one).	
Faulty hall sensor	Non-conducting switches
H_A=1	T5, T4
H_B=1	T1, T6
H_C=1	T3, T2

5.3.1 Fault diagnosis and remedial strategies

Each Hall effect signal of BLDC motor has specific value at each instant of time with respect to permanent magnet rotor position. Electronic commutation is done by decoding the position sensor signals. Decoding rules of Hall Effect signals to choose a proper switching vector of VSI are shown in *Table 5.1*. As it can be seen in table there is no condition that all three hall signals being one or zero at a same time.

$$H_f = H_A + H_B + H_C \tag{5.3.1}$$

Where the value of H_f lies between 1 and 2 (i.e. $1 < H_f < 2$) for each specific electrical angle section. Hall effect sensors Fault Flag (HFF) is introduced for sensor fault detection if H_f value goes over of these limits. HFF is set to '1' if H_f value is more than 2 (it means that one of the position sensor signals is constant one), HFF is set to '-1' if H_f value is less than 1 (itmeans that one of the position sensor signals is constant zero) and HFF is '0' in case of no

fault. Maximum fault detection time is the time of on electrical rotation of rotor which is quite fast.

However identification of faulty sensor is impossible through Hall effect sensor Fault Flag. As the line voltages of BLDC motor are deteriorated due to position sensor failure, the Discrete Fourier transform (DFT) analysis is used for pattern recognition of the line voltages. DFT of line voltages are calculated by (5.3.2) for specific intervals of time. The minimum time interval for proper fault detection is one electrical rotation of motor. Spectral Energy Density (SED) of computed frequency spectrum is determined by (5.3.3). SED difference of successive time intervals are calculated and analyzed to identify the faulty position sensor.

$$V(f)=\sum_{n=0}^{N-1} V_n e^{-j2\pi k\frac{n}{N}} \qquad k=0,1,...,N \tag{5.3.2}$$

$$E_m(f)=|V(f)|^2 \tag{5.3.3}$$

$$\varepsilon_m = E_m(f)-E_{m-1}(f) \tag{5.3.4}$$

Hall effect Identification Flag (HIF) of each phase is introduced for faulty sensor identification. Numeric values are given to HIF of each phase according to SED errors of all three line voltages of BLDC motor as below,

- HIF is '-1' if SED error is negative;
- HIF is '1' if SED error is positive.

A multidimensional knowledge based table was introduced in [28] for position sensors fault diagnosis according to Fault detection and identification flags (HFF and HIF) by analyzing the above expressions (5.3.2) – (5.3.4) for Hall Effect position sensor faults of all phases of a BLDC motor. One of the advantages of this technique is that it is not necessary to know the exact line voltages of BLDC motor for different speed and loads in advance. Multidimensional knowledge based table for position sensor fault diagnosis of BLDC motor is shown in *Table 5.3.3*.

Tab. 5.3.3. Rule based position sensor fault identification table [28].

Fault type	HIF phase A	HIF phase B	HIF phase C	HFF
No fault	X	X	X	0
H_A=0	-1	1	1	-1
H_A=1	1	-1	-1	1
H_B=0	1	-1	1	-1
H_B=1	-1	1	-1	1
H_C=0	1	1	-1	-1
H_C=1	-1	-1	1	1

Once the faulty Hall effect sensor is identified, the corresponding sensor signal to the drive control system is disconnected and is substituted with an automated generated commutation signal by microcontroller. Commutation signal is generated based on 120 electrical degree phase difference from the other two Hall Effect signals. A new and simple method has been introduced to calculate electrical degree delays with respect to the time [32]. If motor speed is known and it does not change during commutation intervals (considering controller keeps the motor speed constant), the time of one electrical degree rotation of BLDC motor can be determined in seconds by (5.3.5), where P is the pole numbers and ω_{ref} is the reference speed of the controller in RPM [32].

$$t = \frac{1}{P/2\left(6 * \omega_{ref}\right)} \tag{5.3.5}$$

5.4 Conclusion

Fault tolerant control system for Hall effect position sensors failure of BLDC motor is discussed. Discrete Fourier transform (DFT) analysis is used for pattern recognition of the line voltages of BLDC motor. A knowledge based table is so useful in identifying the faulty sensors. Hence faulty position sensor is identified through spectral density error of the line voltages; exact knowledge of BLDC motor voltages for various speed and torque loads is not needed. Commutation signal of faulty sensor is generated by microcontroller through correlation between Hall signals. The above studied fault tolerant system is capable to detect, identify and rectify the Hall effect sensor break down in BLDC motor. The system has a simple algorithm and can be implemented with a closed loop control scheme of BLDC motor on a single chip microcontroller. Consequently reliability of BLDC motor drive is improved.

Chapter 6

Five-Phase PM BLDC Drive with Various Supply Modes and Torque Capabilities

6.1 Introduction

Efficiency, economy and flexibility are the major factors fostering the adoption of electric drives for executing key tasks in vehicular and aeronautic applications [3], [12], [15], [34]. In the vehicular sector, electric drives are used since many years for the propulsion of road vehicles; in the aeronautical sector, electric drives have been introduced – within the frame of the so-called more-electric aircraft concept – as actuators for flight control surfaces like rudders, ailerons, and flaps, whilst their use for the propulsion is nowadays limited to airplanes requiring low thrusts like drones or small-scale prototypes.

Commonly, electric drives for such applications have a three-phase structure. In recent times, however, some concerns have emerged in regard to the power capability, efficiency and fault-tolerance of this structure. As a response, more and more importance has been given to multiphase electric drives as they offer an effective solution to the above-mentioned issues. For instance, multiphase motors develop higher torque compared to conventional three-phase machines of equal size, and therefore are well-suited for heavy-duty tasks. Moreover, for a given power rating, they have a higher efficiency thanks to the lower additional losses in the motor and allow for using power electronic switches with lower current capability. However, the most important feature of the multiphase drives is related to their fault-tolerance features, which play a key role in vehicular and aeronautic applications like in any other safety-critical application [34]. In fact, multiphase drives guarantee a real fail-operation behavior in the presence of a fault in either the motor or the motor-supplying converter, although with degraded performance [12], [35].

The most straightforward multiphase structure of an electric drive has a five-phase arrangement. It fulfils the demand of improving power capability, efficiency and fault tolerance of the drive without excessively complicating its structure and, at the same time, maintaining the odd symmetrical properties of the three-phase structure. In particular, the fault tolerance demand is largely met as a five-phase drive can continue to work even with two faulty phases, of course with somewhat lower torque performance and provided that the drive is properly controlled.

Among the various kinds of electric drives, permanent-magnet (PM) brushless (BL) drives have got a reserved place because of their higher torque and power density [17], [36]. Out of the two basic PM BL motor arrangements, the PM BL drives of DC type (BLDC) are widely accepted whenever possible over the PM BL drives of AC type due to their simpler

electromagnetic configuration, easier control requirements and higher torque-per-ampere ratios [37].

Multiphase BLAC drives have been largely studied in the literature [38–41]. Instead, investigation on multiphase BLDC drives has been started only recently and, incidentally, under the prevalent assumption that their phases are supplied with a distorted current formed by a sinusoidal fundamental and some superimposed harmonics [42–55]. In particular, [43] and [44] deal with the issues of modeling a five-phase PM BLDC motor and injecting phase currents of convenient waveform, whereas [45] examines open circuit fault-tolerant capabilities under different types of windings and discusses strategies for the current control under a fault to improve the average motor torque.

This chapter investigates the torque capabilities of a five-phase PM BLDC drive. In contrast to the previous works, operation of the drive with square-wave currents is dealt with and various supply modes are analyzed, differing by the number of simultaneously conducting phases. A comparative evaluation of the torque capabilities is executed by taking the three-phase counterpart as a benchmark; power and phase resistance are also compared [46]. The terminology/parameters used in this chapter with subscripts 3 and 5 denotes three-phase and five-phase PM BLDC drive quantities, respectively.

6.2 Operation of Five Phase PM BLDC drive

Circuit scheme of a five-phase PM BLDC drive with star-connected stator phases and isolated neutral point is shown in *Figure 6.2.1*, where e_j with *j=a, b, c, d, e* is the back-emf of the motor phase j, V_{dc} is the voltage of the DC source feeding the drive, i_{dc} is the current flowing in the DC source, T_1, T_2… and T_{10} are the transistors of the VSI legs, and D_1, D_2 … and D_{10} are the corresponding free-wheeling diodes. To run the motor up to the nominal speed, the DC source voltage is set at the nominal motor voltage, i.e. $V_{dc} = V_N$.

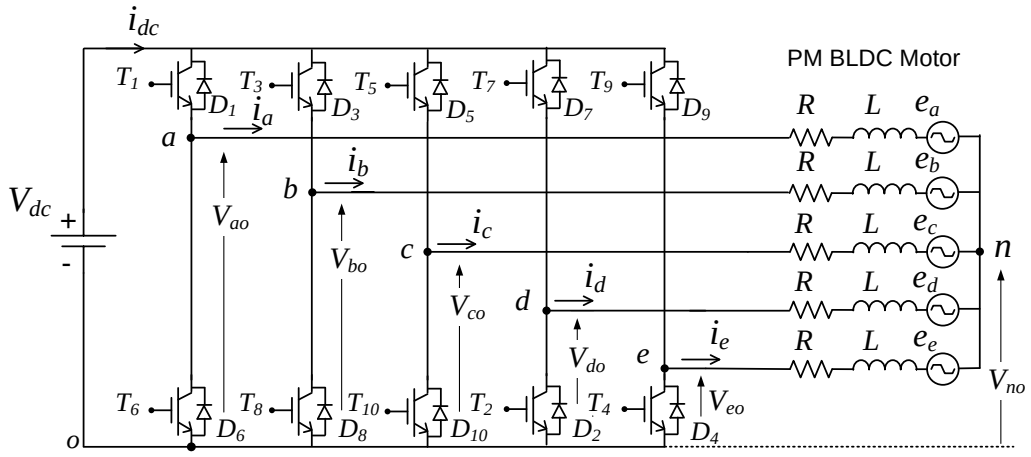

Fig. 6.2.1. Circuit scheme of five-phase PM BLDC drive.

The motor is characterized by a trapezoidal back-emf with positive and negative flat regions,

each of them with a flat region of 4π/5 electrical radians (144°) as depicted in *Figure 6.2.2*, where θ_e is the rotor position in electrical radians. For a phase to produce constant torque, a square-wave current is injected into the motor phases by the VSI, where the positive and negative flat region of current are as long as synchronized with the flat back-emf positive and negative flat regions (i.e. 4π/5 electrical radians), respectively. The commutation phenomena is disregarded for a moment.

By looking at the motor supply over the period, ten different supply intervals can be identified, having an angular length of π/5 electrical radians each. The supply intervals are designated with S1, S2, …, S10 in *Figure 6.2.2* and are defined by the circumstance that, during each supply interval, four specific VSI transistors are conducting, two in the upper side and two in the lower side of the VSI, so that -at any instant- four of the five motor phases are supplied. Conducting transistors rotate from one supply interval to the successive one as illustrated in *Figure 6.2.3*. The supply mode of the motor, where four phases conduct simultaneously with duration of the conduction intervals of 4π/5 for both positive and negative magnitude of the current, is the standard operating way of a five-phase PM BLDC drive.

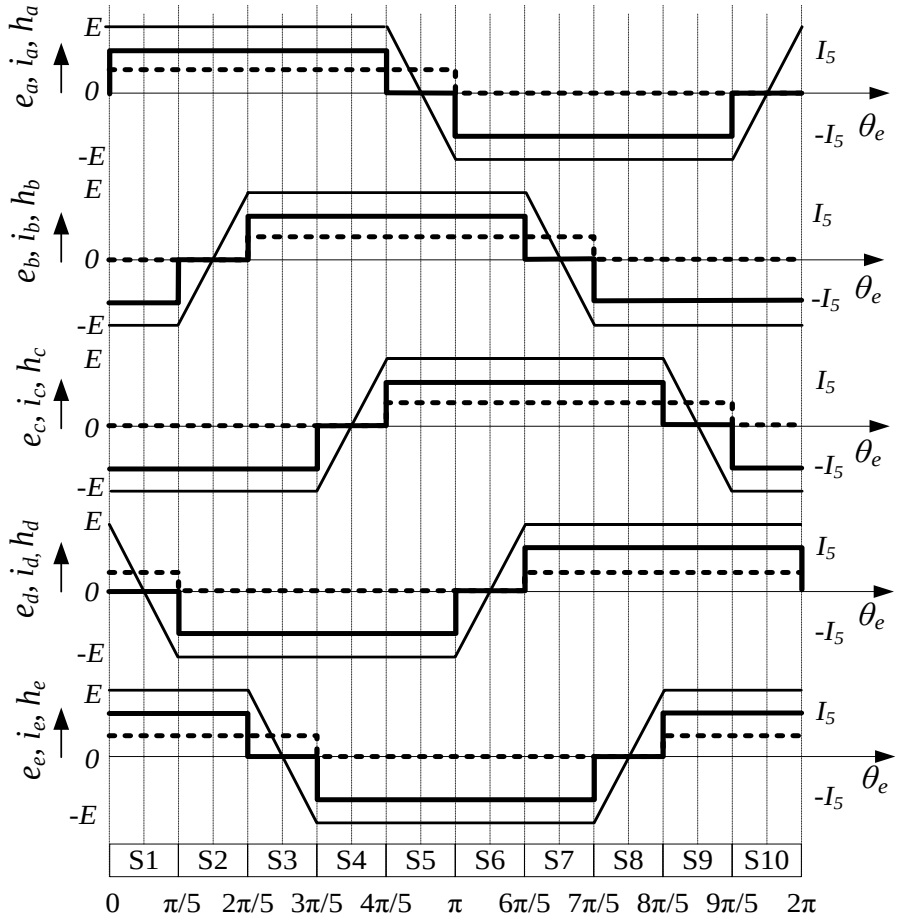

Fig. 6.2.2. Back-emfs (thin line), phase currents (bold line), Hall-sensor signals (dashed line) and supply intervals of five-phase PM BLDC motor.

As an example, *Figure 6.2.2* points out that the conduction interval of phase *a* with positive current magnitude starts at $\theta_e = 0$ and finishes at $\theta_e = 4\pi/5$. The conduction interval embraces four supply intervals, namely S1, S2, S3 and S4. Specifically, during supply interval S1, transistor T1 conducts together with T8, T10 and T9; during supply interval S2 together with T10, T2 and T9, and so on.

To synchronize the phase currents with the back-emfs, five Hall sensors are mounted on the stator of the motor and generate the signals denoted with *h* in *Figure 6.2.2*.

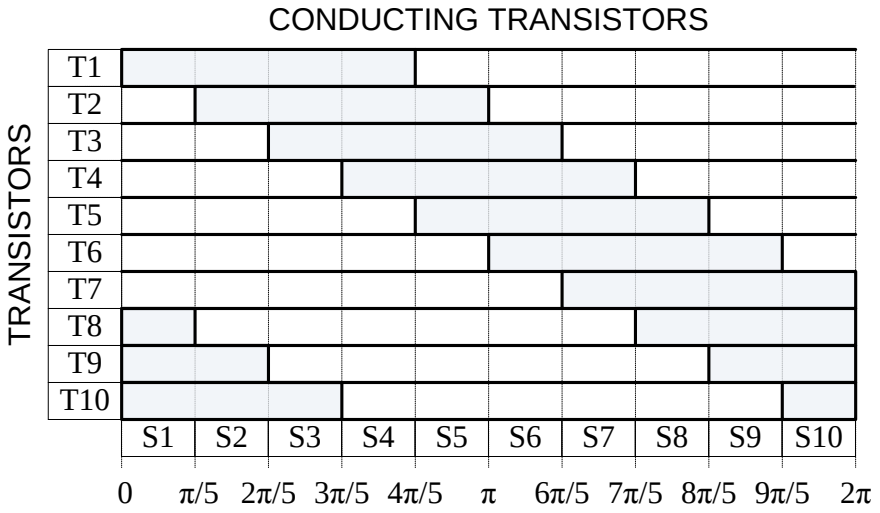

Fig. 6.2.3. Conducting transistors and supply intervals.

6.3 Basic equations

Magnitude E_5 of the phase back-emf in the flat region is given by the back-emf constant k_5 times the motor mechanical speed Ω, i.e. to

$$E_5 = k_5 \Omega \tag{6.3.1}$$

The rotor position θ_e in *Figure 6.2.2* is equal to $\Omega_e t$, where the motor speed in electrical rad/sec Ω_e is related to the motor speed Ω by the number of pole-pairs n_p, i.e.by

$$\Omega_e = n_p \Omega \tag{6.3.2}$$

The phase currents are constrained by the Kirchhoff's current law, i.e. by

$$\sum_{j=a,b,c,d,e} i_j = 0 \tag{6.3.3}$$

The electrical power p_5 that the motor converts into mechanical form is expressed as

$$p_5 = \sum_{j=a,b,c,d,e} e_j i_j \tag{6.3.4}$$

and the corresponding instantaneous torque developed by the motor, assuming that the motor

speed is constant, is

$$\tau_5 = \frac{p_5}{\Omega} \tag{6.3.5}$$

Four phases are simultaneously conducting at any time. This means that the mechanical power (apart from losses) is

$$P_5 = 4E_5 I_5 \tag{6.3.6}$$

and the developed average torque becomes

$$T_5 = 4k_5 I_5 \tag{6.3.7}$$

Note that, in nominal speed conditions, E_5 equals $V_N/2$ and the DC source current I_{dc} is twice I_5.

6.4 Five-phase vs. Three-phase drive

Torque capabilities of a five-phase PM BLDC drive are compared to the three-phase counterpart by taking two motors with equal overall dimensions (stator and rotor diameters, and core lengths). In particular, the conductor of each phase has the total length *l*, including winding overhang portion. Further assumptions for the comparison are as follows:

i) the two motors have the same rotor,
ii) the two motors are equally loaded from a thermal point of view; this means that they have the same total copper losses (P_{Cu}), distributed over the same total copper cross-section area (S_{Cu}),
iii) the two motors have an equal speed range.

It can be noted that, since the two motors have the same core length and the same copper cross section, they also have the same overall copper volume, while the operation of the motor in nominal conditions is considered.

The comparison will be made under two different hypotheses, namely the five-phase and three-phase motors having

i) An equal phase back-emf.
ii) An equal rms value of the phase current.

6.4.1 Equal phase back-emf hypothesis

Let the five-phase and three-phase motors have the same phase back-emf, i.e. let $E_5=E_3=E$. By assumption (iii), the two motors have an equal back-emf constant.

$$k_5 = k_3 = k \tag{6.4.1}$$

By (6.4.1) and as per assumption (i), the two motors have an equal number of series-connected conductors per phase

$$N_{c5} = N_{c3} = N_c \tag{6.4.2}$$

The total copper cross section area for the two motors is

$$S_{Cu5} = 5N_c S_{c5} \tag{6.4.3}$$

$$S_{Cu3} = 3N_c S_{c3} \tag{6.4.4}$$

As per assumption (ii), S_{cu5} and S_{cu3} are equal; then

$$\frac{S_{c5}}{S_{c3}} = \frac{3}{5} \tag{6.4.5}$$

The phase resistance for the two motors is

$$R_5 = \rho_{Cu} \frac{N_c l}{S_{c5}} \tag{6.4.6}$$

$$R_3 = \rho_{Cu} \frac{N_c l}{S_{c3}} \tag{6.4.7}$$

where ρ_{Cu} is the copper resistivity. From (6.4.6) and (6.4.7), it follows that:

$$\frac{R_5}{R_3} = \frac{5}{3} \tag{6.4.8}$$

The copper losses P_{Cu} of the two motors are

$$P_{Cu5} = 5R_5 {I_{rms5}}^2 \tag{6.4.9}$$

$$P_{Cu3} = 3R_3 {I_{rms3}}^2 \tag{6.4.10}$$

As per assumption (ii), $P_{Cu5} = P_{Cu3}$, Then, by considering (6.4.8), it is

$$\frac{I_{rms5}}{I_{rms3}} = \frac{3}{5} \tag{6.4.11}$$

Reminding that a five-phase motor operates with a current conduction interval of $4\pi/5$ and a three-phase motor with a current conduction interval of $2\pi/3$, the following relationships hold between the rms value and the magnitude of the currents in the two cases:

$$I_{rms5} = \sqrt{\frac{4}{5}} I_5 \tag{6.4.12}$$

$$I_{rms3} = \sqrt{\frac{2}{3}} I_3 \tag{6.4.13}$$

On solving (6.4.11) – (6.4.13), we get

$$\frac{I_5}{I_3} = \sqrt{\frac{3}{10}} \tag{6.4.14}$$

Phase self-inductance is proportional to the square of the number of turns, turn length and the air gap section. Then, according to (6.4.2) and the assumptions on the motor dimensions, the two motors have an equal phase self-inductance, i.e. $L_5 = L_3$, apart from small

discrepancies due to leakage component of the inductance and the distribution factor of the windings.

In terms of power, a three-phase PM BLDC drive has two simultaneously conducting phases at each instant and, hence, the electrical power converted into mechanical form and the relevant developed torque are

$$P_3 = 2EI_3; \quad T_3 = 2kI_3 \tag{6.4.15}$$

From (6.3.6), (6.3.7), (6.4.14) and (6.4.15), it results

$$\frac{P_5}{P_3} = \frac{T_5}{T_3} = \sqrt{\frac{6}{5}} \cong 1.095 \tag{6.4.16}$$

Equation (6.4.16) shows that, under the comparison assumptions and the hypothesis of an equal phase back-emf, the torque developed by the five-phase PM BLDC drive is 9.5% greater than the three-phase counterpart.

6.4.2 Equal phase rms current hypothesis

Let the five-phase and three-phase motors have the same rms value of the phase current, i.e. let I_{rms3}= I_{rms5}= I_{rms}. By (6.4.12) and (6.4.13), the magnitude of the current for the two motors are

$$\frac{I_5}{I_3} = \sqrt{\frac{5}{6}} \tag{6.4.17}$$

As per assumption ii), the total copper losses P_{Cu} for the two motors are equal. Therefore the current density σ_{Cu} must be also equal since the copper losses are given by

$$P_{Cu} = \rho_{Cu} V_{Cu} \sigma_{Cu}^{\ 2} \tag{6.4.18}$$

where the copper resistivity ρ_{Cu} and the copper volume V_{Cu} are equal for the two motors. Moreover, the two motors must also have an equal value of the conductor cross section as a consequence of the fact that they have equal values of both the current density and the phase rms current, i.e. it is

$$S_{c5} = S_{c3} = \frac{I_{rms}}{\sigma_{Cu}} \tag{6.4.19}$$

Again as per assumption ii), the total copper cross-section area S_{Cu} for the two motors is equal. Then, from (6.4.3) and (6.4.4), it follows that the ratio between the number of series-connected conductors for the two motors is

$$\frac{N_{c5}}{N_{c3}} = \frac{3}{5} \tag{6.4.20}$$

Therefore the relations between the phase resistance and self-inductance are as follows:

$$\frac{R_5}{R_3} = \frac{3}{5} \tag{6.4.21}$$

$$\frac{L_5}{L_3} = \frac{9}{25} \tag{6.4.22}$$

Being the back-emf constants proportional to the number of series-connected turns per phase, the same ratio as (6.4.20) exists both between the back-emf constants of the two motors

$$\frac{k_5}{k_3} = \frac{3}{5} \tag{6.4.23}$$

and, as per assumption i), between their back-emfs

$$\frac{E_5}{E_3} = \frac{3}{5} \tag{6.4.24}$$

Finally, the electrical power converted into mechanical form and the developed torque for a three-phase drive can here be expressed as

$$P_3 = 2E_3I_3; \quad T_3 = 2k_3I_3 \tag{6.2.25}$$

From (6.3.6), (6.3.7) and (6.4.23) – (6.4.25), the same power and torque relationships as in *Section 6.4.1* (6.4.16) are found under the comparison assumptions and the hypothesis of an equal phase rms current.

6.4.3 Comparision remarks

A five-phase PM BLDC drive has been compared to its three-phase counterpart under the assumptions of motors with equal size and copper volume, and having the same rotor. Comparison has been made at first by assuming an equal back-emf, and then an equal phase rms current. It has been found that, in both the cases, the five-phase PM BLDC drive is capable of developing a torque that is 9.5% higher than the torque developed from the three-phase drives.

6.5 Operation with simultaneous conduction of a reduced number of phases

In *Section 6.2*, the standard supply mode of a five-phase PM BLDC has been discussed. A study is also carried out on the five phase PM BLDC drive to analyze/observe the torque developed by the drive with a reduced number of motor phases that conduct simultaneously. The study will be useful in view of approaching the fault-tolerance management of the drive. Two supply modes are considered:

i) Simultaneous conduction of three motor phases (*Supply mode #3*)
ii) Simultaneous conduction of two motor phases (*Supply mode #2*)

6.5.1 Supply mode #3

When three motor phases conduct contemporaneously, the current enters one phase and outputs from the other two phases or vice versa. In this case, the conduction interval of each motor phase is 3π/5 and the currents in the three phases do not have the same magnitude. Furthermore, by maintaining a current square waveform, it results that the phase currents as shown in *Figure 6.5.1*, where the maximum value is indicated with $I_{5/3}$. *Figure 6.5.2* gives the conducting transistors with the relevant supply intervals and points out that the motor phases start conducting in the mid instant of a supply intervals -as defined for the standard supply mode- and finishes 3π/5 later.

The developed torque is still constant over the supply period and its expression is now given by

$$T_{5/3} = 2k_5 I_{5/3} \tag{6.5.1}$$

whilst the current flowing in the DC source is $I_{5/3}$. The rms value of the phase current is

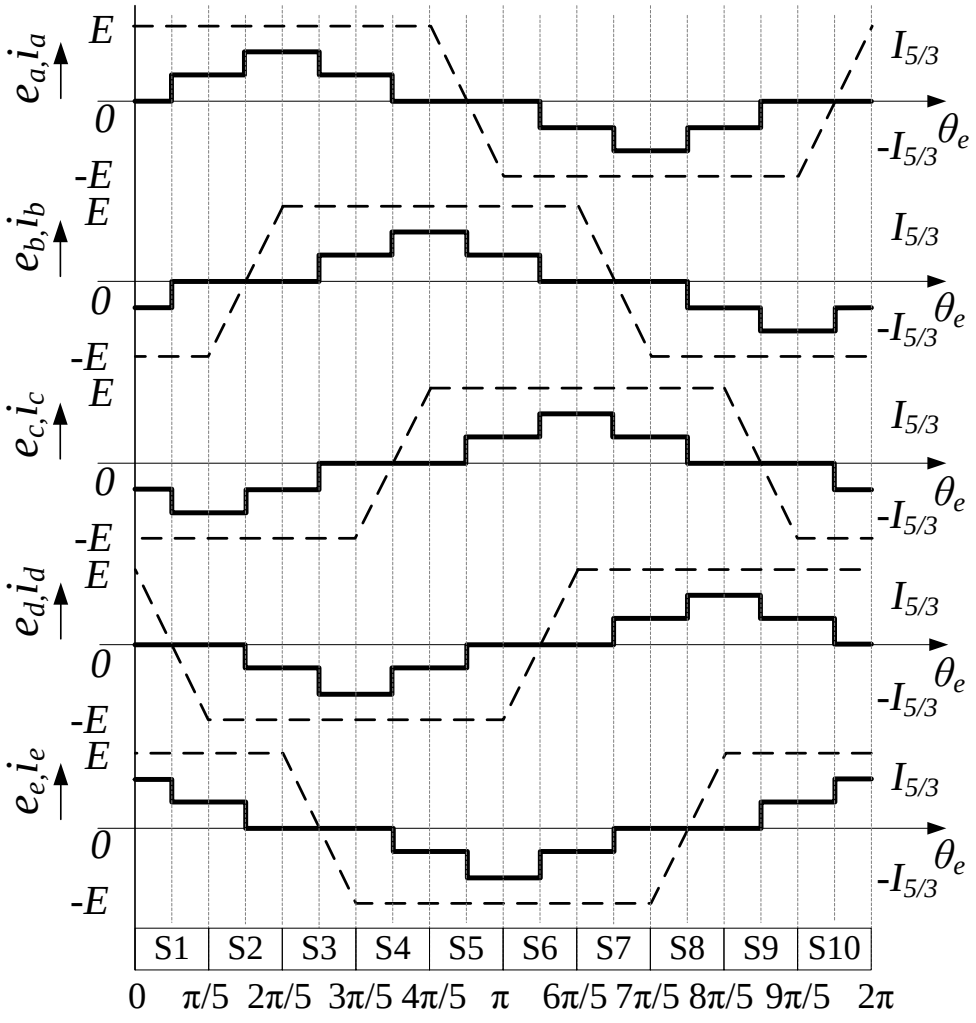

Fig. 6.5.1. Back-emfs (dotted line), phase currents (solid line) of five-phase PM BLDC motor during supply mode #3.

$$I_{rms5/3} = \sqrt{\frac{3}{10}}\, I_{5/3} \tag{6.5.2}$$

For the copper losses to be the same as in the standard supply mode, $I_{rms5/3}$ must be equal to I_{rms5}. Then, by equating (6.4.12) and (6.5.2), it becomes

$$I_{5/3} = 2\sqrt{\frac{2}{3}}\, I_5 \tag{6.5.3}$$

Equations (6.5.1) and (6.5.3) show that the torque developed by the drive under supply mode #3 is

$$T_{5/3} = \sqrt{\frac{2}{3}}\, T_5 \tag{6.5.4}$$

i.e. it is about 0.8 times the torque developed with the standard supply mode. The same relationship applies to the electrical power converted into mechanical form.

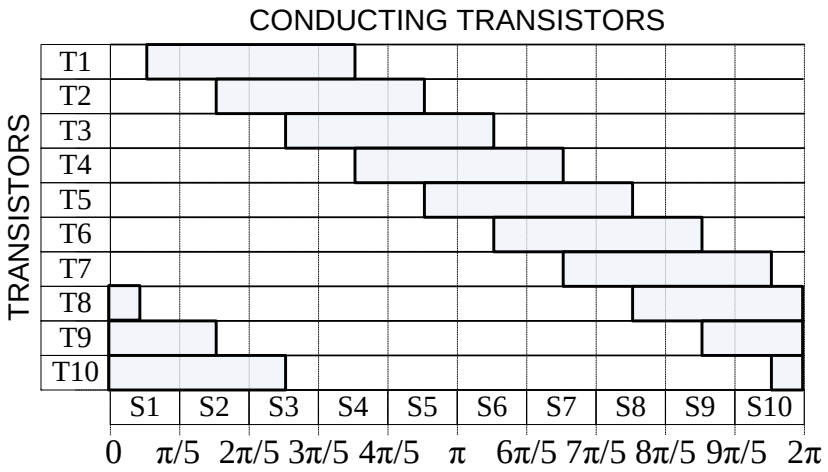

Fig. 6.5.2. Conducting transistors and supply intervals during supply mode #3.

6.5.2 Motor phase current allocation

With the simultaneous conduction of three motor phases, the currents can be allocated at the center of the flat-zone of the relevant back-emfs as illustrated in *Figure 6.5.1*. This allocation, however, requires an interpolation of the Hall signals to find out the starting (and ending) angle of the current conduction intervals. The problem can be circumvented by shifting the currents in advance by π/10 electrical radians so as to align their beginning with the flat region of the relevant back-emfs. The shift does not change the power and torque profile of the drive and, then, their values. The new allocation is illustrated in *Figure 6.5.3*.

The last result is an evidence of the existence of some degree of freedom in locating the current conduction intervals with respect to the back-emf waveform when the intervals are less than 4π/5. In particular, in *Figure 6.5.3* the phase currents are shifted by π/10 from the

allocation at the center of the flat back-emf region. This implies that the fundamental component of the currents is no longer in phase with the fundamental component of the back-emfs; in spite of this, the electrical power converted into mechanical form and, hence, the developed torque does not change. The result might seem surprising because the power associated to the fundamental components of the phase back-emfs and currents actually changes in the two cases. Indeed, their magnitudes do not vary while their power displacement is 1 for the supply current allocation in *Figure 6.5.1* and less than 1 in *Figure 6.5.3*. Nevertheless the result is consistent with the fact that the electrical power converted into mechanical form is produced not only by the fundamental components of the phase back-emfs and currents, but also by their higher order harmonics, including the harmonics multiple of three. Hence, what actually happens when moving the supply current allocation of *Figure 6.5.1* to the one in *Figure 6.5.3* is that i) the contribution of the fundamental components of phase back-emfs and currents to the electrical power converted into mechanical form decreases, and ii) the decrease is compensated for by the increase in the contribution of the other harmonics. An analytical formulation of this assertion is as follows:

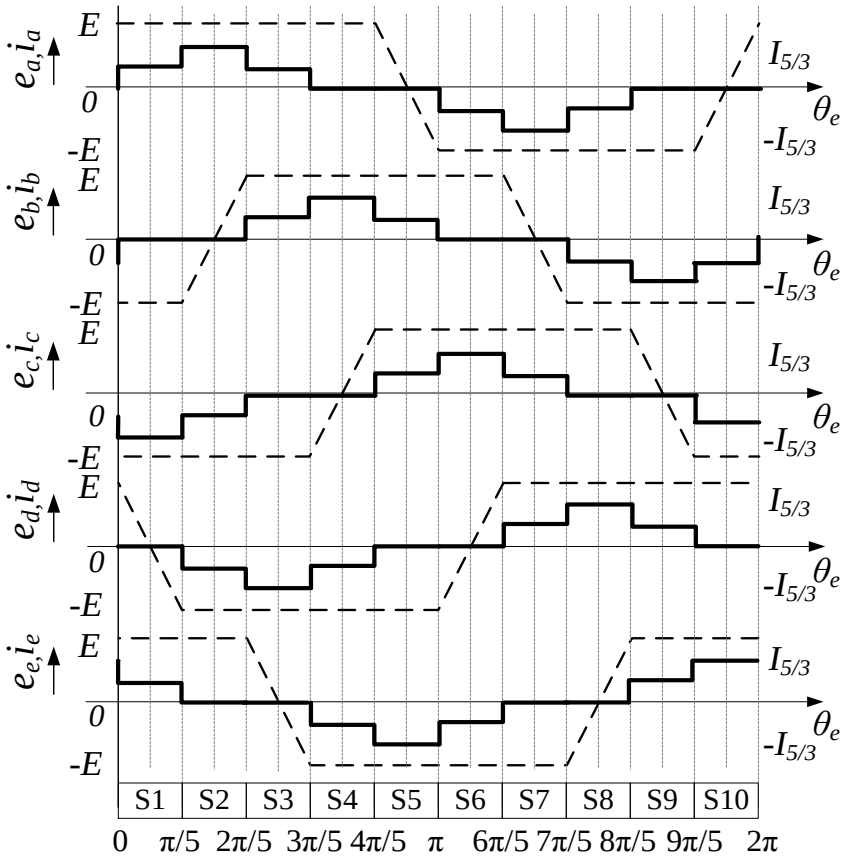

Fig. 6.5.3. Convenient motor phase current allocation in supply mode #3.

Let us consider the waveforms of phase back-emfs and currents in *Figure 6.5.1* and, for the sake of simplifying the computation, let us move the origin of the abscissa axis at $\theta_e = -\pi/10$. The back-emf of phase *a* can be expanded in Fourier series as follows:

$$e(\theta_e) = E\sum_{n=1}^{\infty} \hat{E}_n \sin(n\theta_e) \tag{6.5.5}$$

where n is an odd integer and the coefficients $\hat{E}_n$ are non-dimensional quantity expressed as

$$\hat{E}_n = \frac{40}{\pi^2 n^2}(-1)^{\frac{n-1}{2}} \cos\left(\frac{2n\pi}{5}\right) \tag{6.5.6}$$

In turn, the current of the phase a can be expanded in Fourier series as follows:

$$i(\theta_e) = I_{5/3}\sum_{n=1}^{\infty} \hat{I}_n \sin(n\theta_e) \tag{6.5.7}$$

where n is still an odd integer and the coefficients $\hat{I}_n$ are non-dimensional quantities expressed as

$$\hat{I}_n = \frac{8}{n\pi}(-1)^{\frac{n-1}{2}} \cos^2\left(\frac{n\pi}{10}\right)\sin\left(\frac{n\pi}{10}\right) \tag{6.5.8}$$

It can be readily verified that the coefficients $\hat{I}_n$ with n multiple of 5 are zero. The phase angles between harmonics of the same order of the phase back-emfs and currents are zero.

For the supply current allocation in *Figure 6.5.3*, the coefficients of $\hat{I}_n$ and, of course of $\hat{E}_n$, do not change while the phase angles are now given by

$$\varphi_n = n\frac{\pi}{10} \tag{6.5.9}$$

Tab. 6.5.2.1. Harmonic contribution to the power

Harmonic order	Fourier coefficients		$P_n/(EI_{5/3}) = \hat{E}_n\hat{I}_n\cos(\varphi_n)$	
	Phase back-EMF($\hat{\mathbf{E}}_\mathbf{n}$)	Phase current ($\hat{\mathbf{i}}_\mathbf{n}$)	Centered	Shifted
1	1.2524	0.7118	0.4457	0.4239
3	0.3643	-0.2373	-0.0432	-0.0254
5	0.1621	0	0	0
7	0.0669	-0.1017	-0.0034	0.002
9	0.0155	0.0791	0.0006	-0.0006
11	-0.0104	0.0647	-0.0003	0.0003
13	-0.0194	-0.0548	0.0005	-0.0003
15	-0.018	0	0	0
17	-0.0113	-0.0419	0.0002	0.0001
19	-0.0035	0.0375	-0.0001	-0.0001
21	0.0028	0.0339	0	0
23	0.0062	-0.309	-0.0001	-0.0001
25	0.0065	0	0	0
		SUM	**0.4**	**0.4**

Table 6.5.2.1 reports the harmonics of order up to 25 for $\hat{E}_n$ and $\hat{I}_n$ together with the contribution of the back-emf and current harmonics to the electrical power converted into mechanical form for a phase, expressed as a fraction of $EI_{5/3}$. The total power is obtained by multiplying the value of power in the table by 5 (the number of the phases). The table clearly shows that the total power of a phase remains constant for the two supply current allocations. Another outcome that emerges from the table is that, apart from the fundamental component, the major contribution to the power is given by the harmonics of order 3 and 7.

6.5.3 Supply mode #2

When two motor phases conduct contemporaneously, the current enters one phase and exits another phase. Then the conduction interval of each motor phase is 2π/5. By maintaining a current square waveform, it results that the currents have the waveform in *Figure 6.5.4*, where the maximum current is indicated with $I_{5/2}$. *Figure 6.5.5* gives the conducting transistors with the relevant supply intervals and points out that the motor phases start conducting at the beginning of a supply interval like in the standard supply mode and finishes two supply intervals later instead of four. Similarly to supply mode #3, the current conduction can be shifted in advance of 2π/5 electrical radians without modifying the resultant torque.

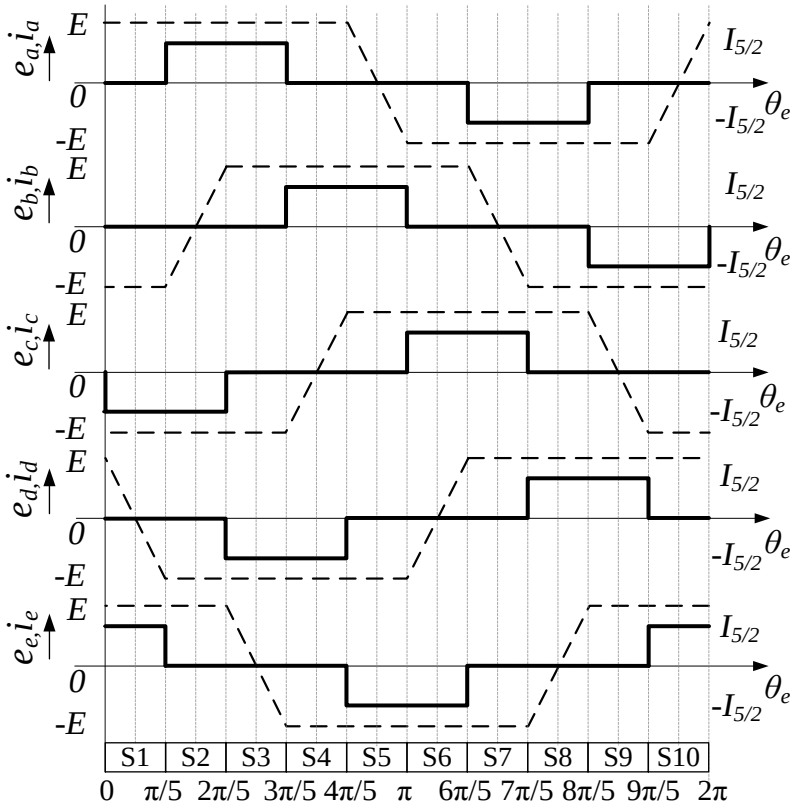

Fig. 6.5.4. Back-emfs (dotted line), phase currents (solid line) with supply mode #2, and supply intervals of five-phase PM BLDC motor.

The developed torque is still constant over the supply period and its expressions is given by

$$T_{5/2} = 2k_5 I_{5/2} \tag{6.5.10}$$

whilst the current flowing in the DC source is $I_{5/2}$.The rms value of the phase current is

$$I_{rms5/2} = \sqrt{\frac{2}{5}}\, I_{5/2} \tag{6.5.11}$$

For the copper losses to be the same as in the standard supply mode, $I_{rms5/2}$ must be equal to I_{rms5}. Then, by equating (6.4.12) and (6.5.11), it results

$$I_{5/2} = \sqrt{2}\, I_5 \tag{6.5.12}$$

Equations (6.5.10) and (6.5.12) show that the torque developed by the drive under supply mode #2 is equal to

$$T_{5/2} = \frac{1}{\sqrt{2}} T_5 \tag{6.5.13}$$

i.e. it is about 0.7 times the torque developed with the standard supply mode. The same relationship applies to the electrical power converted into mechanical form. Note that the torque here is not too much less than the value obtained for the supply mode #3.

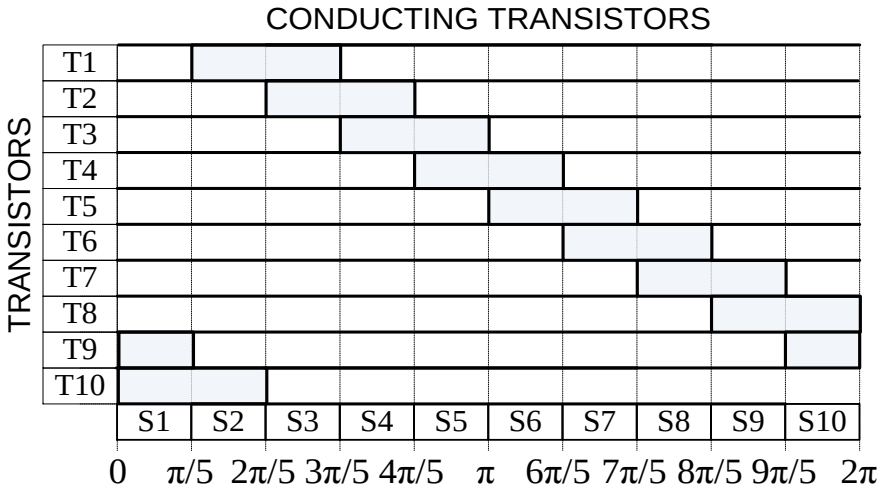

Fig. 6.5.5. Conducting transistors and supply intervals during supply mode #2

6.6 Conclusion

This chapter deals with the torque capabilities of a PM BLDC drive with a five-phase structure, which is a promising solution for its simplicity with respect to the ones with a greater number of phases to attain high torque, better efficiency and fault-tolerant features. Differently from what is usually done in the literature, the five-phase PM BLDC drive has been investigated by assuming the motor supplied with square-wave currents. Firstly the analysis started with the torque capabilities of a five-phase PM BLDC drive compared to a

three-phase counterpart having a motor with equal dimensions and magnetic structure. From the comparison it has been found that the five-phase PM BLDC drive is able to develop a torque 9.5% higher than the three-phase one. Later on the analysis is carried with the torque capabilities of the five-phase PM BLDC drive when the simultaneous conduction does not involve four motor phases like in the standard supply. As a feasibility, two supply modes have been evaluated, where three or two phases are conducting simultaneously with conduction intervals of $3\pi/5$ and $2\pi/5$, respectively. It has been found that in these supply modes the torque capability of a five-phase PM BLDC drive decreases of about 20% and 30% respectively, compared to the standard supply. Therefore, it does not appear convenient to use these supply modes in a healthy five-phase motor; however, their study has represented a preliminary analysis of the drive behavior in faulty conditions, i.e. when one or more motor phases are out-of-service.

Chapter 7

Analytical Study of the Behavior of Five-Phase PM BLDC Drive Under Square Wave Phase Currents

7.1 Introduction

Five-phase PM BLDC drives are characterized by a trapezoidal phase back emf with two flat portions whose length in electrical radians is $4\pi/5$ [42–43]. Like the three-phase PM BLDC drives, the five-phase PM BLDC drives require the injection of square-wave phase currents synchronized with the flat portion of the back-emfs for the drives to develop constant torque with maximum torque-per-ampere factor. In the existing literature, however, five-phase PM BLDC drives with sinusoidal-like phase currents have been mostly investigated [43–44], [47] in spite of the fact that their set-up needs a high-resolution transduction of the rotor position for the current synchronization. Less attention, instead, has been paid to the five-phase PM BLDC drives with square-wave current supply even if they have a more robust set-up due to the use of less troubling Hall sensors.

In this chapter the five-phase PM BLDC drive is investigated with square-wave supply. Injection and removal of steeply edged currents from the motor phases are limited by the phase inductances and the finite value of the drive supply voltage, causing the deviation of the current waveform from the ideal shape and the ensuing onset of unwanted effects on the drive torque. Focus is on the study of these effects as they are the main inconveniences in the use of a square-wave current supply. Such a study has been faced and experimentally validated in [20] for a three-phase PM BLDC drive. The study for a five-phase PM BLDC drive presents some differences with respect to three-phase counterpart. Indeed, while the motor phases are in parallel two at a time during the constant current supply, all the five

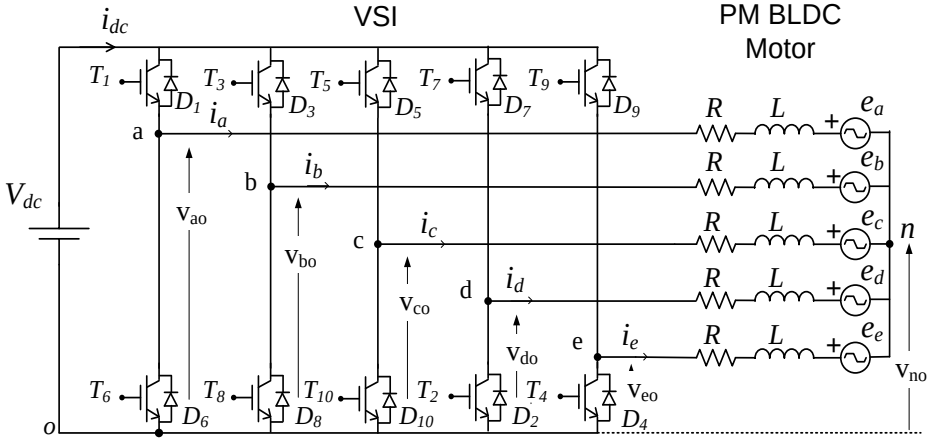

Fig. 7.1. Circuit scheme of a five-phase PM BLDC drive.

phases are conducting during the commutations. Furthermore, during the commutations, some of the phases are solicited with a fixed voltage whilst the other ones can be solicited with adjustable voltages, giving rise to many possible transients of the phase currents, which are analyzed in detail.

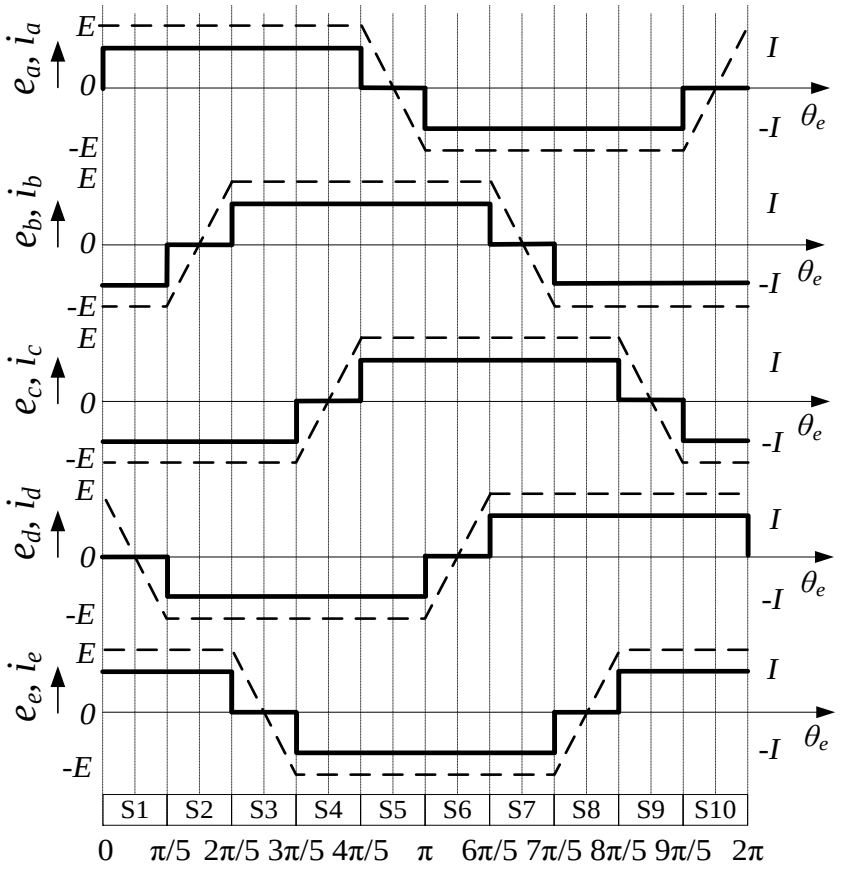

Fig. 7.2. Back-emfs (dashed line), phase currents (bold line), and supply intervals of five-phase PM BLDC motor.

7.2 Five phase PM BLDC drive

The circuit scheme of a 5-phase PM BLDC drive with no neutral connection is shown in *Figure 7.1*, where the motor is represented by its equivalent circuit and the voltage source inverter (VSI) that supplies the motor is represented with its five legs. In the figure, R and L and e_j with $j=a, b, c, d, e$ are the resistance, the self-inductance and the back-emfs of the phases.

In this chapter, square waveforms are assumed for the motor phase currents, thus disregarding the commutation phenomena. Phase back-emfs and currents of the motor are drawn in *Figure 7.2* as a function of the rotor position θ_e in electrical radians. Both the back-emfs and the currents of the phases are displaced by $2\pi/5$ apart. The relations between θ_e, the motor speed Ω_e in electrical rad/s, and the motor speed Ω in mechanical rad/s are

$$\theta_e = \Omega_e t; \quad \omega_e = n_p \Omega \tag{7.2.1}$$

where n_p is the number of pole pairs.

The magnitude E of the phase back-EMF's is proportional to the motor speed according to

$$E = k\Omega \tag{7.2.2}$$

where k is the motor constant. The instantaneous electrical power p converted into mechanical form is

$$p = \sum_{j=a,b,c,d,e} e_j i_j \tag{7.2.3}$$

Hence, the instantaneous torque developed by the drive is calculated as

$$\tau = p/\Omega \tag{7.2.4}$$

For the current supply shown in *Figure 7.2*, p is equal to *4EI*, where *I* is the square-wave current magnitude. Therefore the torque is constant and proportional to *I*, i.e.

$$T = 4kI \tag{7.2.5}$$

The rms value of the currents in the motor phases is [53]

$$I_{rms} = \sqrt{\frac{4}{5}} I \tag{7.2.6}$$

With respect to a three-phase PM BLDC drive, in a 5-phase one the following facts are observed:

- The torque expression contains the coefficient 4 instead of 2; this is due to the fact that 4 motor phases instead of 2 are conducting in each supply interval.
- The phase currents contain harmonics multiple of 3 whilst do not contain harmonics multiple of 5; this is due to the fact that the phase currents are shifted by $2\pi/5$ instead of $\pi/3$.
- For a given value of *I*, the rms value of the phase currents is greater in the 5-phase case; this is due to the fact that the phases conduct the current for a longer interval.

By neglecting the voltage drop on the phase resistance, the following relations hold in nominal conditions between the DC source voltage, the back-emf magnitude, the drive speed, the rms phase current and the motor torque:

$$V_N = 2E_N; \Omega_N = \frac{V_N}{2k}; I_{rms,N} = \sqrt{\frac{4}{5}} I_N; T_N = 4kI_N \tag{7.2.7}$$

Where subscript N stand for the nominal condition.

The average value I_{dc} of the DC link current is given by

$$I_{dc} = \frac{4EI}{V_N} \tag{7.2.8}$$

for motor speed and phase current below the nominal values. In nominal conditions, I_{dc} becomes equal to $2I_N$.

Current behavior is obtained from the following phase voltage equations, written in matrix form:

$$\mathbf{v} = \mathbf{L}\frac{d\mathbf{i}}{dt} + \mathbf{e} \tag{7.2.9}$$

where **v**, **i, e** and **L** are respectively the vector of the voltages applied to the motor phases, the vector of the currents flowing into the motor phases, the vector of the phase back-emfs and the inductance matrix. The vectors **v**, **i, e** are expressed as

$$\mathbf{v} = \begin{vmatrix} v_{ao} - v_{no} \\ v_{bo} - v_{no} \\ v_{co} - v_{no} \\ v_{do} - v_{no} \\ v_{eo} - v_{no} \end{vmatrix}, \quad \mathbf{i} = \begin{vmatrix} i_a \\ i_b \\ i_c \\ i_d \\ i_e \end{vmatrix}, \quad \mathbf{e} = \begin{vmatrix} e_a \\ e_b \\ e_c \\ e_d \\ e_e \end{vmatrix} \tag{7.2.10}$$

The matrix **L,** by neglecting the leakage inductance of the motor phases and by recognizing that the phases are shifted of $2\pi/5$ each other, can be expressed as

$$\mathbf{L} = L\begin{vmatrix} 1 & \cos\left(\frac{2\pi}{5}\right) & \cos\left(\frac{4\pi}{5}\right) & \cos\left(\frac{6\pi}{5}\right) & \cos\left(\frac{8\pi}{5}\right) \\ \cos\left(\frac{8\pi}{5}\right) & 1 & \cos\left(\frac{2\pi}{5}\right) & \cos\left(\frac{4\pi}{5}\right) & \cos\left(\frac{6\pi}{5}\right) \\ \cos\left(\frac{6\pi}{5}\right) & \cos\left(\frac{8\pi}{5}\right) & 1 & \cos\left(\frac{2\pi}{5}\right) & \cos\left(\frac{4\pi}{5}\right) \\ \cos\left(\frac{4\pi}{5}\right) & \cos\left(\frac{6\pi}{5}\right) & \cos\left(\frac{8\pi}{5}\right) & 1 & \cos\left(\frac{2\pi}{5}\right) \\ \cos\left(\frac{2\pi}{5}\right) & \cos\left(\frac{4\pi}{5}\right) & \cos\left(\frac{6\pi}{5}\right) & \cos\left(\frac{8\pi}{5}\right) & 1 \end{vmatrix} \tag{7.2.11}$$

For drive operation below the nominal speed and current, chopping of the leg transistors is necessary to regulate the phase currents. Hereafter, it is assumed to chop only the upper transistors of the two legs carrying on the current entering in the motor phases (unipolar VSI command). According to the conventions of *Figure 7.1*, this means that the relevant currents are positive. Let *j* be the leg that is chopped. The terminal voltage of the phase *j* is

$$v_{jo} = \delta_j V_N \tag{7.2.12}$$

where δ_j is the chopping duty-cycle. *Table 7.2.1* reports the conducting devices during each one of the ten $\pi/5$-long supply intervals that form the supply period.

Tab. 7.2.1. Conducting devices vs. supply intervals.

Phase/ Supply Interval	***a***	***B***	***c***	***d***	***e***
S1	T_1, D_6	T_8	T_{10}	-	T_9, D_4
S2	T_1, D_6	-	T_{10}	T_2	T_9, D_4
S3	T_1, D_6	T_3, D_8	T_{10}	T_2	-
S4	T_1, D_6	T_3, D_8	-	T_2	T_4
S5	-	T_3, D_8	T_5, D_{10}	T_2	T_4
S6	T_6	T_3, D_8	T_5, D_{10}	-	T_4
S7	T_6	-	T_5, D_{10}	T_7, D_2	T_4
S8	T_6	T_8	T_5, D_{10}	T_7, D_2	-
S9	T_6	T_8	-	T_7, D_2	T_9, D_4
S10	-	T_8	T_{10}	T_7, D_2	T_9, D_4

7.3 Phase current behaviour around commutation

7.3.1 Just before commutation

The commutation at θ_e=0 is examined as a template and operation at nominal current is considered as the worst-case situation. Before the commutation as shown in *Figure 7.3.1(a)*, the transistors T_1 and T_6 of the leg *a* are OFF, the transistors T_7 and T_9 of the legs *d* and *e* are chopped with duty-cycles δ_d and δ_e, and the transistors T_8 and T_{10} of the legs *b* and *c* are kept ON. By imposing in (7.2.9) that the currents of the phases *d* and *e* are regulated at I_N, it is

$$\delta_d = \delta_e = \frac{2E}{V_N} \tag{7.3.1}$$

whilst the terminal voltages of the phases *b* and *c* are

$$v_{bo} = 0; \quad v_{co} = 0 \tag{7.3.2}$$

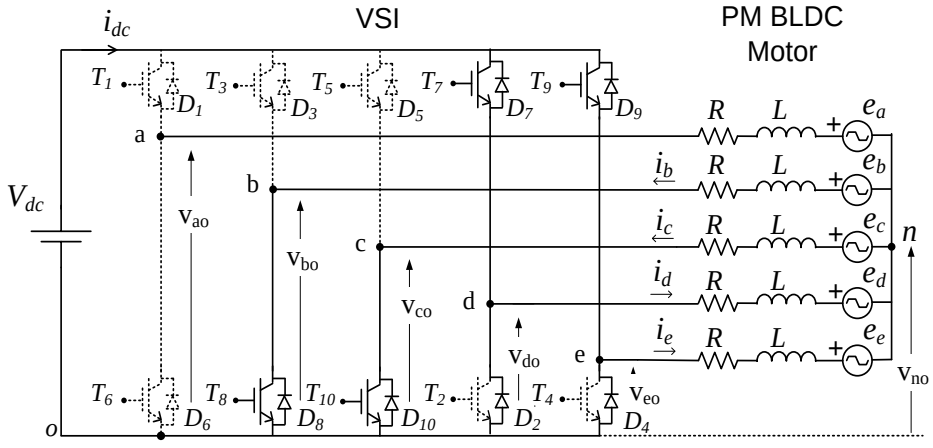

(a)

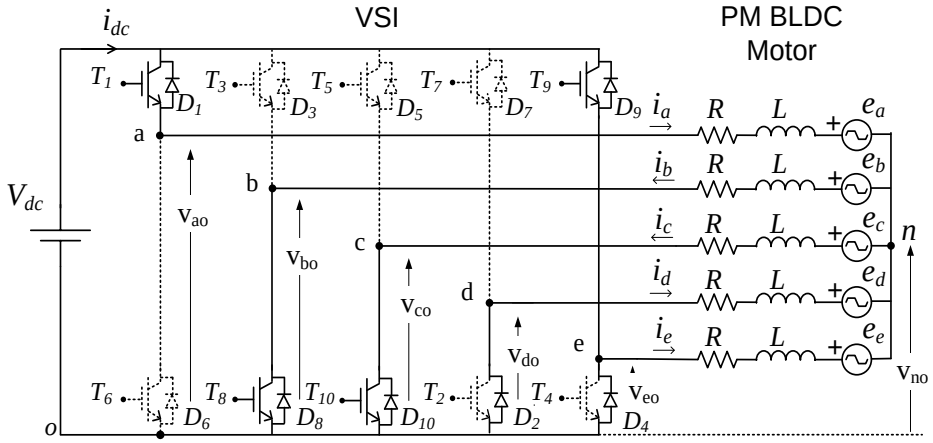

(b)

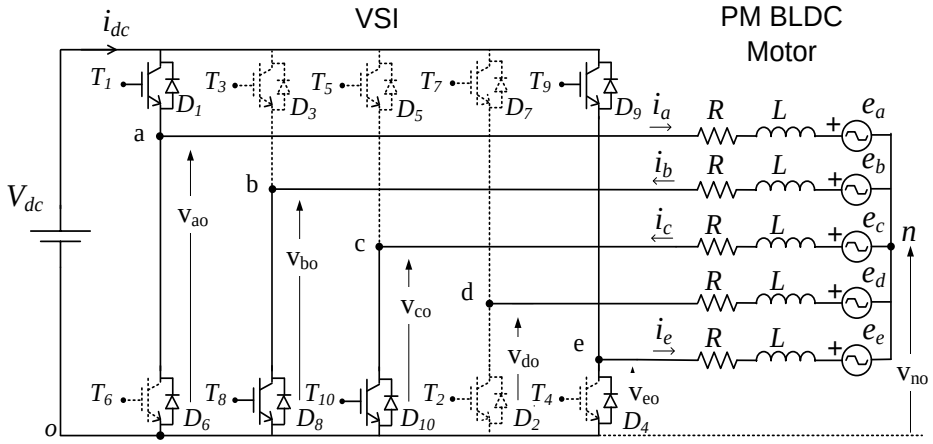

(c)

Fig. 7.3.1. Phase currents a) before; b) during and c) after the commutation θ_e= 0.

7.3.2 First commutation sub interval

At the commutation time $\theta_e = 0$, T_1 is turned ON to allow the incoming current i_a to reach the nominal value I_N, T_7 is turned OFF to force the outgoing current i_d to vanish by circulating through D_2 whilst T_{10} is kept ON. Then it is

$$v_{ao} = V_N ; \quad v_{do} = 0 \tag{7.3.3}$$

Regarding the switch T_9, it can be switched either ON or OFF or chopped as before commutation, i.e. by (7.3.1). In all the cases, the current of phase *e* undergoes variations of distinct amount.

- For T_9 ON, the current i_e increases of I_N like the phase current i_a (the incoming current) since the two phases are subjected to the same terminal voltage.
- For T_9 OFF, the phase current i_e falls toward zero value.
- At last, for T_9 chopped by (7.3.1), the phase current i_e is no more regulated at I_N due to the change equivalent circuit which leads towards the change in the neutral point voltage v_{no}.

The solution adopted here is to continue to chop T_9 by updating its duty-cycle (δ_e) during the commutation, so as to maintain the current i_e regulated at I_N. Furthermore, T_8 is no more kept ON but the upper transistor in the same leg (i.e. T_3) is chopped to maintain the current i_b regulated at $-I_N$. This is in favor of reducing the effects of the commutation on the motor torque and, in addition, simplifies the analysis of the current behavior during the commutation since i) only three currents, namely i_a, i_c and i_d, are subjected to transients, and ii) the sum of the three currents is zero, i.e.

$$i_a + i_c + i_d = 0 \tag{7.3.4}$$

This leads to drive operation that looks like in the three-phase case but, as a matter of fact, it is quite different since these three phases (7.3.4) are not equally shifted in the space.

By assuming here and throughout the paper that the commutation interval is short enough to approximate the back-emf e_d of the outgoing phase with its flat-top magnitude E along the commutation interval, the voltage equation of the mesh formed by the motor phases *a* and *c*, and that one of the mesh formed by the motor phases *c* and *d* become

$$\left.\begin{aligned} 2L\left(1-\cos\frac{4\pi}{5}\right)\frac{di_a}{dt} + L\left(1-\cos\frac{2\pi}{5}\right)\frac{di_d}{dt} - V_N + 2E = 0 \\ L\left(1-\cos\frac{2\pi}{5}\right)\frac{di_a}{dt} + 2L\left(1-\cos\frac{2\pi}{5}\right)\frac{di_d}{dt} + 2E = 0 \end{aligned}\right\} \tag{7.3.5}$$

Solving the system in (7.3.5) with the time *t* expressed in terms of θ_e gives the rate of change of phase currents i_a and i_d, as follows

$$\left.\begin{aligned} \frac{di_a}{d\theta_e} &= \frac{0.306}{n_p \Omega L}\left(V_N - E\right) \\ \frac{di_d}{d\theta_e} &= -\frac{1}{n_p \Omega L}\left(0.153V_N + 1.29E\right) \end{aligned}\right\} \tag{7.3.6}$$

Substituting the derivatives of the currents into the terminal voltages of the phases *b* and *e* gives the duty-cycles of the legs *b* and *e*, as shown below

$$\delta_b = 0.618 \;;\; \delta_e = 0.618 - 1.236\left(\frac{E}{V_N}\right) \tag{7.3.7}$$

From (7.3.7) it is observed that δ_e falls within the range 0 – 1 while E varies from 0 to $V_N/2$, thus demonstrating the feasibility of the solution adopted.

Both the incoming and outgoing current transients take time to be completed. From (7.3.6), the angular interval θ_r that i_a takes to rise to I_N (rising interval) and the angular interval θ_v that i_d takes to vanish (vanishing interval) are calculated. The results do not apply together since, as soon as one of the two commutating currents reaches its final value, operation of the circuit changes. The two intervals come out to be

$$\theta_r = \frac{3.27 n_p L I_N}{k}\frac{E}{\left(V_N - E\right)}; \quad \theta_v = \frac{n_p L I_N}{k}\frac{E}{0.153V_N + 1.29E} \tag{7.3.8}$$

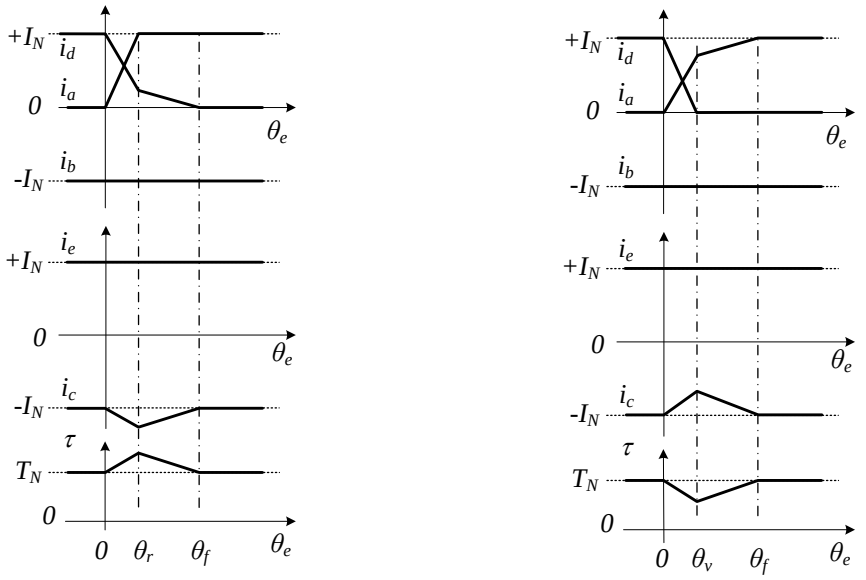

(a) (b)

Fig. 7.3.2. Current and torque transients during commutation in (a) low-speed zone and (b) high-speed zone.

By (7.3.8), θ_r is equal to θ_v for a distinct value E_d of the back-emf and a corresponding value Ω_d of the motor speed, where $E_d=0.096V_N$ and $\Omega_d=0.19\Omega_N$. This means that

i) for $E=E_d$, i_a reaches the final value I_N at the same time as i_d vanishes,
ii) for $E<E_d$, i_a reaches the final value I_N before that i_d vanishes so that it continues to evolve until vanishing, and
iii) for $E>E_d$, i_d vanishes before that i_a reaches the final value I_N so that it continues to evolve until reaching I_N.

In terms of speeds, this means that the transients of the incoming and outgoing currents take the same time for $\Omega = \Omega_d$, the transients of the incoming current is faster for $\Omega < \Omega_d$ (low-speed zone) and slower for $\Omega > \Omega_d$ (high-speed zone).

From above, it emerges that the commutation interval consists of two subintervals. In the first subinterval both the commutating currents are subjected to transients toward their final values. During the second subinterval only the current that did not reach its final value is subjected to transient. The angular interval taken by the slowest commutation current to reach its final value is denoted as θ_f and constitutes the commutation interval.

During the commutation interval, the non-commutating negative phase current i_c undergoes a deviation Δi_c from the steady-state value of $-I_N$. For a constant value of i_b and i_e, it can be readily realized that Δi_c is given by

$$\Delta i_c = I_N - i_a - i_d \tag{7.3.9}$$

Eq. (7.3.9) attains its maximum magnitude at the end of the first subinterval of commutation. The transients of both the commutating currents and the non-commutating current in the two

speed zones are exemplified in *Figure 7.3.2*. The traces clearly show the different behavior of the currents in the two speed zones. Therefore it is convenient to study the current behavior and the ensuing torque characteristics separately in each speed zone. The same occurs in a three-phase drive but the speed that separates the low-speed zone from the high-speed one in a five-phase drive is much less than in the three-phase counterpart. Moreover, differently from a three-phase drive, one notes that here i) the motor has a phase that conducts a current in the same direction as the incoming current, and ii) the motor has two non-commutating phases that conduct currents in the same direction as the outgoing current.

7.3.3 Second commutation sub-interval

7.3.3.1 Low speed zone ($\Omega < 0.19\Omega_N$)

In the low-speed zone, incoming current i_a reaches the required value I_N before outgoing current i_d vanishes. The rising interval θ_r of i_a is given by the first equation of (7.3.8). By (7.3.6) and (7.3.8), the value of i_d at θ_r is

$$i_d(\theta_r) = \left(\frac{0.5V_N - 5.22E}{V_N - E}\right) I_N \tag{7.3.10}$$

For $\theta_e > \theta_r$, T_1 is no more kept ON but it is chopped to maintain the current of the phase a regulated at I_N. At the same time, chopping of T_3 and T_9 is continued to maintain the currents of the phases *b* and *e* regulated at $-I_N$ and I_N, respectively, whilst chopping of T_5 and T_7 has to be started to enable the outgoing current to vanish. The duty-cycles of T_5 and T_7 can be selected within a certain range. For simplicity, an equal value is taken for them, set at

$$\delta_c = \delta_d = 0.618 \tag{7.3.11}$$

From (7.2.9) and (7.3.11), the rate of change of i_d in the second subinterval of commutation and the duty-cycles of T_3 and T_9 are calculated in

$$\frac{di_d}{dt} = -\frac{1.44E}{L} \tag{7.3.12}$$

$$\delta_b = 0.618\left(1 + \frac{E}{V_N}\right);\ \delta_e = 0.618\left(1 - \frac{E}{V_N}\right) \tag{7.3.13}$$

Current i_d vanishes for

$$\theta_f - \theta_r = \frac{n_p L I_N}{k} \frac{0.34V_N - 3.62E}{V_N - E} \tag{7.3.14}$$

By summing the first equation of (7.3.8) to (7.3.14), the commutation interval is obtained as

$$\theta_f = \frac{0.34 n_p L I_N}{k} \tag{7.3.15}$$

From (7.3.9) and (7.3.10), the amplitude of Δi_c at θ_r is equal to

$$\Delta i_c(\theta_r) = -i_d(\theta_r) = -\left(\frac{0.5V_N - 5.22E}{V_N - E}\right) I_N \tag{7.3.16}$$

7.3.3.2 High speed zone ($\Omega > 0.19\Omega_N$)

In the high-speed zone, outgoing current i_d vanishes before i_a reaches the required value I_N. The vanishing interval θ_v of i_d is given by the second equation of (7.3.8). By (7.3.6) and (7.3.8), the value of i_a at θ_v is

$$i_a(\theta_v) = \left[\frac{0.306(V_N - E)}{0.153V_N + 1.29E} \right] I_N \tag{7.3.17}$$

For $\theta_e > \theta_v$, T_1 is kept ON, and T_3 and T_9 are chopped until the current i_a reaches the required value I_N. From (7.2.9), the rate of change of i_a and the duty-cycles of T_3 and T_9 are calculated in

$$\frac{di_a}{dt} = \frac{0.276(V_N - 2E)}{L} \tag{7.3.18}$$

$$\delta_b = 0.5\left(1 - \frac{2E}{V_N}\right) \; ; \; \delta_e = 0.809 + 0.382\frac{E}{V_N} \tag{7.3.19}$$

Current i_a reaches I_N for

$$\theta_f - \theta_v = \frac{n_p L I_N}{k} \frac{3.62\left(-0.153V_N + 1.59E\right)E}{(V_N - 2E)(0.153V_N + 1.29E)} \tag{7.3.20}$$

By summing the second equation of (7.3.8) to (7.3.20), the commutation interval is obtained as

$$\theta_f = \frac{n_p L I_N}{k} \frac{(0.446V_N + 3.77E)E}{(V_N - 2E)(0.153V_N + 1.29E)} \tag{7.3.21}$$

From (7.3.9) and (7.3.17), the amplitude of Δi_c at θ_v is equal to

$$\Delta i_c(\theta_v) = I_N - i_a(\theta_v) = \frac{-0.153V_N + 1.59E}{0.153V_N + 1.29E} I_N \tag{7.3.22}$$

7.4 Torque characteristics

The instantaneous torque developed by the drive, obtained by applying (7.2.3) and (7.2.4) and the first Kirchhoff's principle to the neutral point, is given by

$$\tau(\theta_e) = -2k\left[i_b(\theta_e) + i_c(\theta_e)\right] \tag{7.4.1}$$

Equation (7.4.1) shows that the torque is equal to the opposite of the sum of the non-commutating negative currents. Similar torque equations can be derived for the other supply intervals and in the two speed zones as shown in *Figure 7.2*. Then the effective torque, given by the average value of the instantaneous torque over the supply period (that coincides with the average value over the supply interval), is

$$T = 4kI_N - 2k\frac{5}{\pi}\int_0^{\theta_f} \Delta i_c(\theta_e) d\theta_e \tag{7.4.2}$$

and the toque ripple, defined as the peak-to-peak torque, is

$$\Delta T = 2k\left|\Delta i_c(\theta_M)\right| \tag{7.4.3}$$

where θ_M is equal to the θ_r for low-speed zone and to θ_v for high-speed zone.
By substituting (7.3.15) and (7.3.16) in (7.4.2) and (7.4.3), the effective torque and the torque ripple of a five-phase PM BLDC drive operating in the low-speed zone are formulated as a function of E (and then, by (7.2.2), of the motor speed) are expressed as follows

$$T = 4kI_N + \frac{5n_pLI_N^2}{\pi}\left(\frac{0.17V_N - 1.77E}{V_N - E}\right) \tag{7.4.4}$$

$$\Delta T = \frac{0.5V_N - 5.22E}{V_N - E}2kI_N \tag{7.4.5}$$

By substituting (7.3.21) and (7.3.22) in (7.4.2) and (7.4.3), the effective torque and the torque ripple of a five-phase PM BLDC drive operating in the high-speed zone are formulated as a function of E, are expressed as follows

$$T = 4kI_N - \frac{5n_pLI_N^2}{\pi}\left[\frac{E(0.446V_N + 3.77E)(-0.153V_N + 1.59E)}{(V_N - 2E)(0.153V_N + 1.29E)^2}\right] \tag{7.4.6}$$

$$\Delta T = \left|\frac{-0.153V_N + 1.59E}{0.153V_N + 1.29E}\right|2kI_N \tag{7.4.7}$$

From (7.4.4) and (7.4.6) it is observed that the motor torque

i) Is higher than the nominal value of a small amount at low speeds,
ii) Is equal to the nominal value for $\Omega=\Omega_d$, and
iii) Has a significant drop, especially when the speed approaches the nominal value, at high speeds.

From (7.4.5) and (7.4.7) it is observed that the torque ripple

i) Is zero at $\Omega=\Omega_d$, and
ii) Increases at both high and low speeds.

7.5 Base Speed

Let us define the base speed Ω_B as the maximum speed at which the incoming current reaches I_N at least before that the successive commutation starts, i.e. at the end of the $\pi/5$ length of the supply interval. Under this situation, θ_f coincides with $\pi/5$. Base speed is obtained by equating (7.3.21) to $\pi/5$ and by solving the following expression for E, as shown below

$$\frac{n_pLI_N}{k}\frac{(0.446V_N + 3.77E)E}{(V_N - 2E)(0.153V_N + 1.29E)} = \frac{\pi}{5} \tag{7.5.1}$$

7.6 Study Case

The study case of a 5-phase PM BLDC drive meant for the propulsion of light road vehicles is here considered to exemplify the above findings. Nominal quantities and parameters of the drive are listed in *Table 7.6.1*.

Figure 7.6.1 plots the commutation interval θ_f in the low-speed zone and in the high-speed zone as a function of motor speed. The graphs point out that i) the commutation interval is constant in the low-speed zone whilst it increases notably in the high-speed zone, reaching the value of $\pi/5$ at the base speed.

Tab. 7.6.1 PM BLDC Drive Data.

Data	Symbol	Value
Supply voltage	V_N	48 V
Nominal motor current	I_N	25 A
Nominal torque	T_N	32 Nm
Nominal speed	Ω_N	75 rad/s
Pole pairs	n_p	8
Phase inductance	L	50 μH
Motor constant	k	0.32 V·s/rad

The motor torque and the torque ripple are plotted in *Figure 7.6.2* with the blue dotted line and the red solid line, respectively. The graphs show that the motor torque continuously drops with the increase in speed and exhibts a torque drop of about 19% and a torque ripple of about 39% of the nominal torque at the base speed. After the base speed, the system fails to complete the commutation within the maximum duration i.e. a supply interval for a duration of $\pi/5$. Therefore the torque drastically droops and reaches to zero after the base speed as shown in *Figure 7.6.2*.

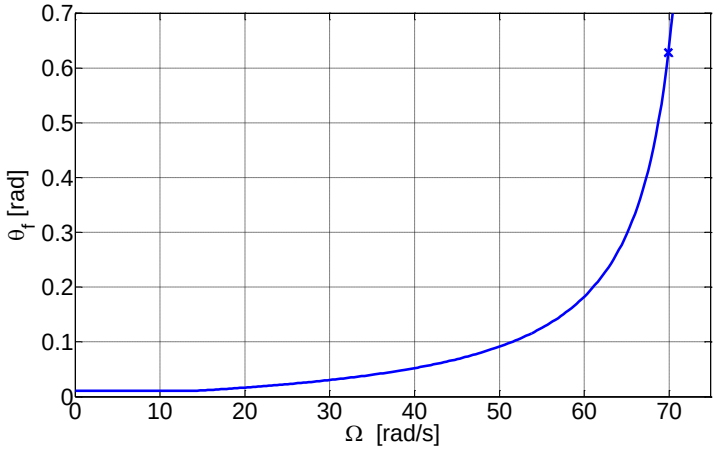

Fig. 7.6.1. Commutation interval vs. motor speed.

Base speed results in 70 rad/s, which is about 6.6% lower than the nominal speed. Working conditions at the base speed are highlighted by stars in *Figure 7.6.1* and Figure *7.6.2.*

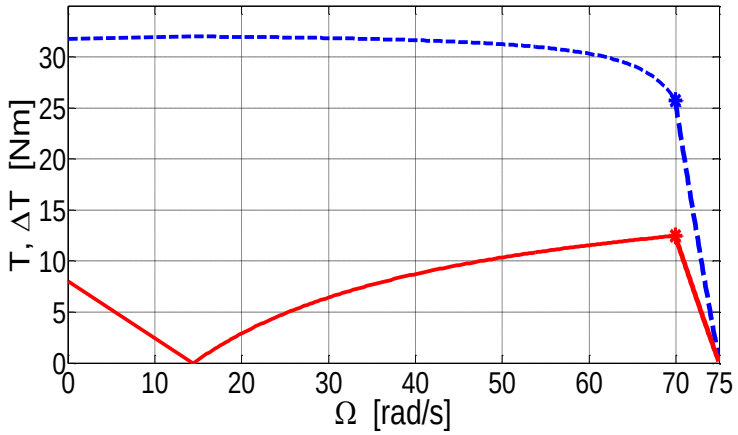

Fig. 7.6.2. Torque (blue dashed line) and torque ripple (red solid line) vs. motor speed.

7.7 Conclusion

This chapter deals with the five-phase PM BLDC drives with square-wave current supply of the motor phases. Current behavior during phase commutations has been analyzed for low- and high-speed operation by keeping regulated the current of two non-commutating phase, one situated on the same side of the phase of the incoming current and the other one in the opposite side. This basically entails that the current behavior reproduces that one in a three-phase PM BLDC drive. Resulting expressions, however, are quite divergent from the three-phase case for both the current excursion of the non-commutating phase and the length of the commutation interval because of the different space shift of the motor phases. The study has divided the speed range into two zones each of them having a proper behaviour of the phase currents during the phase commutations. The calculated motor torque exhibits a continuous drop with the speed whilst the calculated torque ripple is high at high speeds. The theoretical results on the motor torque have been verified by drive data which was executed on a PM BLDC drive meant for propulsion of light road vehicles.

Chapter 8

An Algebraic Approach to Determine the Current Supply in a Faulty Five-Phase PM BLDC Drive

8.1 Introduction

Nowadays the electric drives are more oftenly used in safety-critical applications, turning the efforts of their design towards the development of solutions able to tolerate a fault [34]. For example, in the aerospace industry there is an increasing adoption of electrical drives to substitute for the heavy hydraulic and mechanical systems. The relevant drives are expected to be fault-tolerant as human life is tightly related to their trustworthy operation. Similar issues are encountered in the automotive industry, with regard to the propulsion drives especially of the purely electric vehicles.

Permanent magnet (PM) brushless (BL) drives are used since long time in the industry thanks to their high torque-per-ampere capabilities [48]. Recently, they have become popular in transportation too [17], [37]. Among the two different types of PM BL drives, namely those with sinusoidal back-emf (BLAC) and with trapezoidal back-emf (BLDC), the latter ones are preferred within the framework of more-electric aircraft as flight control actuators, for instance (f.i.) positioning ailerons, flaps, and rudders [3], [36]. They are also preferred for the propulsion of light-duty electric vehicles such as city cars and scooters [49]. Design of fault-tolerant electrical drives has pushed for the use of multiphase drives as they are able to operate under one or more faulty phases although with downsized performance [12] [35], [50]. The most promising structure for a multiphase drive has five phases because of its lower complexity with respect to topologies with higher phase count.

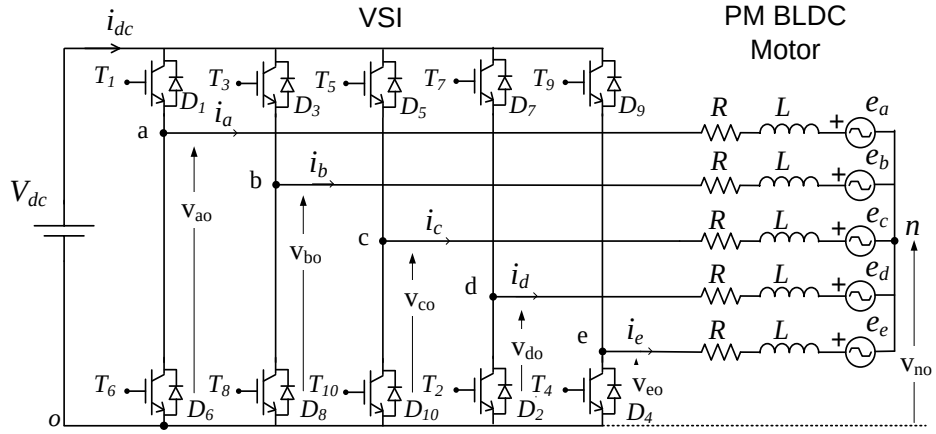

Fig. 8.1. Circuit representation of a five-phase PM BLDC drive.

Here in this chapter an algebraic approach is proposed [51–52], to set up a model of a five-phase PM BLDC drive that is valid not only in healthy conditions but also under faulty conditions, as long as the model is modified with fault-specific constraints. Drive faults due to the opening of one or more phases are here considered. The modified model provides not only scheduling and magnitude of the currents in the surviving phases but also maximum magnitude of the currents and maximum torque developed by the motor. After illustrating the way of constraining the model, this approach is applied to the case of one or more open phase faults. A single switch fault in any of the five leg VSI, is realized as open circuit phase fault by isolating the faulty leg from the drive and the algorithm is applied to determine the appropriate reference phase current sequence. The phase current supply strategy of the surviving motor phases with open phase faults is analyzed by calculating the motor torque for an rms value of the working phase currents equal to the rated one.

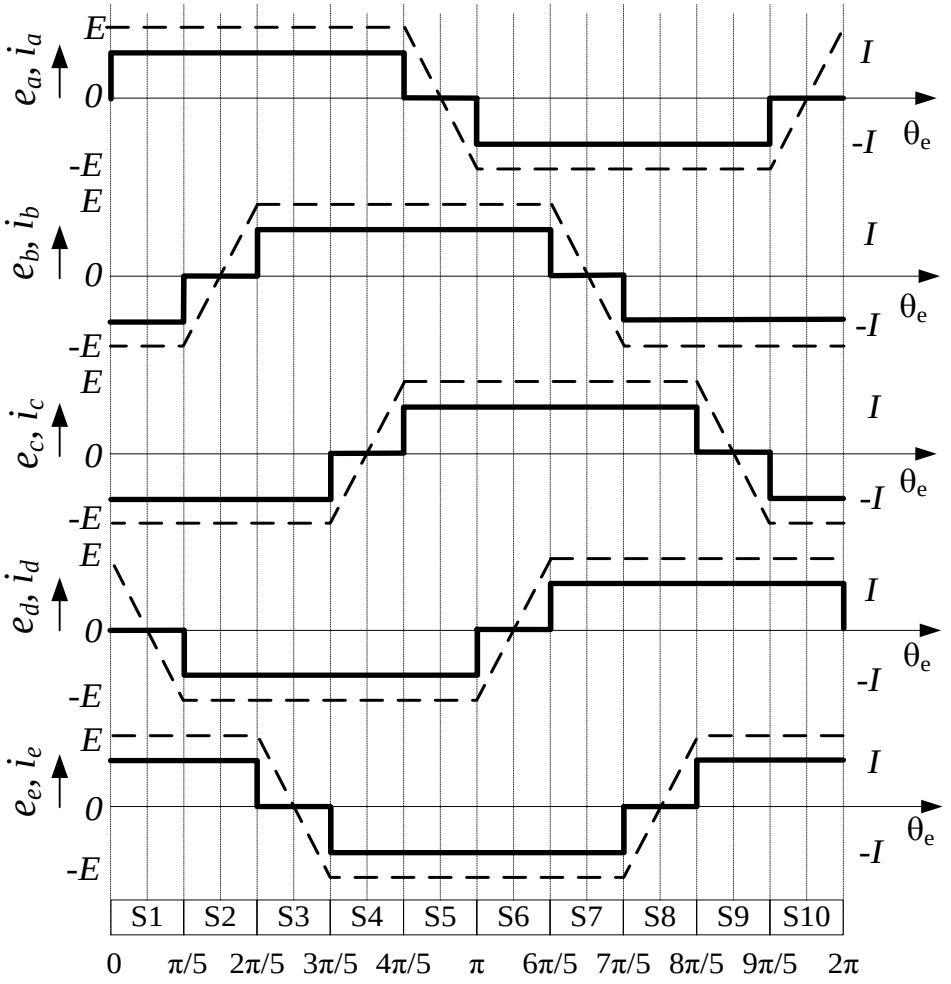

Fig. 8.2. Back-emfs (dashed line), phase currents (bold line), and supply intervals of five-phase PM BLDC drive.

8.2 Five phase PM BLDC drive

The circuit scheme of a 5-phase PM BLDC drive with an Y-connected, neutral-isolated is shown in *Figure 8.1*. The motor is represented by its equivalent circuit where R, L and e_j with with $j=a, b, c, d, e$ are the resistance, the self-inductance and the back-emfs of the phases, and the voltage source inverter (VSI) supplying the motor is represented by its five legs. The DC link at the VSI input is fed by the voltage source V_{dc}, with V_{dc} set at the nominal motor voltage V_N to fully exploit the motor voltage ratings. The mutual inductances between the phases of the motor are not indicated in the figure.

Hereafter within this chapter, the following assumptions are made: i) ideal square waveforms for the motor phase currents, thus disregarding the commutation phenomena and the current ripple due to the chopper control of the voltage at the motor terminals, ii) steady-state operation of the drive, and iii) negligible voltage drop across the motor phase resistances and the VSI.

Phase back-emfs and currents of the motor are drawn in *Figure 8.2* as a function of the rotor position θ_e in electrical radians. Both the back-emfs and the currents of the phases are displaced by $2\pi/5$ apart. The relations between the rotor position θ_e, the motor speed Ω, and the motor speed Ω_e in electrical rad/s are

$$\theta_e = \Omega_e t; \quad \omega_e = n_p \Omega \tag{8.2.1}$$

where n_p is the number of pole pairs.

The magnitude E of the phase back-EMF is proportional to the Ω according to

$$E = k\Omega \tag{8.2.2}$$

where k is the motor constant. The instantaneous electrical power p converted into mechanical form can be expressed in terms of power entering in the back-emfs

$$p = \sum_{j=a,b,c,d,e} e_j i_j \tag{8.2.3}$$

or of power generated by the DC link voltage source

$$p = V_{dc} i_{dc} \tag{8.2.4}$$

where I_{dc} is the continuous component of the DC-link current. From p, the instantaneous torque τ developed by the motor is calculated as

$$\tau = p / \Omega \tag{8.2.5}$$

For the square-wave current supply of *Figure 7.2*, p is constant and equal to $4EI$, where I is the phase current magnitude; then torque τ is also constant and given by

$$T = 4kI \tag{8.2.6}$$

Moreover, the rms value of the currents in the motor phases is [53]

$$I_{rms} = \sqrt{\frac{4}{5}} I \tag{8.2.7}$$

With respect to a 3-phase PM BLDC drive, a 5-phase one differs in the following features:

- The torque expression contains the coefficient 4 instead of 2; this is due to the fact that four motor phases, instead of two are conducting at the same time,
- The currents contain harmonics multiple of 3 whilst do not contain harmonics multiple of 5; this is due to the fact that the currents are shifted each other by 2π/5 instead of π/3,
- For a given value of *I*, the rms value of the phase currents is $\sqrt{6/5}$ times greater than in the 3-phase drive; this is due to the fact that the phases conduct the current for a longer angular interval.

In normal conditions, the following relations hold between the back-emf magnitude, the motor speed, the rms phase current, the motor torque and the motor voltage and current:

$$V_N = 2E_N;\ \Omega_N = \frac{V_N}{2k};\ I_{rms,N} = \sqrt{\frac{4}{5}} I_N;\ T_N = 4kI_N \tag{8.2.8}$$

8.3 Drive model

From *Figure 8.2* one realizes that the motor supply period is divided into ten supply intervals of equal length, each lasting π/5 electrical radians.

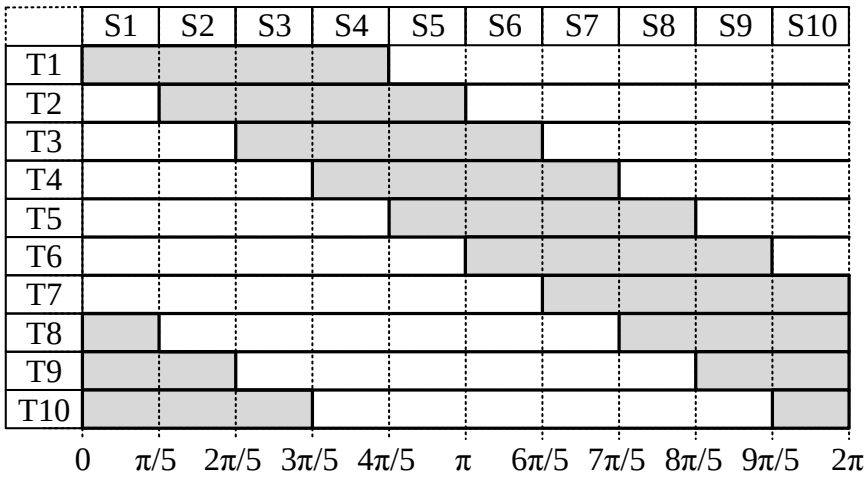

Fig. 8.3.1 Switching scheme in healthy conditions. T1..T10 are the VSI switches; S1..S10 are the supply intervals.

Figure 8.3.1 summarizes the on/off states of the VSI transistors T1, T2, ..., T10 (grey means *on*, white means *off*) over the supply period. Each supply interval i.e. S1, S2,…, S10 are identified by the states of the ten VSI transistors during that particular interval. Therefore *Figure 8.3.1* can be seen as a sequence of the VSI states over the supply period, shortly termed as VSI state.

The VSI state can be expressed in a matrix form. To do this,

i) The *on* and *off* states of a transistor are associated to the digits 1 and 0, respectively,

ii) Let *n*, with *n*=1, 2….10, be the generic supply interval.

The transistor state column-vector $\mathbf{T}_n$ for the *n*-th supply interval is of size 10x1 and is defined as follows: the *i*-th element of $\mathbf{T}_n$ represents the state of the *i*-th transistor (where *i* =1, 2….10). Of course, two transistors of a leg cannot be *on* at the same time, whilst they can be both *off*. For example, for the supply interval S3, $\mathbf{T}_3$ is given by

$$\mathbf{T}_3 = \begin{bmatrix} 1 & 1 & 1 & 0 & 0 & 0 & 0 & 0 & 0 & 1 \end{bmatrix}^T \tag{8.3.1}$$

The VSI state matrix **S** is built up by columns, where the column *n* is given by $\mathbf{T}_n$. The matrix has the size of 10x10 and is expressed as

$$\mathbf{S} = \begin{bmatrix} 1 & 1 & 1 & 1 & 0 & 0 & 0 & 0 & 0 & 0 \\ 0 & 1 & 1 & 1 & 1 & 0 & 0 & 0 & 0 & 0 \\ 0 & 0 & 1 & 1 & 1 & 1 & 0 & 0 & 0 & 0 \\ 0 & 0 & 0 & 1 & 1 & 1 & 1 & 0 & 0 & 0 \\ 0 & 0 & 0 & 0 & 1 & 1 & 1 & 1 & 0 & 0 \\ 0 & 0 & 0 & 0 & 0 & 1 & 1 & 1 & 1 & 0 \\ 0 & 0 & 0 & 0 & 0 & 0 & 1 & 1 & 1 & 1 \\ 1 & 0 & 0 & 0 & 0 & 0 & 0 & 1 & 1 & 1 \\ 1 & 1 & 0 & 0 & 0 & 0 & 0 & 0 & 1 & 1 \\ 1 & 1 & 1 & 0 & 0 & 0 & 0 & 0 & 0 & 1 \end{bmatrix} \tag{8.3.2}$$

In a PM BLDC drive with square-wave current supply, the phase currents during each supply interval are directly related to the corresponding states of the leg transistors. When one of the two transistors of a leg is *on*, the current flows in the connected phase, entering into it if the upper transistor is *on*, or leaving from it if the lower transistor is *on*. When both the transistors of a leg are *off*, no current flows into the connected phase. According to the conventions in *Figure 7.1*, the phase currents are positive when entering into the motor and negative in the opposite case.

A) Phase current supply

A phase current column-vector $\mathbf{C}_n$ of size 5x1 can be defined for the *n*-th supply interval, where the *j*-th element of $\mathbf{C}_n$ is the current in the phase *j*. For example, for the supply interval S3, $\mathbf{C}_3$ is given by

$$\mathbf{C}_3 = \begin{bmatrix} 1 & 1 & -1 & -1 & 0 \end{bmatrix}^T I \tag{8.3.3}$$

Of course, the sum of the phase currents, given by the sum of the elements of $\mathbf{C}_n$, must be zero to meet the first Kirchhoff's law applied to the motor neutral point.

The phase current supply is defined as the sequence of the phase currents over the supply period, and can be also expressed in a matrix form. The matrix is designated with **M** and is built up by columns, where the column *n* is given by $\mathbf{C}_n$. Therefore **M** has the size 5x10 and is expressed as

$$\mathbf{M}=\begin{bmatrix} 1 & 1 & 1 & 1 & 0 & -1 & -1 & -1 & -1 & 0 \\ -1 & 0 & 1 & 1 & 1 & 1 & 0 & -1 & -1 & -1 \\ -1 & -1 & -1 & 0 & 1 & 1 & 1 & 1 & 0 & -1 \\ 0 & -1 & -1 & -1 & -1 & 0 & 1 & 1 & 1 & 1 \\ 1 & 1 & 0 & -1 & -1 & -1 & -1 & 0 & 1 & 1 \end{bmatrix} I \tag{8.3.4}$$

It can be readily proved that

$$\mathbf{M=HS} \tag{8.3.5}$$

where

$$\mathbf{H}=\begin{bmatrix} 1 & 0 & 0 & 0 & 0 & -1 & 0 & 0 & 0 & 0 \\ 0 & 0 & 1 & 0 & 0 & 0 & 0 & -1 & 0 & 0 \\ 0 & 0 & 0 & 0 & 1 & 0 & 0 & 0 & 0 & -1 \\ 0 & -1 & 0 & 0 & 0 & 0 & 1 & 0 & 0 & 0 \\ 0 & 0 & 0 & -1 & 0 & 0 & 0 & 0 & 1 & 0 \end{bmatrix} \tag{8.3.6}$$

H is termed Hall matrix. Its rows can be built up from the signals of the Hall sensors. Indeed, let us consider the *n*-th Hall sensor. The *i*-th element of the *n*-th row is i) 1 when the signal of the Hall sensor commands entering of the current into the phase, ii) 0 when either the current is kept flowing into the phase or the current is not allowed to flow, and iii) -1 when the signal of the Hall sensor commands removal of the current from the phase.

To complete the model of the drive, the back-emf state matrix **B** is defined as

$$\mathbf{B}=\begin{bmatrix} 1 & 1 & 1 & 1 & 0 & -1 & -1 & -1 & -1 & 0 \\ -1 & 0 & 1 & 1 & 1 & 1 & 0 & -1 & -1 & -1 \\ -1 & -1 & -1 & 0 & 1 & 1 & 1 & 1 & 0 & -1 \\ 0 & -1 & -1 & -1 & -1 & 0 & 1 & 1 & 1 & 1 \\ 1 & 1 & 0 & -1 & -1 & -1 & -1 & 0 & 1 & 1 \end{bmatrix} E \tag{8.3.7}$$

The matrix has size 5x10 and is built up by rows. The *j*-th row refers to the back-emf of the phase *j* and its *n*-th element gives the amplitude of the back-emf in the supply interval *n*, with the exception of the intervals when the back-emf changes from +*E* to –*E* or vice versa where the elements are set at 0.

B) Phase current rms value and DC link current

By observing, each row of **M** represents the current in the phase *j* of the motor over the supply period and the phase current is constant in each supply interval, it can be readily obtained the following quantities like the rms value of the phase current and the continuous component of the DC link current over the supply period, expressed in vector form.

The rms value of the currents in the motor phases can be expressed as

$$\mathbf{I}_{rms} = \sqrt{\frac{1}{2\pi} diagc\left(\mathbf{M}\mathbf{M}^T\right)\frac{\pi}{5}} \tag{8.3.8}$$

where *diagc* is an operator that produces the column-vector $\mathbf{I}_{rms}$ of size 5x1 by picking up the diagonal elements of the matricial argument. It can be recognized that the *j*-th element of $\mathbf{I}_{rms}$ gives the rms value of the current in the phase *j*.

The continuous component of the DC-link current over the supply period can be expressed as

$$\mathbf{I}_{dc} = \frac{1}{V_{dc}}\left[\frac{1}{N} diagr\left(\mathbf{M}^T\mathbf{B}\right)\right] \tag{8.3.9}$$

where *diagr* is an operator that produces the row-vector $\mathbf{I}_{dc}$ of size 1x10 by picking up the diagonal elements of the matricial argument, and N is the minimum number of phases connected to any of the two DC link rails. For an healthy drive, it is N=2. It can be recognized that the *n*-th element of $\mathbf{I}_{dc}$ gives the continuous component of the DC-link current in the supply interval *n*.

C) Drive model

Matrices (8.3.4), (8.3.7), (8.3.8) and (8.3.9) altogether constitute the model of the drive in healthy conditions.

8.4 Constraints applying to BLDC drive model

An open phase fault may occur when either a motor phase or a leg of the VSI supplying the motor experiences an open-circuit failure. Under an open phase fault, the drive model must be constrained according to the following conditions:

A) Fulfilment of First Kirchhoff's law

By applying the first Kirchhoff law to the motor with no neutral connection, the total current entering into the motor must equate the total current leaving the motor at any time. This means that the sum of the elements of all the columns of **M** must be zero.

B) Invariance of phase rms current

Losses in a motor phase are related to the rms value of the current flowing in it. To avoid phase overheating, the rms value of the current in any of the surviving phases must not exceed the nominal value.

C) Rule on current flow

Equations (8.2.3) and (8.2.5) clearly show that, for a phase to develop a positive instantaneous torque, the current must have the same sign as the back-emf in that phase. This condition could be met by allowing the current to flow in a phase while the back-emf changes from $+E$ to $-E$ or vice versa, on condition that the current has the same sign as the back-emf. However, in healthy conditions such a current supply

is not used and the current is made to flow only during the flat regions of the back-emf to avoid the uprising of a relevant torque ripple. The same is applied for the faulty case operation of the drive. It appears quite obvious that the above-selected rule on the current flow is in favor of keeping low the torque ripple rather than of maximizing the motor torque. Let it be noted that the adoption of this rule for a faulty drive entails that the modified phase current supply matrix maintains the size and the 0 elements of **M**.

8.5 BLDC drive operation during open phase faults

8.5.1 Single open phase fault

The model derived in *Section 8.3* and the constraints mentioned in *Section 8.4* are utilized to modify the supply current of the motor phases when one phase is open.

With no restriction, phase *a* is assumed as the open phase. Of course, this implies that there is no current in phase *a*; moreover, this implies that, during the supply intervals where phase *a* should be conducting, the magnitude of the currents in the other phases are altered. F.i., during the supply interval S1, the current enters only into phase *e* and outputs from phases *b* and *c*. Then, the current in the latter two phases can not be equal to the current in phase *e*.

The phase current supply matrix under phase *a* open, designated with $\mathbf{M}_{F1}$, is built up in 3 steps. The first step consists in zeroing all the elements of the row of **M** corresponding to phase *a*, this yields the following tentative current sequence state matrix ($\mathbf{M}'_{F1}$)

$$\mathbf{M}'_{F1} = \begin{bmatrix} 0 & 0 & 0 & 0 & 0 & 0 & 0 & 0 & 0 & 0 \\ -1 & 0 & 1 & 1 & 1 & 1 & 0 & -1 & -1 & -1 \\ -1 & -1 & -1 & 0 & 1 & 1 & 1 & 1 & 0 & -1 \\ 0 & -1 & -1 & -1 & -1 & 0 & 1 & 1 & 1 & 1 \\ 1 & 1 & 0 & -1 & -1 & -1 & -1 & 0 & 1 & 1 \end{bmatrix} I_{F1} \tag{8.5.1}$$

where I_{F1} denotes the current magnitude for this faulty case.

The second step consists in testing the fulfillment of condition *A)* in *Section 7.4* for each column of the modified matrix. If not fulfilled, the elements of the only one phase, if any, connected to either the positive or the negative DC link rail along a supply interval are left at 1 or -1 whilst the elements of the other phases are modified in an equal way so as the sum of the elements of the column is 0. This yields the following phase current supply matrix:

$$\mathbf{M}_{F1} = \begin{bmatrix} 0 & 0 & 0 & 0 & 0 & 0 & 0 & 0 & 0 & 0 \\ -0.5 & 0 & 1 & 1 & 1 & 0.5 & 0 & -1 & -1 & -1 \\ -0.5 & -0.5 & -0.5 & 0 & 1 & 0.5 & 0.5 & 0.5 & 0 & -1 \\ 0 & -0.5 & -0.5 & -0.5 & -1 & 0 & 0.5 & 0.5 & 0.5 & 1 \\ 1 & 1 & 0 & -0.5 & -1 & -1 & -1 & 0 & 0.5 & 1 \end{bmatrix} I_{F1} \tag{8.5.2}$$

By (8.5.2), the currents flowing in the suviving phases have the pattern plotted in *Figure 8.5.1*. The third step consists in fulfilling condition *B)* in *Section 8.4*. By (8.3.8) and (8.5.2),

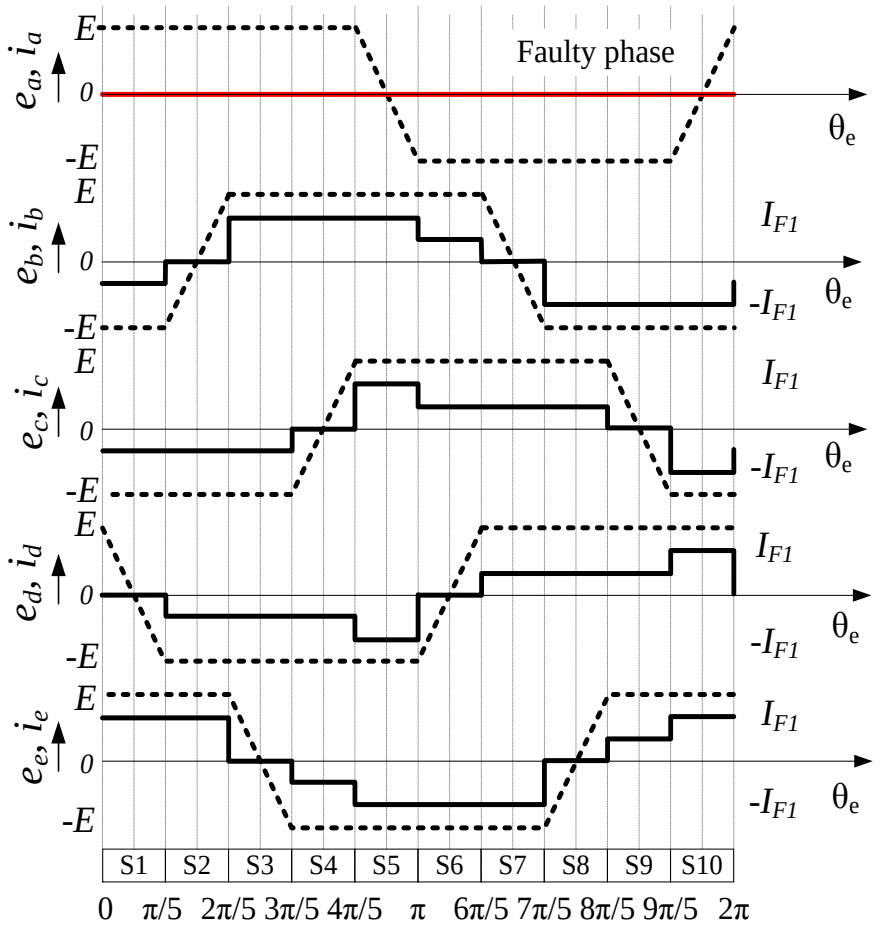

Fig. 8.5.1. Phase currents in a 5-phase PM BLDC drive under phase *a* open.

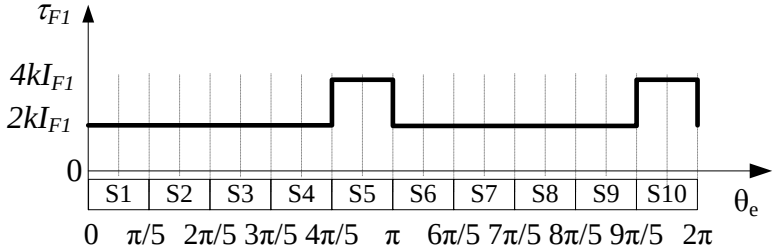

Fig. 8.5.2. Instantaneous motor torque in a 5-phase PM BLDC drive under phase *a* open.

the phase current rms value column-vector, designated with $\mathbf{I}_{rms,F1}$, becomes

$$I_{rms,F1} = \left[0 \quad \sqrt{\frac{13}{20}} \quad \sqrt{\frac{7}{20}} \quad \sqrt{\frac{7}{20}} \quad \sqrt{\frac{13}{20}}\right]^T I_{F1} \tag{8.5.3}$$

Equation (8.5.3) shows that the phases *b* and *e* are the most solicited ones. Then, by equating the rms value of their currents to the nominal value given in (8.2.8), it comes out that the maximum magnitude of I_{F1} is

$$I_{F1,M} = \sqrt{\frac{16}{13}} I \cong 1.09 I_N \tag{8.5.4}$$

It is worth to note that $I_{F1,M}$ is greater than I_N because the surviving phases conduct a current

less than the maximum magnitude in some supply intervals.

From (8.3.7), (8.3.9) and (8.5.2) the DC-link current continuous component row-vector becomes

$$\mathbf{I}_{dc,F1} = \frac{E}{V_{dc}}\begin{bmatrix}2 & 2 & 2 & 2 & 4 & 2 & 2 & 2 & 2 & 4\end{bmatrix} I_{F1} \tag{8.5.5}$$

By (8.5.5), the electrical power converted into mechanical form is not constant along the supply period. The same occurs for the instantaneous motor torque that, therefore, exhibits a ripple of peak-to-peak amplitude equal to $2kI_{F1}$, as shown in *Figure 8.5.2*. The maximum motor torque, given by the average value of the instantaneous torque over the supply period when I_{F1} is equal to its maximum magnitude, results in

$$T_{F1,M} = \frac{3}{5}\sqrt{\frac{16}{13}}\left(4kI_N\right) \approx 0.67T_N \tag{8.5.6}$$

The output power is, however, reduced compared to the one delivered in healthy conditions. More precisely, the maximum available power is two third of the nominal value.

8.5.2 Two faulty phases

When a two-open phase fault occurs, the behavior of the drive may vary according to the respective location of the open phases. There are two different cases for the open phase locations: adjacent and non-adjacent. They are modeled individually in the next Subsections.

8.5.2.1 Adjacent two-open phase fault (f.i. phase *a* and *b*)

With no restriction, *a* and *b* are taken as the open phases. As there is no current in phases *a* and *b*, it follows that the currents in the other phases are altered during the supply intervals where phase *a* and *b* should be conducting. For instance (f.i.)

i) during the supply interval S2, the current enters into the motor only through phase *e* and leaves the motor from phases *c* and *d*, split into two equal fractions,

ii) during the supply interval S3, there is no any current flow into the motor, and so on.

The phase current supply matrix under phase *a* and *b* open is designated with $\mathbf{M}_{F2a}$, and is built up in 3 steps. The first step consists in zeroing all the elements of the rows of **M** corresponding to phase *a* and *b*, which yields the following tentative motor phase current sequence state matrix ($\mathbf{M}'_{F2a}$)

$$\mathbf{M}'_{F2a} = \begin{bmatrix} 0 & 0 & 0 & 0 & 0 & 0 & 0 & 0 & 0 & 0 \\ 0 & 0 & 0 & 0 & 0 & 0 & 0 & 0 & 0 & 0 \\ -1 & -1 & -1 & 0 & 1 & 1 & 1 & 1 & 0 & -1 \\ 0 & -1 & -1 & -1 & -1 & 0 & 1 & 1 & 1 & 1 \\ 1 & 1 & 0 & -1 & -1 & -1 & -1 & 0 & 1 & 1 \end{bmatrix} I_{F2a} \tag{8.5.7}$$

where I_{F2a} denotes the current magnitude for this faulty case.

The second step consists in testing the fulfilment of condition *A)*, stated in *Section 8.4*, for each column of (8.5.7). If the condition is not fulfilled, the elements of the only one phase, if any, connected to either the positive or the negative DC-link rail during a supply interval are left at 1 or -1 whilst the elements of the other phases are equally modified so as the sum of the elements of the column is 0. This yields the following phase current supply matrix:

$$\mathbf{M}_{F2a} = \begin{bmatrix} 0 & 0 & 0 & 0 & 0 & 0 & 0 & 0 & 0 & 0 \\ 0 & 0 & 0 & 0 & 0 & 0 & 0 & 0 & 0 & 0 \\ -1 & -0.5 & 0 & 0 & 1 & 1 & 0.5 & 0 & 0 & -1 \\ 0 & -0.5 & 0 & 0 & -0.5 & 0 & 0.5 & 0 & 0 & 0.5 \\ 1 & 1 & 0 & 0 & -0.5 & -1 & -1 & 0 & 0 & 0.5 \end{bmatrix} I_{F2a} \tag{8.5.8}$$

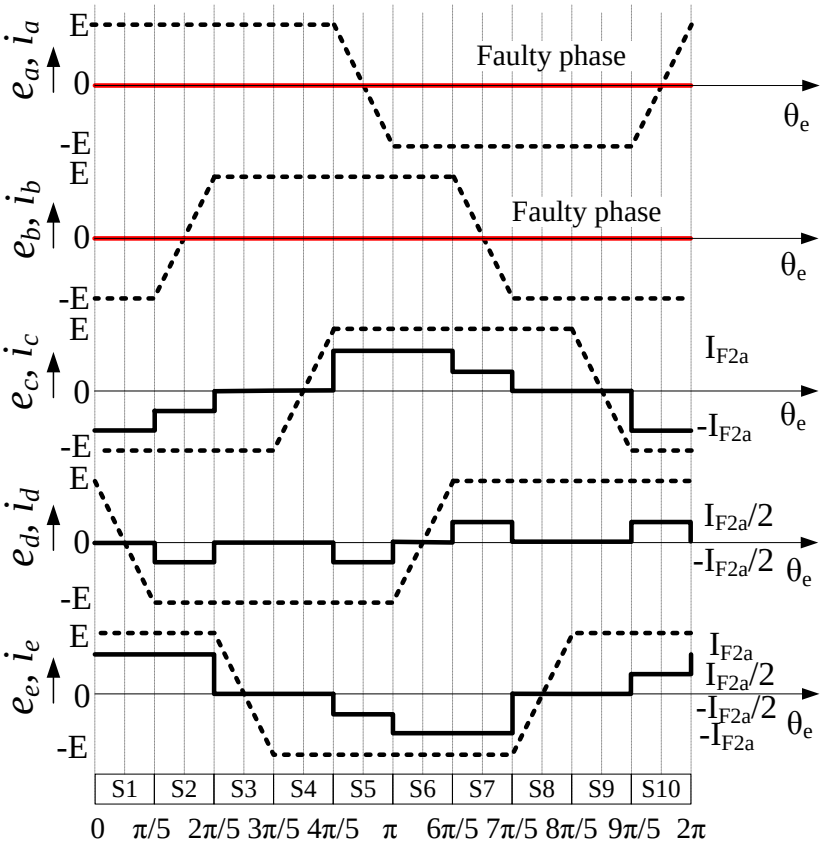

Fig. 8.5.3. Phase currents in a 5-phase PM BLDC drive under phases *a* and *b* open.

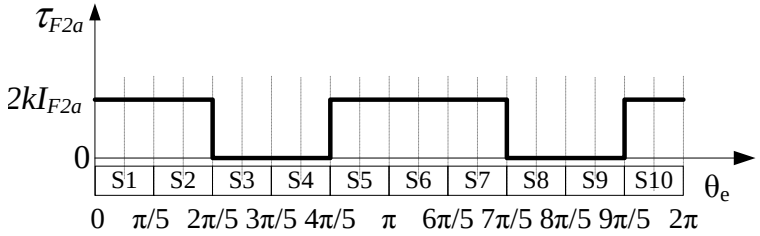

Fig. 8.5.4. Instantaneous torque in a 5-ph PM BLDC drive under phases *a* and *b* open.

By (8.5.8), the currents flowing in the surviving phases have the pattern plotted in *Figure 8.5.3*.

The third step consists in meeting condition *B)* in *Section 8.4*. By (8.3.8) and (8.5.8), the phase current rms value column-vector under phases *a* and *b* open, designated with $\mathbf{I}_{rms,F2a}$, becomes

$$I_{rms,F2a} = \begin{bmatrix} 0 & 0 & \sqrt{\frac{9}{20}} & \sqrt{\frac{1}{10}} & \sqrt{\frac{9}{20}} \end{bmatrix}^T I_{F2a} \tag{8.5.9}$$

Equation (8.5.9) shows that the phases *c* and *e* are the most solicited ones. By equating the rms value of their currents to the nominal value, it comes out that the maximum magnitude of I_{F2a} as

$$I_{F2a,M} = \frac{4}{3} I_N \tag{8.5.10}$$

It is worth to note that $I_{F2a,M}$ is greater than I_N because the surviving phases conduct a current less than the maximum magnitude in some supply intervals.

From (8.3.7), (8.3.9) and (8.5.8), the DC-link current continuous component row-vector under phases *a* and *b* open, designated with $\mathbf{I}_{dc,F2a}$, becomes

$$\mathbf{I}_{dc,F2a} = \frac{E}{V_{dc}} \begin{bmatrix} 2 & 2 & 0 & 0 & 2 & 2 & 2 & 0 & 0 & 2 \end{bmatrix} I_{F2a} \tag{8.5.11}$$

By (8.5.11), the electrical power converted into mechanical form is not constant along the supply period. Since the same occurs for the instantaneous motor torque, the drive exhibits a torque ripple of peak-to-peak amplitude equal to $2kI_{F2a}$, as shown in *Figure 8.5.4*. The maximum motor torque, given by the average value of the instantaneous torque over the supply period when I_{F2a} is equal to its maximum magnitude, results in

$$T_{F2a} = \frac{2}{5}(4kI_N) = 0.4T_N \tag{8.5.12}$$

Thus, not to exceed the rated copper losses in the most loaded phases, the motor offers only 40% of the nominal torque of a five-phase PM BLDC motor.

8.5.2.2 Non-adjacent two-open phase fault (f.i. phases *a* and *c*)

With no restriction, phase *a* and *c* are taken as the open phases. Differently from the previous location of the open phases, the motor is flowed by current in all the supply intervals. By constraining the model of the healthy drive with conditions *A)* and *B)*, stated in *Section 8.4* and specified for the faulty case under analysis, one obtains

i) By applying the condition *A)* in *Section 8.4*, the phase current supply matrix $\mathbf{M}_{F2b}$ under phases *a* and *c* open becomes

$$\mathbf{M}_{F2b} = \begin{bmatrix} 0 & 0 & 0 & 0 & 0 & 0 & 0 & 0 & 0 & 0 \\ -1 & 0 & 1 & 1 & 1 & 1 & 0 & -1 & -1 & -1 \\ 0 & 0 & 0 & 0 & 0 & 0 & 0 & 0 & 0 & 0 \\ 0 & -1 & -1 & -0.5 & -0.5 & 0 & 1 & 1 & 0.5 & 0.5 \\ 1 & 1 & 0 & -0.5 & -0.5 & -1 & -1 & 0 & 0.5 & 0.5 \end{bmatrix} I_{F2b} \tag{8.5.13}$$

where I_{F2b} denotes the current magnitude for this faulty case. By (8.5.13), the currents flowing in the surviving phases have the pattern plotted in *Figure 8.5.5*.

ii) the phase current rms value column-vector under phases *a* and *c* open, designated with $\mathbf{I}_{rms,F2b}$,

$$I_{rms,F2b} = \begin{bmatrix} 0 & \sqrt{\frac{4}{5}} & 0 & \sqrt{\frac{1}{2}} & \sqrt{\frac{1}{2}} \end{bmatrix}^T I_{F2b} \tag{8.5.14}$$

Eq. (8.5.14) shows that the phase *b* is the most solicited one. By equating the rms value of its current to the nominal value, it comes out that the maximum magnitude of I_{F2b} is

$$I_{F2b,M} = I_N \tag{8.5.15}$$

It is worth to note that $I_{F2b,M}$ is equal to I_N because the current conduction along the supply period in the surviving phase *b* replicates that one of a healthy drive.

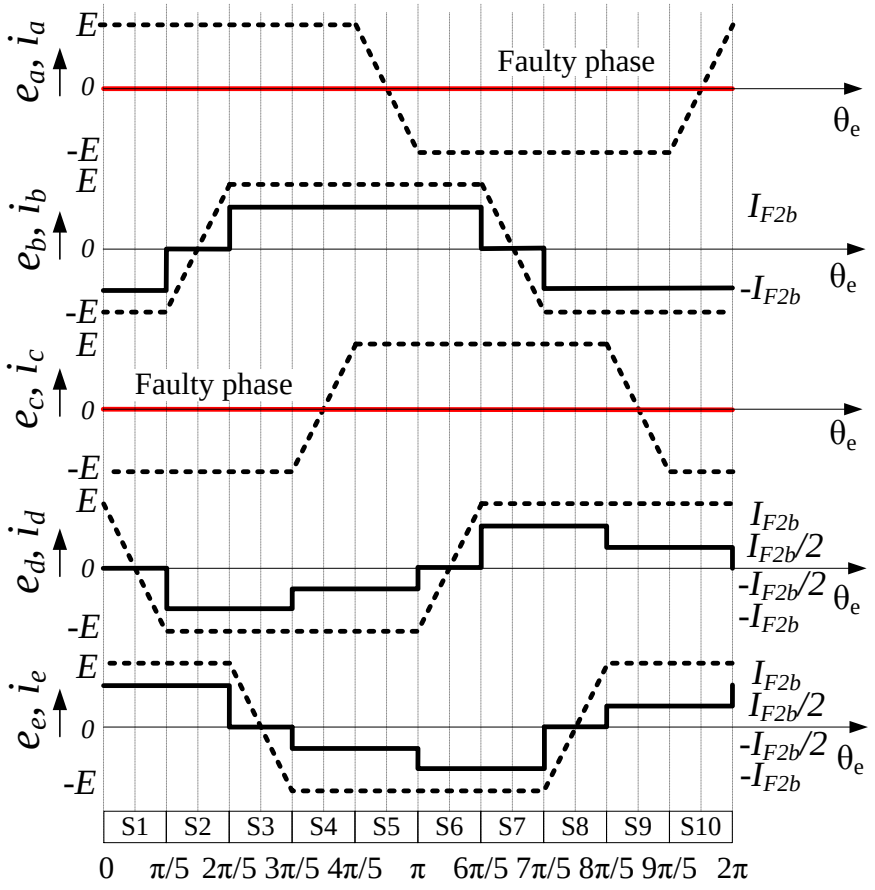

Fig. 8.5.5. Phase currents in a 5-ph PM BLDC drive under phases *a* and *c* open.

iii) the DC-link current continuous component row-vector under phases *a* and *c* open, designated with $\mathbf{I}_{dc,F2b}$

$$i_{dc,F2b} = \frac{E}{V_{dc}}\begin{bmatrix}2 & 2 & 2 & 2 & 2 & 2 & 2 & 2 & 2 & 2\end{bmatrix} I_{F2b} \tag{8.5.16}$$

By (8.5.16), the electrical power converted into mechanical form is constant along the supply period, and the drive does not exhibit any torque ripple. The maximum motor torque, developed when I_{F2b} is equal to its maximum magnitude, results in

$$T_{F2b,M} = \frac{1}{2}(4kI_N) = 0.5T_N \tag{8.5.17}$$

The motor offers 50% of the nominal torque of a five-phase PM BLDC motor.

8.5.3 Three faulty phases

Like with two-open phase fault, the behavior of the drive under three-open phase fault may vary according to the respective location of the open phases. Again there are two different locations, with two of the three open phases that are adjacent or non-adjacent. They are modeled individually in the next Subsections. However, it can be realized right now that for both the locations there is no current flow in the motor during some supply intervals. Indeed, two of the open phases are necessarily adjacent, leading to the same situation encountered for the adjacent two-open phase fault. Moreover, since one of the two surviving phases must be connected to the positive DC-link rail and the other one to the negative, the two phases conduct the same current for an equal interval.

8.5.3.1 Adjacent three-open phase fault (f.i. phase *a, b,* and *c*)

With no restriction, *a, b* and *c* are taken as the open phases. By constraining the model of the healthy drive with conditions *A)* and *B),* stated in *Section 8.4* and specified for the faulty case under analysis, one obtains

i) the phase current supply matrix $\mathbf{M}_{F3a}$ under phases *a, b,* and *c* open becomes,

$$\mathbf{M}_{3Fa} = \begin{bmatrix} 0 & 0 & 0 & 0 & 0 & 0 & 0 & 0 & 0 & 0 \\ 0 & 0 & 0 & 0 & 0 & 0 & 0 & 0 & 0 & 0 \\ 0 & 0 & 0 & 0 & 0 & 0 & 0 & 0 & 0 & 0 \\ 0 & -1 & 0 & 0 & 0 & 0 & 1 & 0 & 0 & 0 \\ 0 & 1 & 0 & 0 & 0 & 0 & -1 & 0 & 0 & 0 \end{bmatrix} I_{F3a} \tag{8.5.3.1}$$

where I_{F3a} denotes the current magnitude for this faulty case. By (8.5.3.1), the currents flowing in the surviving phases have the pattern plotted in *Figure 8.5.6.*

ii) the phase current rms value column-vector under phases *a, b* and *c* open, designated with $\mathbf{I}_{rms,F3a}$,

$$I_{rms,F3a} = \begin{bmatrix} 0 & 0 & 0 & \sqrt{\frac{1}{5}} & \sqrt{\frac{1}{5}} \end{bmatrix}^T I_{F3a} \tag{8.5.3.2}$$

Equation (8.5.3.2) confirms that the phases *d* and *e* are equally solicited. By equating the rms value of their currents to the nominal value, it comes out that the maximum magnitude of I_{F3a} is

$$I_{F3a,M} = 2I_N \tag{8.5.3.4}$$

It is worth to note that $I_{F3a,M}$ is twice as great as I_N because the current conduction interval of the surviving phases is one fourth of that in the healthy drive

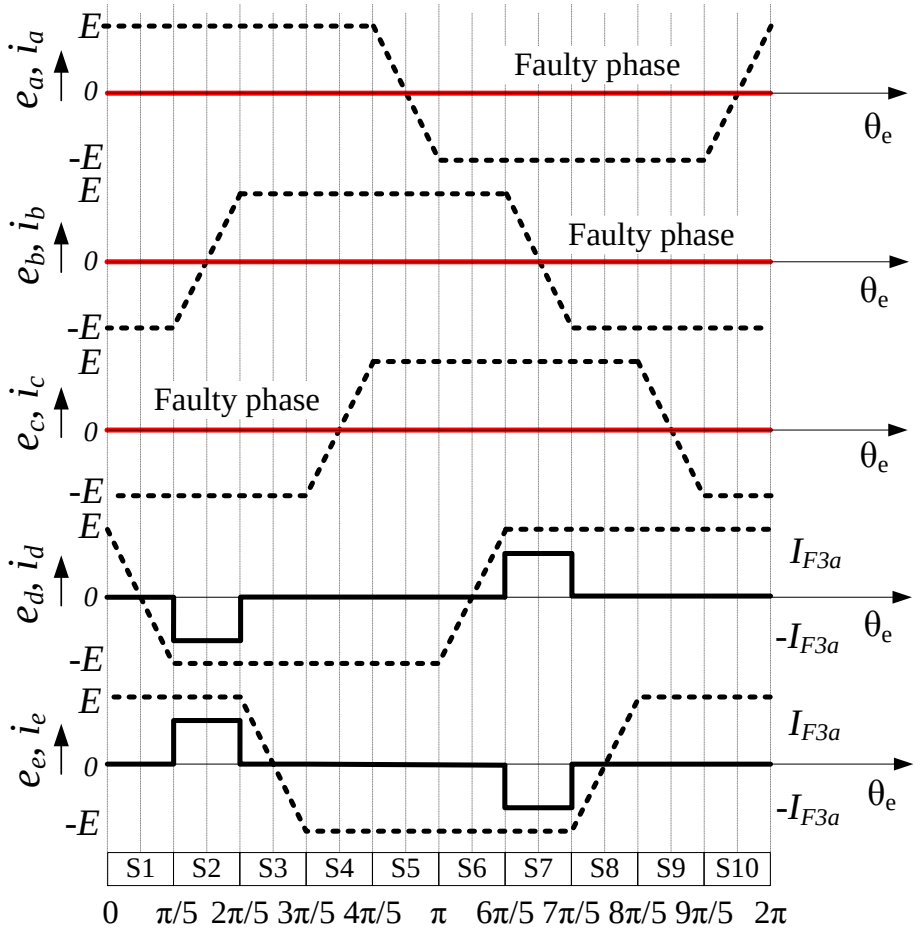

Fig. 8.5.6. Phase currents in a 5-phase PM BLDC drive under phases *a*, *b* and *c* open.

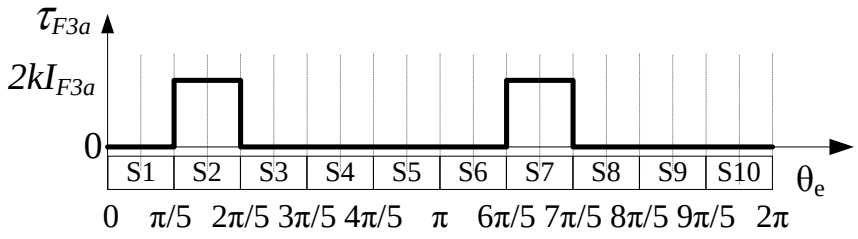

Fig. 8.5.7. Instantaneous torque in a 5-ph PM BLDC drive under phases *a*, *b* and *c* fault.

iii) the DC-link current continuous component row-vector under phases *a*, *b* and *c* open, designated with $\mathbf{I}_{dc,F3a}$,

$$i_{dc,F3a} = \frac{E}{V_{dc}}\begin{bmatrix}0 & 2 & 0 & 0 & 0 & 0 & 2 & 0 & 0 & 0\end{bmatrix} I_{F3a} \tag{8.5.3.5}$$

Eq. (8.5.3.5) shows that the electrical power converted into mechanical form is not constant along the supply period, thus originating a torque ripple. The peak-to-peak amplitude of the ripple is $2kI_{F3a}$, as shown in *Figure 8.5.7*. The maximum motor torque, given by the average value of the instantaneous torque over the supply period when I_{F3a} is equal to its maximum magnitude, results in

$$T_{F3a,M} = \frac{1}{5}\left(4kI_N\right) = 0.2T_N \tag{8.5.3.6}$$

The motor offers only 20% of the nominal torque of a five-phase PM BLDC motor

8.5.3.2 Non-adjacent three-open phase fault (f.i. phases *a, b* and *d*)

With no restriction, *a, b* and *d* are taken as the open phases. By constraining the model of the healthy drive with conditions *A)* and *B)* stated in *Section 8.4* and specified for the faulty case under analysis, one obtains

i) the phase current supply matrix under phases *a, b,* and *d* open, designated with $\mathbf{M}_{F3b}$,

$$\mathbf{M}_{F3b} = \begin{bmatrix} 0 & 0 & 0 & 0 & 0 & 0 & 0 & 0 & 0 & 0 \\ 0 & 0 & 0 & 0 & 0 & 0 & 0 & 0 & 0 & 0 \\ -1 & -1 & 0 & 0 & 1 & 1 & 1 & 0 & 0 & -1 \\ 0 & 0 & 0 & 0 & 0 & 0 & 0 & 0 & 0 & 0 \\ 1 & 1 & 0 & 0 & -1 & -1 & -1 & 0 & 0 & 1 \end{bmatrix} I_{F3b} \tag{8.5.3.7}$$

where I_{F3b} denotes the current magnitude for this faulty case. By (8.5.3.7), the currents in the surviving phases have the pattern plotted in *Figure 8.5.8*.

ii) the phase current rms value column-vector under phases *a, b* and *c* open, designated with $\mathbf{I}_{rms,F3b}$,

$$I_{rms,F3b} = \begin{bmatrix} 0 & 0 & \sqrt{\frac{3}{5}} & 0 & \sqrt{\frac{3}{5}} \end{bmatrix}^T I_{F3b} \tag{8.5.3.8}$$

Equation (8.5.3.8) confirms one more time that the phases *b* and *e* are equally solicited. By equating the rms value of their currents to the nominal value, it comes out that the maximum magnitude of I_{F3b} is

$$I_{F3b,M} = \sqrt{\frac{4}{3}}\, I_N \tag{8.5.3.9}$$

It is worth to note that $I_{F3b,M}$ is $\sqrt{4/3}$ as great as I_N because the current conduction interval

of the surviving phases is three fourths of that in the healthy drive.

iii) the DC-link current continuous component row-vector under phases *a*, *b* and *c* open, designated with $\mathbf{I}_{dc,F3b}$,

$$i_{dc,F3b} = \frac{E}{V_{dc}}\begin{bmatrix}2 & 2 & 0 & 0 & 2 & 2 & 2 & 0 & 0 & 2\end{bmatrix} I_{F3b} \qquad (8.5.3.10)$$

By (8.5.3.10), the electrical power converted into mechanical form is not constant along the supply period, thus originating a torque ripple. The peak-to-peak amplitude of the ripple is $2kI_{F3b}$, as shown in *Figure 8.5.9*.

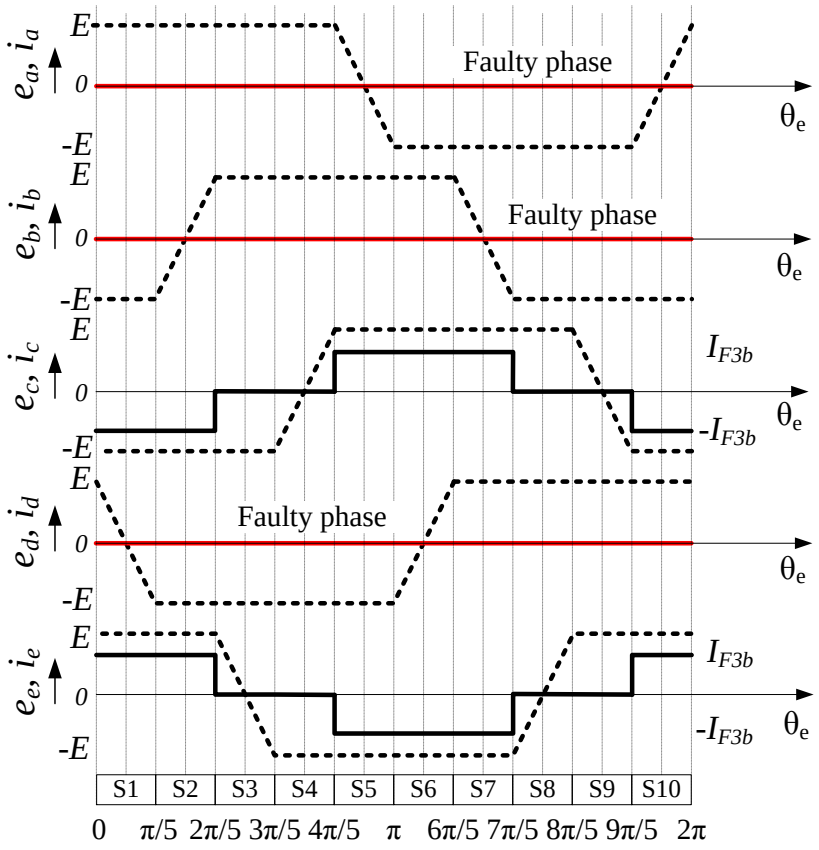

Fig. 8.5.8. Phase currents in a 5-phase PM BLDC drive under phases *a*, *b* and *d* open.

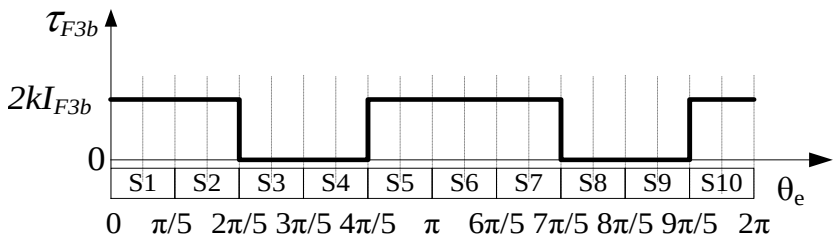

Fig. 8.5.9. Instantaneous torque in a 5-phase PM BLDC drive under phases *a*, *b* and *d* open.

The maximum motor torque, given by the average value of the instantaneous torque over the supply period when I_{F3b} is equal to its maximum value, results in

$$T_{F3b,M} = \frac{3}{10}\sqrt{\frac{4}{3}}\left(4kI_N\right) \cong 0.35T_N \tag{8.5.3.11}$$

The motor offers only 34.7% of the nominal torque of a five-phase PM BLDC motor.

8.6 Study case

A 5-phase PM BLDC drive meant for the propulsion of light-duty electric vehicles is examined to exemplify the above findings. Parameters and nominal quantities of the drive are listed in *Table 8.6.1*.

Tab. 8.6.1 PM BLDC Drive data.

Data	Symbol	Value
Supply voltage	V_N	48 V
Nominal motor current	I_N	25 A
Nominal torque	T_N	32 Nm
Nominal speed	Ω_N	75 rad/s
Pole pairs	n_p	8
Phase inductance	L	50 μH
Motor constant	k	0.32 V·s/rad

The 5-phase PM BLDC drive is simulated in PSIM environment under open phase fault cases discussed in *Section 8.5*. The phase current supply matrix (**M**) is used to set the reference of the scheduling and magnitude for the current controllers while the maximum magnitude ($I_{F,M}$) is used to limit their outputs. The current controller implemented in the simulation are of hysteresis type.

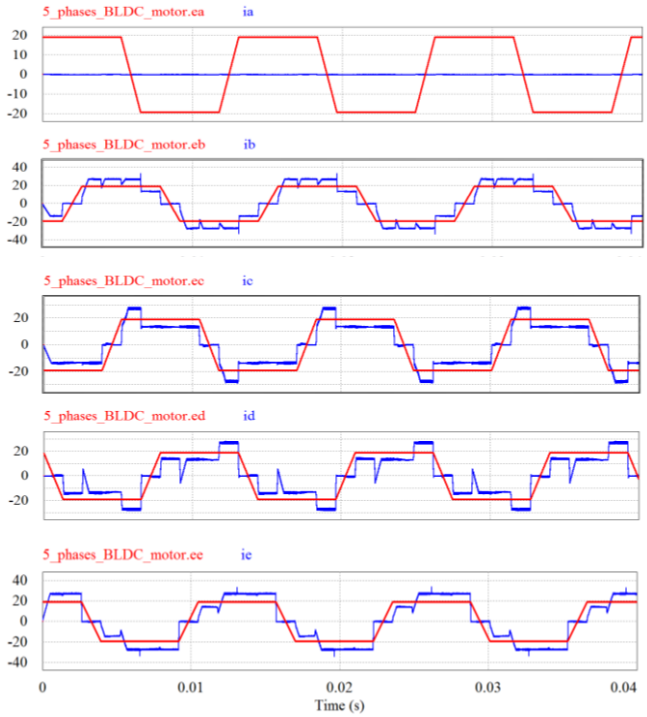

(a) Phase currents (blue line) and back-EMFs (red line)

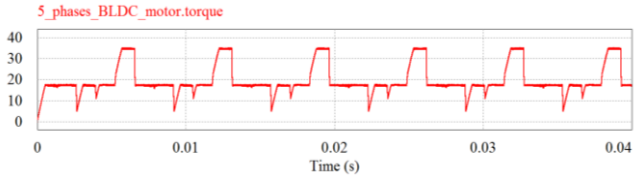

(b) Motor torque

Fig. 8.6.1. Simulation of a 5-phase PM BLDC drive with phase *a* open, which is operated at 80% of the nominal speed.

The phase currents and the motor torque obtained at 80% of the nominal speed are reported in *Figures 8.6.1(a)* and *8.6.1(b)*, respectively. The plots shows that the modified model runs appropriately, giving the expected phase current supply. The ripple visible in both the phase currents and the instantaneous motor torque is due to the commutation phenomena. A detailed analysis of the commutation phenomena and of their effect can be found in [53].

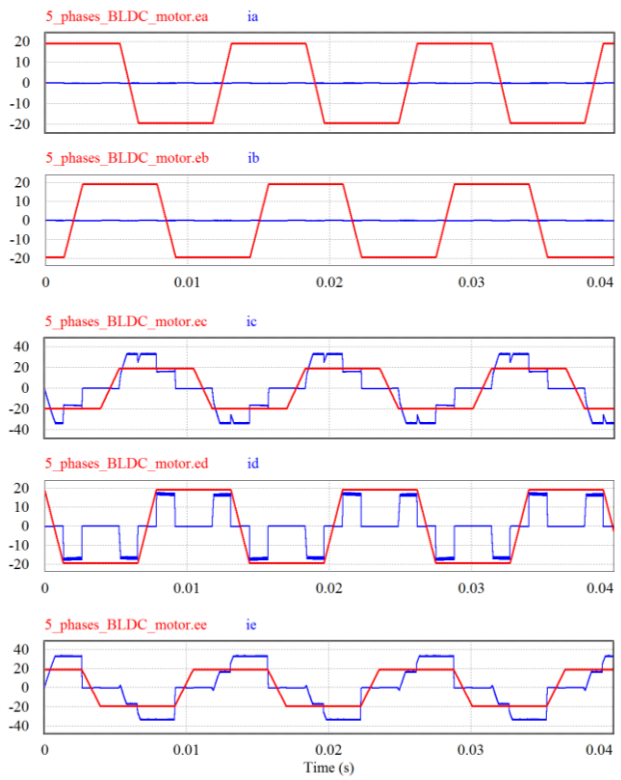

(a) Phase currents (blue line) and back EMFs (red line)

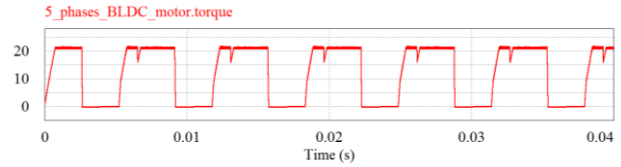

(b) Motor torque

Fig. 8.6.2. Adjacent two-open phase faults

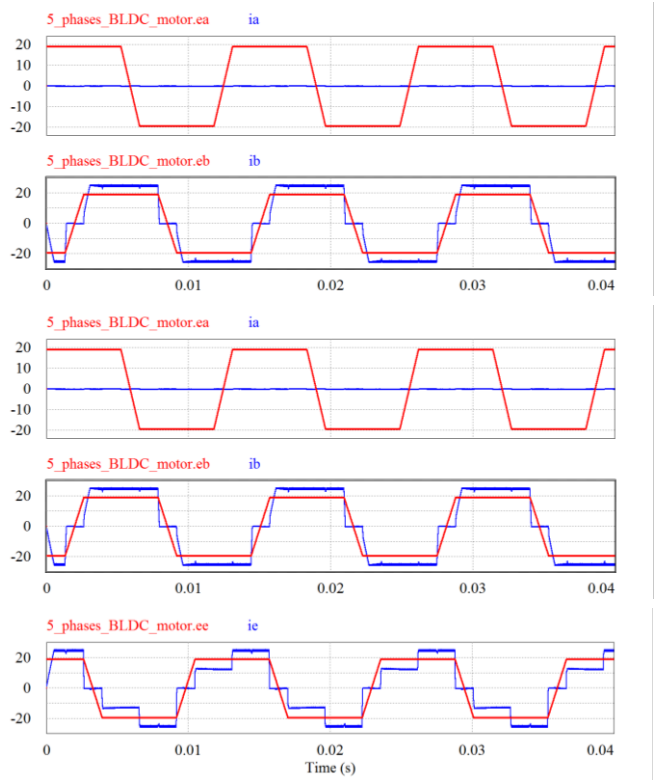

(c) Phase currents (blue line) and back EMFs (red line)

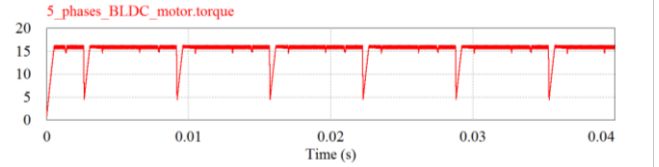

(d) Motor torque

Fig. 8.6.3. Non-Adjacent two-open phase faults

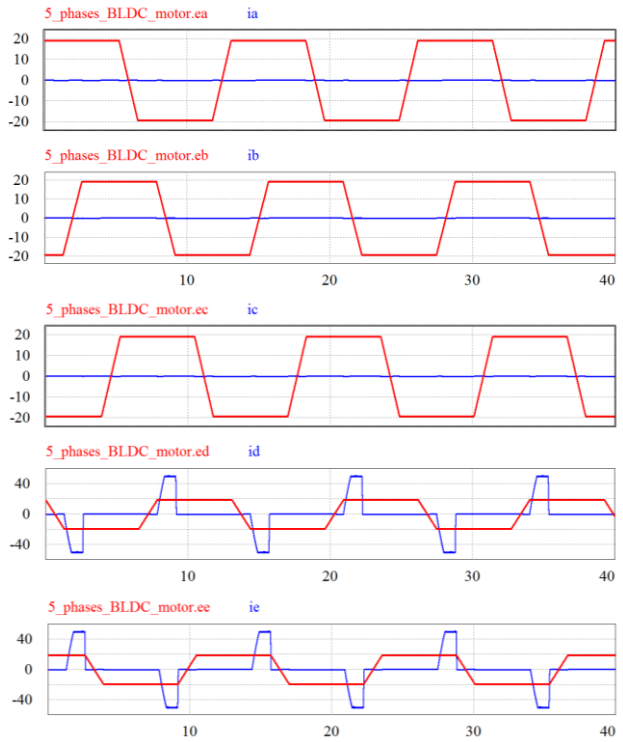

(a) Phase currents (blue line) and Back EMFs (red line)

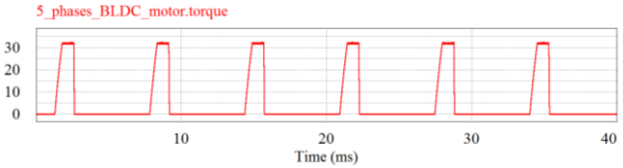

(b) Motor Torque

Fig. 8.6.4. Adjacent three-open phase faults

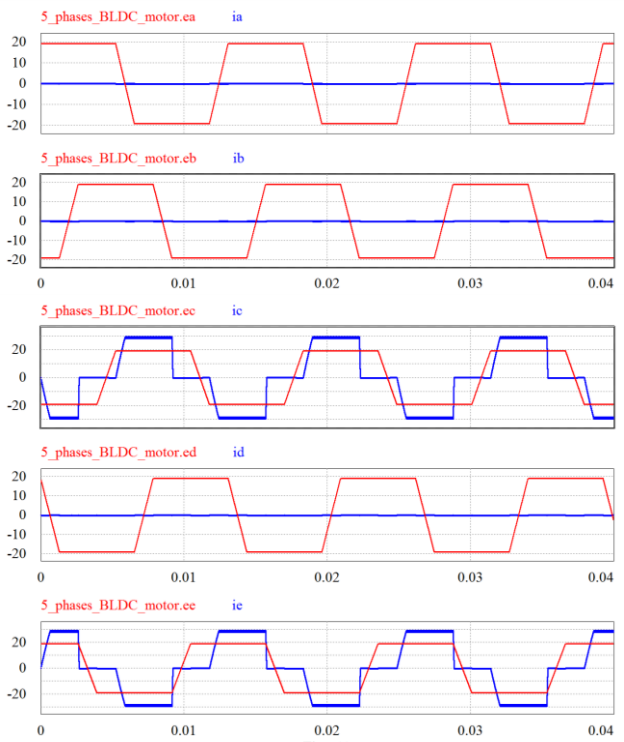

(c) Phase currents (blue line) and Back EMFs (red line)

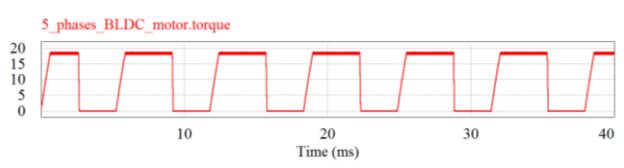

(d) Motor Torque

Fig. 8.6.5. Non-adjacent three-open phase faults

The phase currents and the motor torque obtained under adjacent and non-adjacent two-open phase faults running at 80% of the nominal speed are reported in *Figure 8.6.2* and *Figure 8.6.3*, respectively. Explicitly, the maximum motor torque for two-open phase faults passes from 50% of the nominal torque if the faulty phases are non-adjacent to 40% if they are adjacent. For three-open phase faults plotted in *Figure 8.6.4* and *Figure 8.6.5*, the maximum motor torque passes from 35% of the nominal torque if the faulty phases are non-adjacent to 20% if they are adjacent. Regarding the torque ripple, the best situation occurs with non-adjacent two-open phase fault since the drive does not exhibit any ripple. Instead, in the other case with two open phases and in all the cases with three open phases, the drive is affected by a ripple whose peak-to-peak amplitude is *2k* times the magnitude of the current supply.

8.7 Conclusion

A five-phase BLDC motor drive has been reviewed with the main operating principle of the drive and an algebraic model describing the drive operation in healthy conditions has been described. Then some constraints, applying to both healthy and faulty operation, have been identified. Based on these premises, the current sequence has been derived to supply the machine in case of open phase faults. It has been analyzed that, with the proposed current sequence, the power that can be extracted from the drive as well as the torque waveform change depends not only on the number of faulty (open) phases, but also on their relative location. It has been demonstrated that, with the proposed current sequence, the drive can deliver a ripple-free torque for a single open phase fault whose value reduces to 63% of the rated one. With two open phases the drive can deliver 40% and 50% of its rated power depending on whether the two-open phases are adjacent or non-adjacent, respectively. Furthermore, in the former case the output torque exhibits a ripple, while in the latter case is ripple-free. As regards the faulty scenario with three-open phases, it has been demonstrated that the drive can deliver 20% or 34.7% of its rated power depending on whether the open phases are adjacent or not, respectively. In this case, for both adjacent and non-adjacent three-open phases, a ripple arises in the output torque.

Appendix - A

Dependability

The motor drive supplied by a power electronic converter with a control circuitry makes the major systems in an aircraft. Due to increase in the electronic components and drive systems the complexity of the systems and their handling is also getting higher and higher, and the chance of a fault impeding the delivery of the service has become greater than ever. This aspect is particularly important for the safety-critical systems [12], i.e. for the systems the outage of which can harm people, subsystems (things) or the environment. The underlying reason for this attention is that electronic circuitry is thought to be less robust in withstanding adverse situations, such as physical stresses, than the mechanical or hydraulic devices that they have replaced.

The system is a composition of devices grouped into a single entity with the goal of delivering a service. The system is made up of many simpler systems called subsystems which are meant to make the desired work/service to happen. The result of cumulative functions carried out by a system is known as service. The service delivered by a system can be correct or incorrect. The key concepts of dependability theory that focus on the characteristics of the service are as follows:

i) Threats
ii) Attributes
iii) Enforcing techniques

A1. Threats

The threats are phenomena that impair the dependability of a system. For the purpose of their classification, a system is modelled by three hierarchical layers: operational, processing and physical. As per [34] the system can be represented by the three-layer model of *Table A1* where each layer is identified by the activity done.

Tab. A1 Three layer model of dependability theory

Layer	Threaten
Operational (service delivering)	Failure
Processing (information processing, if any)	Error
Physical (devices and interactions)	Fault

A failure is a deviation of external state of a system from its true value which may lead to error and further fault. Errors may occur in the system that processes information items like

data or signals. It may be due to the improper maintenance of the system, user flaws in using the system. A fault is a deviation of the regular operation of device from the predicted/expected one and is stimulated due to the physical phenomenon like mechanical or electrical stresses, wearing, aging, heating and so on.

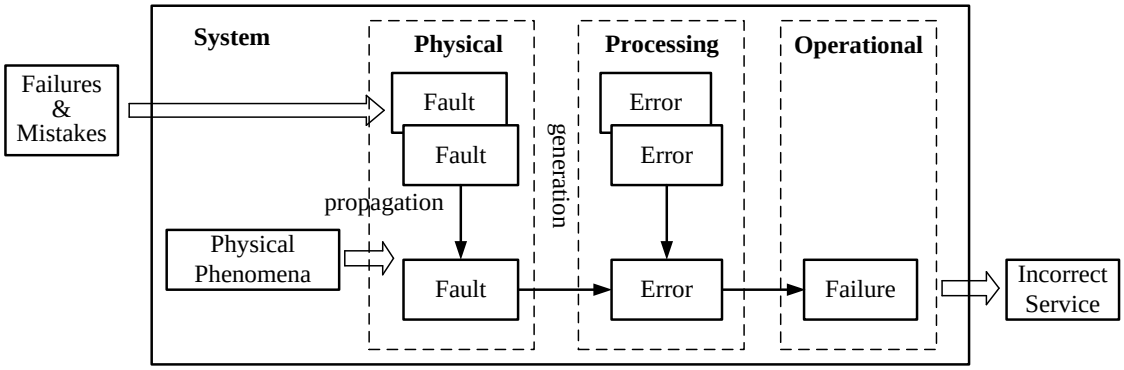

Fig. A1. Failure mechanism [34].

Failure may be of different types based on the contest like domain, propagation, detectability, perception, and different consequences. *Figure A1* illustrates the two basic failure mechanisms: generation and propagation. The rule holds that a failure is generated by an error and an error by a fault, being a fault the trigerring-off source of a failure according to a cascade generation mechanism. Faults and errors can be also caused by other faults and

Tab. A2 Fault classification.

CONTEXT		FAULT TYPE
Nature		Hardware fault
		Software fault
Persistence (or duration)		Permanent fault (a fault continuously or regularly recurring in the time)
		Transient fault (a fault bounded in time and not recurring)
		Intermittent fault (a transient fault the activation of which is not systematically reproducible)
Origin	Place	External fault
		Internal fault
	Phenomenon	Natural fault
		Human fault
	Phase of occurrence	Development fault
		Operational fault
	Modality	Malicious fault
		Deliberate fault
		Accidental fault
		Incompetence fault
Activity		Dormant fault (a fault not causing an error)
		Active fault (a fault causing an error)
		Latent fault (a fault with no manifestation or detected)

errors though a propagation mechanism occurring within the same layer. A failure is recognized by the user leads to either a system outage or a fault in the fed systems. A detailed fault classifications is listed in *Table A2*.

A2. Attributes

Attributes are quantities that measure the dependability of a system. The main attributes are reliability, availability, maintainability, and safety. The first three are expressed by probabilistic figures, while the safety is a property that the system has or does not have.

- Reliability is the probability that a system carries out the correct service at the time $t > 0$ for a given set of operating conditions, provided that the correct service is done at the time $t = 0$. High reliability means long time intervals before the system fails. The expected time for a system to fail is the mean time to failure (MTTF). It is a statistical value and therefore the length of the observation interval needed to determine the MTTF should be infinite.
- Maintainability is the probability that a system delivers the correct service at the time $t > 0$, provided that the correct service is not done at the time $t = 0$ and the system is under a repair process. High maintainability means short downtime for the system. The expected time for a system to be repaired is the mean time to repair (MTTR). It is also a statistical value.
- Availability is the probability that a system delivers the correct service at the time $t > 0$, without specifying whether or not the service is correct at the time $t = 0$ but assuming that the repair process starts immediately after the detection of the incorrect service. High availability means long uptime of the system. As a function of MTTF and MTTR, the availability is expressed as follows:

$$A = \frac{MTTF}{MTTF + MTTR} \tag{A1}$$

- Safety, according to the dependability theory, is a property that a system either has or does not have. Safety is important for safety-critical applications and is the ability of a system to show a safe behaviour in the presence of a fault that would lead to an unacceptable failure.

A3. Enforcing Techniques

Enforcement techniques are intended to improve the dependability of a system, safety included; they act by preventing, tolerating, removing, and forecasting a fault. In *Table A3*, the techniques and their actions are detailed. The fault-tolerance techniques are the most popular ones since, unlike the other techniques, they work on an operating system and make it tolerant to an intervening fault. They are closely illustrated in the next subsection.

Regarding fault-prevention techniques, also termed design for reliability techniques, the traditional approach begins with the specification of the reliability of a system and studies how to allocate the MTTFs of the items (subsystems) of a system so it meets the required

reliability. The MTTFs of the items, in turn, are defined according to statistical models mainly obtained from historical data, possibly scaled to account for reliability degradation due to usage stresses. Recently, initiated in the manufacturing of the integrated circuits, an approach termed physics of failure has emerged as a more effective fault-prevention technique to improve the MTTFs of the items and then the reliability of a system [54]. The approach consists of analysis of the physical phenomena relevant to the faults and then to the failure of the item. Identification of the root cause of the faults and the development of a failure model that gives the MTTF of the item. It is a matter of evidence that a better knowledge of the failure mechanisms of an item helps to determine the actions to undertake during the design stage of the item to increase its MTTF.

Tab. A3 Dependability enforcing techniques.

Enforcement technique	Action
Fault prevention	Aimed at avoiding the occurrence of a fault. Applied during the design, development, and test stages of the system.
Fault removal	Aimed at finding and eradicating a fault. Applied at the setup of the system to verify the fulfillment of the dependability requirements. Able to start diagnosis and corrective procedures.
Fault tolerant	Aimed at tolerating a fault. Applied on an operating system and implemented by redundancy.
Fault forecasting	Aimed at evaluating the dependability performance. Based on measurement or computation of the system attributes.

REFERENCES

[1] Y. Song and B. Wang, "Survey on reliability of power electronic systems," *IEEE Trans. Power Electron.*, vol. 28, no. 1, pp. 591–604, Jan. 2013.

[2] M. Salehifa, R. S. Arashloo, J. M. Moreno-Equilaz, V. Sala, L. Romeral, "Fault Detection and Fault Tolerant Operation of a Five Phase PM Motor Drive Using Adaptive Model Identification Approach," *IEEE Journal of emerging and selected topics in power electronics*, vol. 2, no. 2, pp. 212–223, June 2014.

[3] X. Roboam, B. Sareni, and A.D. Andrade, "More Electricity in the Air: Toward Optimized Electrical Networks Embedded in More-Electrical Aircraft," *IEEE Ind. Electron. Mag.*, vol. 6, no. 4, pp. 6-17, Dec. 2012.

[4] X. Roboam, "New trends and challenges of electrical network embedded in more electrical aircraft," in Proc. IEEE International Symposium on Industrial Electronics(ISIE), June 2011, pp. 26 – 31.

[5] Advisory Council for Aeronautics Research in Europe. (2010, June). Aeronautics and Air Transport: Beyond Vision 2020 Towards 2050 [Online]. Available: http://bookshop.europa.eu/en/aeronotics-and-air-transport-pbKI3211857/

[6] K. Emadi and M. Ehsani, "Aircraft power systems: technology, state of the art, and future trends," *IEEE Aerospace and Electron. Systems Mag.*, vol. 15, no. 1, pp. 28 – 32, Jan. 2000.

[7] J.A. Weimer, "Electrical power technology for the more electric aircraft," in Proc. AIAA/IEEE Digital Avionics Systems (DASC), October 1993, pp. 445-450.

[8] W. G. Homeyer, E. E. Bowless, S. P. Lupan, C. Rodriguez, P. S. Walia, N. M. Shah, and M. A. Maldonado, "Advanced power converters for more electric aircraft applications," in Proc. IECEC, 1996,vol. 1, pp. 137 – 142.

[9] M. David Kankam, "A survey of Power Electronics applications in Aerospace Technologies," in Proc. 36th Intersociety Energy Conversion Engineering Conference(IECEC), Georgia, July - August 2001, pp. 1 – 6.

[10] J. A Rosero, J. A. Ortega, E. Aldabas, and L. Romeral, "Moving towards a more electric aircraft," *IEEE Aerospace Electron. Mag.*, vol. 22, no. 3, pp. 3-9, Mar. 2007.

[11] I. Moir, "The all-electric aircraft-major challenges," in Proc. IEE Colloquium on All Electric Aircraft, 1998, pp. 2/1-2/6.

[12] A. Boglietti, A. Cavagnino, A. Tenconi, and S. Vaschetto, "The safety critical electric machines and drives in the more electric aircraft: A survey," in Proc. IEEE 35th Annu. Conf. Ind. Electron., Nov. 2009, pp. 2587 - 2594.

[13] D. Kŕahenb̈uhl, C. Zwssig, H. Weser, and J.W. Kolar, "A miniature 500000-r/min electrically driven turbocompressor," *IEEE Trans. Ind. Appl.*, vol. 46, no. 6, pp. 2459-2466, 2010.

[14] J. A. Weimer, “The role of electric machines and drives in the more electric aircraft,” in Proc. IEEE IEMDC, 2003, vol. 1, pp. 11–15.

[15] W. Cao, B.C. Mecrow, G.J. Atkinson, J.W. Bennett, and D.J. Atkinson, “Overview of electric motor technologies used for more electric aircraft (MEA),” *IEEE Trans. Ind. Electron.*, vol. 59, no. 9, pp. 3523-3531, Sep. 2012.

[16] T.J.E. Miller, “Brushless permanent-magnet and reluctance motor Drives,” Clarendon Press, Oxford 1989.

[17] K. T. Chau, C. C. Chan, and C. Liu, “Overview of Permanent-Magnet Brushless Drives for Electric and Hybrid Electric Vehicles,” *IEEE Trans. Ind. Electron.*, vol. 55, pp. 2246-2257, June 2008.

[18] A.M. El-Refaie, “Motors/Generators for Traction/Propulsion Applications: A Review,” *IEEE Vehicle Tech. Magazine*, vol. 8, no. 1, pp. 90-99, Mar. 2013.

[19] R. Carlson, M. Lajoie-Mazenc, and J.C.d.S. Fagundes, “Analysis of torque ripple due to phase commutation in brushless DC drives,” *IEEE Trans. Ind. App.*, vol. 28, pp. 287-292, 1992.

[20] M. Bertoluzzo, G. Buja, R.K. Keshri and R. Menis, “Analytical Study of Torque vs. Speed Characteristics of PM brushless DC drives”, in Proc. of 38th Annual Conf. on IEEE Industrial Electronics Society (IECON), 2012, pp. 1684-1689.

[21] B. Mecrow, A. G. Jack, J. A. Haylock and J. Coles, “Fault-tolerant permanent magnet machine drives,” *IEE Proc. Electr. Power Appl.*, Vol. 143, pp 437 - 442, 1996.

[22] R. Errabelli and P. Mutschler, “Fault-tolerant voltage source inverter for permanent magnet drives,” *IEEE Trans. Power Electron.*, vol. 27, no. 2, pp. 500–508, Feb. 2012.

[23] A. Tashakori and M. Ektesabi, “Fault Diagnosis of In-wheel BLDC Motor Drive for Electric Vehicle Application,” in Proc. IEEE Intelligent Vehicle Symposium, 2013, pp. 925-930

[24] S. Bolognani, M. Zordan, and M. Zigliotto, “Experimental fault-tolerant control of PMSM drive,” *IEEE Tram. Ind. Electron.*, vol. 47, pp. 1134-1141, Oct. 2000.

[25] B.-K. Lee, T.-H. Kim, and M. Ehsani, “On the feasibility of four-switch three-phase BLDC motor drives for low cost commercial applications: Topology and control,” *IEEE Trans. Power Electron.*, vol. 18, no. 1,pp. 164–172, Jan. 2003.

[26] S. H. Park, T. S. Kim, S. C. Ahn, and D. S. Hyun, “A simple current control algorithm for torque ripple reduction of brushless DC motor using four-switch three-phase inverter,” in IEEE 34th Annual Power Electron. Spec. Conf., 2003, vol. 2, pp. 574–579.

[27] R.K. Jha, S. Garlapati, R.K. Keshri, and G. Buja, “Remedial control strategies for a three-phase PM BLDC drive under VSI faults,” in Proc. of IEEE International conference on power electronics, Drives and Energy Systems (PEDES), India, Dec. 2014, pp. 1-6.

[28] A. Tashakori and M.Ektesabi, "A simple fault tolerant control system for Hall Effect sensors failure of BLDC motor," in Proc. of 8th IEEE Conf. on Industrial Electronics and Applications, June 2014, pp.1011–1016.

[29] E. Balaban, A. Saxena, P. Bansal, K.F. Goebel, and S. Curran, "Modeling, Detection, and Disambiguation of Sensor Faults for Aerospace Applications," *IEEE Sensors Journal*, vol. 9, no. 12, pp.1907–1917, Dec. 2009.

[30] N. B. Samoylenko, Q. C. Han, and J. Jatskevich, "Dynamic performance of brushless dc motors with unbalanced hall sensors," *IEEE Trans. on Energy Conversion*, vol. 23, no. 3, pp. 752–763, 2008.

[31] Y.-S. Jeong, S.-K. Sul, S. Schulz, and N. Patel, "Fault detection and fault-tolerant control of interior permanent-magnet motor drive system for electric vehicle," *IEEE Trans. on Ind. Applications*, vol. 41,no. 1, pp. 46–51, 2005.

[32] A. Tashakori and M. Ektesabi, "Stability analysis of sensorless bldc motordrive using digital pwm technique for electric vehicles," in Proc. of 38th Annual Conf. on IEEE Industrial Electronics Society, IECON2012, October 2012, pp. 4898–4903.

[33] J. G. Webster, The Measurement, Instrumentation, and Sensors Handbook. Boca Raton, FL: CRC Press, 1999.

[34] G. Buja and R. Menis, "Dependability and Functional Safety: Applications in Industrial Electronics Systems," *IEEE Ind. Electron. Mag.*, vol. 6, no. 3 pp. 4-12, Sep. 2012.

[35] L.D. Lillo, L. Empringham, P.W. Wheeler, S. Khwan-on, C. Gerada, M.N. Othman, and X. Huang, "Multiphase power converter drive for fault-tolerant machine development in aerospace applications," *IEEE Trans. on Ind. Electron.*, vol. 57, no. 2, pp. 575–583, Feb. 2010.

[36] B. Mecrow, J. Cullen, and P. Mellor, "Editorial - Electrical machines and drives for the more electric aircraft," *IET Electric Power Applications*, vol. 5, no.1, pp. 1-2, Jan. 2011.

[37] Z. Q. Zhu, and D. Howe, "Electrical Machines and Drives for Electric, Hybrid, and Fuel Cell Vehicles," *IEEE Proceedings*, vol. 95, no. 4, pp. 746-765, Apr. 2007.

[38] A.V. Brazhinkov and N.N. Dovzhenko, "Control potentials and advantages of multiphase AC drives," in Proc. of 29th IEEE Power Electronics Specialists Conf. (PESC), May 1998, vol. 2, pp. 2108 - 2114.

[39] L. Parsa, "On advantages of multi-phase machines," in Proc. of 31st Annual Conf. on IEEE Industrial Electronics Society (IECON), 2005, pp. 6-10.

[40] P. Martin, F. Meibody-Tabar, and B. Davat, "Multiple-phase permanent magnet synchronous machine supplied by VSIs, working under fault conditions," in Conf. Record of IEEE-IAS Annual Meeting, 2000, vol. 3, pp. 1710-1717.

[41] J. Figueroa, J. Cros, and P. Viarouge, "Generalized transformations for polyphase phase-modulated motors," *IEEE Transaction on Energy Conversion*, vol. 21, no. 2, pp. 332–341, Jun. 2006.

[42] M. Godoy Simòes and P. Vieira Jr., "A Five-phase brushless DC machine direct drive system," *EPE Journal*, vol. 14, no. 3, pp. 15-24, August 2004.

[43] L. Parsa and H.A. Toliyat, "Five-Phase Permanent-Magnet Motor Drives," *IEEE Trans. on Ind. Appl.*, vol. 41, no. 1, pp. 30-37, Jan/Feb. 2005.

[44] S. Dwari and L. Parsa, "Fault-Tolerant Control of Five-Phase Permanent-Magnet Motors With Trapezoidal Back EMF," *IEEE Trans. on Ind. Electron.*, vol. 58, no. 2, pp. 476-485, Feb. 2011.

[45] A. Mohammadpour and L. Parsa, "A Unified fault-tolerant current control approach for five-phase PM motors with trapezoidal back EMF under different stator winding connections," *IEEE Trans. on Power Electron.*, vol. 28, no. 7, pp. 3517-3527, Jul. 2013.

[46] R. Keshri, S. Garlapati, A. Tessarolo, and G. Buja, "Torque capabilities of a five-phase PM BLDC drive vs. a three-phase one and various supply modes," in Proc. of IEEE International Electric Vehicle Conf. (IEVC), Dec. 2014, pp. 1-8.

[47] A. Mohammadpour, S. Sadeghi, and L. Parsa, "A Generalized Fault-Tolerant Control Strategy for Five-Phase PM Motor Drives Considering Star, Pentagon, and Pentacle Connections of Stator Windings," *IEEE Trans. Ind. Electron.*, vol. 61, no. 1, pp. 63-75, Jan. 2014.

[48] P. Pillay and R. Krishnan, "Application characteristics of permanent magnet synchronous and brushless DC motors for servo drives," *IEEE Trans. on Industry Applications*, vol.27, no.5, pp.986-996, Sept. /Oct. 1991.

[49] G. Buja and M. Bertoluzzo, "Development of electric propulsion systems for light electric vehicles," *IEEE Trans. on Ind. Inform.*, vol.7, no.3, pp.428-435, Aug. 2011.

[50] A.V. Brazhinkov and N.N. Dovzhenko, "Control potentials and advantages of multiphase AC drives," in Proc. of 29th IEEE Power Electronics Specialists Conference (PESC), 1998, pp.2108-2114.

[51] S. Garlapati, G. Buja, and A. Tessarolo, "An Algebraic Approach to Determine the Current Supply in a Faulty 5-Phase PM BLDC Drive. Part I – Model Setup and its Application to the case of One Open Phase Fault," in Proc. of IEEE Conf. on Sustainable Mobility Applications, Renewables and Technology (SMART), 2015.

[52] S. Garlapati, G. Buja, and A. Tessarolo, "An Algebraic Approach to Determine the Current Supply in a Faulty 5-Phase PM BLDC Drive. Part II – Application to the Cases of Two and Three Open Phase Faults," in Proc. of IEEE Conf. on Sustainable Mobility Applications, Renewables and Technology (SMART), 2015.

[53] S. Garlapati, G. Buja, M. Bertoluzzo, R. Keshri "Commutation effects on motor current and torque in five-phase PM BLDC drives," in Proc. of 40th Annual Conf. on IEEE Industrial Electronics Society (IECON), 2014, pp. 3204-3209.

[54] V. P. Nelson, "Fault-tolerant computing: Fundamental concepts," in *Computer*, vol. 23, no. 7, pp. 19–25, Jun. 1990.

[55] J.W. Bennett, B. C. Mecrow, A. G. Jack, and D. J. Atkinson, "A prototype electrical actuator for aircraft flaps," *IEEE Trans. Ind. Appl.*, vol. 46, no. 3, pp. 915–921, May/Jun. 2010.

[56] J. W. Bennett, B. C. Mecrow, A. G. Jack, D. J. Atkinson, C. Sewell, G. Mason, S. Sheldon, and B. Cooper, "Choice of drive topologies for electrical actuation of aircraft flaps and slats," in Proc. IEE Conf. Power Electron., Mach. Drives, Edinburgh, U.K., Mar. 2004, pp. 332–337.

[57] Farhad Aghili, "Fault-Tolerant Torque Control of BLDC Motors," *IEEE Trans. Power Electronics*, vol. 26, no. 2, Feb. 2011.

[58] B. G. Park, T. Kim, J. Ryu, and D. Hyun, "Fault tolerant strategies for BLDC motor drives under switch faults," in Conf. Rec. 41st IEEE IAS Annu. Meeting, 2006, vol. 4, pp. 1637–1641.

[59] R. Spee and A. K. Wallace, "Remedial Strategies for Brushless DC drive failures," *IEEE Trans. Industry Applications*, vol. 26, No. 2, pp.259-266, March/April 1990.

[60] M. Naidu, S. Gopalakrishnan, and T.W. Nehl, "Fault-tolerant permanent magnet motor drive topologies for automotive x-by-wire systems," *IEEE Trans. Ind. Appl.*, vol. 46, no. 2, pp. 841-848, March/April 2010.

[61] M. Villani, M. Tursini, G. Fabri, L. Castellini, "Fault-Tolerant PM Brushless DC drive for aerospace application," in Proc. of XIX International Conference on Electrical Machines (ICEM), Sept. 2010, pp.1-7,.

[62] B. G. Park, K.-J. Lee, R. Y. Kim, T.-S. Kim, J. S. Ryu, and D. S. Hyun, "Simple fault diagnosis based on operating characteristic of brushless direct-current motor drives," *IEEE Trans. Ind. Electron.*, vol. 58, no. 5, pp. 1586–1593, May 2011.

[63] M. G. Simoes and P. Vieira, "A high-torque low-speed multiphase brushless machine - A perspective application for electric vehicles," *IEEE Trans. Ind. Electron.*, vol. 49, no. 5, pp.1154 -1164, 2002.

[64] X. Huang, A. Goodman, C. Gerada, Y. Fang, and Q. Lu, "A Single Sided Matrix Converter Drive for a Brushless DC Motor in Aerospace Applications," *IEEE Trans. Ind. Electron.*, vol. 59, no. 9, pp. 3542-3552, 2012.

[65] R. Burgos, Gang Chen, F. Wang, D. Boroyevich, W.G. Odendaal, J.D. Van Wyk, "Reliability-Oriented Design of Three-Phase Power Converters for Aircraft Applications," *IEEE Trans. Aerospace and Electron. Sys.*, vol. 48, no. 2, pp. 1249-1263, April 2012.

[66] W. Zhang, D. Xu, P. N. Enjeti, H. Li, J. T. Hawke, and H. S. Krishnamoorthy, “Survey on Fault-Tolerant Techniques for Power Electronic Converters,” *IEEE Transactions on Power Electronics* vol. 29, no. 12 , pp. 6319-6331, 2014.

[67] A. G. Jack, B. C. Mecrow, and J. A. Haylock, “A comparative study of permanent magnet and switched reluctance motors for high-performance fault-tolerant applications,” *IEEE Trans. Ind. Applicat.*, vol. 32, pp. 889–895, July/Aug. 1996.

LIST OF PUBLICATIONS

Peer reviewed International conferences (IC)

IC1. S. Garlapati, G. Buja, and A. Tessarolo, "An Algebraic Approach to Determine the Current Supply in a Faulty 5-Phase PM BLDC Drive. Part I – Model Setup and its Application to the case of One Open Phase Fault," in. Proc. of IEEE Conf. on Sustainable Mobility Applications, Renewables and Technology (SMART), 2015.

IC2. S. Garlapati, G. Buja, and A. Tessarolo, "An Algebraic Approach to Determine the Current Supply in a Faulty 5-Phase PM BLDC Drive. Part II – Application to the cases of Two and Three Open Phase Faults," in Proc. of IEEE Conf. on Sustainable Mobility Applications, Renewables and Technology (SMART), 2015.

IC3. R. Keshri, S. Garlapati, A. Tessarolo, and G. Buja, "Torque capabilities of a five-phase PM BLDC drive vs. a three-phase one and various supply modes," in Proc. of IEEE International Electric Vehicle Conference (IEVC), Dec. 2014, pp. 1-8.

IC4. S. Garlapati, G. Buja, M. Bertoluzzo, and R.K. Keshri, "Commutation effects on motor current and torque in five-phase PM BLDC drives," in Proc. of 40th Annual conference of IEEE Industrial Electronics Society, IECON'2014, TX-USA, Nov. 2014, pp. 3204 – 3209.

IC5. Rupesh Kumar Jha, S. Garlapati, R.K. Keshri, and G. Buja, "Remedial control strategies for a three-phase PM BLDC drive under VSI faults," in Proc. of IEEE International conference on power electronics, Drives and Energy Systems (PEDES), India, Dec. 2014, pp. 1-6.